ÄSPÖLABORATORIET

INTERNATIONAL COOPERATION REPORT 95-03

Groundwater degassing and two-phase flow: Pilot hole test report

Jil T Geller
Earth Sciences Division,
Lawrence Berkeley National Laboratory

Jerker Jarsjö
Water Resources Engineering,
Royal Institute of Technology

August 1995

Supported by U.S. DOE, USA and SKB, Sweden

SVENSK KÄRNBRÄNSLEHANTERING AB
SWEDISH NUCLEAR FUEL AND WASTE MANAGEMENT CO
BOX 5864 S-102 40 STOCKHOLM
TEL. +46-8-665 28 00 TELEX 13108 SKB TELEFAX +46-8-661 57 19

ISSN 1104-3210
ISRN SKB-ICR--95/03--SE

GROUNDWATER DEGASSING AND TWO-PHASE FLOW: PILOT HOLE TEST REPORT

Jil T Geller
Earth Sciences Division,
Lawrence Berkeley National Laboratory

Jerker Jarsjö
Water Resources Engineering,
Royal Institute of Technology

August 1995

Supported by U.S. DOE, USA and SKB, Sweden

Revision 1.0

GROUNDWATER DEGASSING AND TWO-PHASE FLOW: PILOT HOLE TEST REPORT

Jil T. Geller

Earth Sciences Division, Lawrence Berkeley National Laboratory

Jerker Jarsjö

Water Resources Engineering, Royal Institute of Technology

August 9, 1995

Keywords: Degassing, Two-Phase Flow, Gas Measurement, Blasting, Transmissivity, Storativity, Fractured Rock, Hydrologic Testing

ABSTRACT

A pilot hole test was conducted to support the design of the Degassing of Groundwater and Two-Phase Flow experiments planned for the Hard Rock Laboratory, Äspö, Sweden. The test consisted of a sequence of constant pressure borehole inflow tests (CPTs) and pressure recovery tests (PRTs) in borehole KA2512A. The test sequence was designed to detect degassing effects from the change in transmissivity/hydraulic conductivity, and storativity/specific storage when the borehole pressure is lowered below the groundwater bubble pressure. A bubble pressure estimate of 300 kPa was calculated from earlier gas contents measurements in KA2511A and KA2598A. Borehole KA2512A was drilled while maintaining the borehole pressure greater than 1500 kPa to prevent the possible formation of a gas phase and ensure that single phase flow behavior could be well characterized. The entire 37.3 m of the borehole section was tested without packers. Flow response to pressure changes in CPTs occurred rapidly. Flowrates fluctuated before attaining a steady trend, probably due to effective stress changes when borehole pressure was reduced for the first time. These factors, along with the rapid response of the borehole to pressure changes, decreased the sensitivity of the single-well analysis for specific storage. The analysis of the pressure response in the monitoring well, KA2511A, provided more reliable estimates of the specific storage. The relationship between borehole pressure and steady-state flowrates was linear over borehole pressures of 1500 kPa (abs) down to 120 kPa (abs) during testing in December 1994, indicating that processes that may change hydraulic conductivity at low borehole pressures, such as degassing, calcite precipitation or turbulence, did not occur to a measurable degree. The gas contents of water from KA2512A, KA2598A, KA3010A and KA3067A were measured by two methods which indicated the volume of evolved gas per known volume of liquid at atmospheric pressure. These methods indicated a gas contents in KA2512A on the order of 0.5% v/v, in which case it is possible that pressures below the groundwater bubble pressure were not attained in the formation. Samples from other boreholes had higher gas contents (ranging from 1 to 3% v/v). Test results during January and February of 1995 suggest that degassing may have occurred. One CPT at a borehole pressure equal to 120 kPa (abs) indicated a 20% decrease compared to the hydraulic conductivity measured at a borehole pressure of 1500 kPa (abs); the latter value was 10% lower than the hydraulic conductivity measured in December, 1994. The volumetric gas content measured during this time was 1% v/v. However, the hydraulic conductivity in a subsequent CPT test at 120 kPa, returned to within the standard deviation of previous measurements.

TABLE OF CONTENTS

LIST OF FIGURES

EXECUTIVE SUMMARY

This report describes a pilot hole test to support the design of the Degassing of Groundwater and Two-Phase Flow experiments planned for the Hard Rock Laboratory, Äspö, Sweden. These experiments will investigate the development of two-phase flow conditions in the near-drift region and their effect on hydraulic test interpretation. One hypothesis is that liquid flow rates are reduced due to the evolution of two phase flow conditions that evolve as a result of groundwater degassing upon pressure reduction. This will be tested by measuring the steady-state inflow to a single borehole as a function of borehole pressure. This relationship is linear for single liquid phase conditions; deviations from linearity at low borehole pressures may indicate the presence of a gas phase. The first tests at borehole pressures above the partial pressure of the dissolved gases (or bubble pressure) establish the linear trend between borehole pressure and flowrates; however, there is concern that depressurization of the borehole during drilling and packer installation may irreversibly disturb the initial conditions of the flow system by allowing the formation of a gas phase.

Equipment exists to drill a borehole while maintaining formation pressure; however, the development and construction of a packer system that could be installed without depressurization would be costly and its performance uncertain. To assess the need for such a packer system, a pilot hole test was conducted in borehole KA2512A. This borehole was drilled while maintaining water pressure above the estimated partial pressure of the dissolved gases. The entire 37.3 m of the borehole section was tested without packers. One water-flowing fracture occurred at the end of the borehole. The pilot hole test provided the opportunity to test the degassing hypothesis and investigate whether other mechanisms at low borehole pressures could cause a change in transmissivity, including effective stress changes, calcite precipitation and turbulence.

The pilot hole test sequence had four phases: (1) characterize the flow system for single-phase conditions by a series of tests at borehole pressures above the estimated bubble pressure; (2) allow two-phase flow conditions to develop by reducing the borehole pressure to atmospheric pressure and measure the change in transmissivity; (3) repeat tests of the first phase to observe any hysteresis as the flow system returned to single liquid phase conditions and measure the time required for resaturation; and (4) a long-term test at atmospheric borehole pressures to observe any time-dependence in degassing effects.

In test phases (1) through (3), the relationship between borehole pressure and inflow rate was linear over borehole pressures ranging from 1500 kPa (abs) down to 120 kPa (abs). The low gas contents measured in KA2512A (0.5% v/v) indicate that during phase (2), water pressures below the bubble pressure may not have been achieved with the equipment configuration used. (On-site gas content measurements were made of the volume of gas evolving when the water pressure was reduced to atmospheric.) The results show no evidence of other processes that might reduce transmissivity at low borehole pressures, such as calcite precipitation, increase in effective stress or turbulence. An analysis of the transient CPT data by type-curve matching for spherical flow geometry gave a hydraulic conductivity value of 1.2×10^{-6} m/s which did not vary significantly with borehole pressure.

The first CPTs of phase (4), which began 25 days following phase (3), indicated that the hydraulic conductivity measured at a borehole pressure of 1500 kPa (abs) was 10%, or one standard deviation, below the mean hydraulic conductivity measured in phases (1) through (3). At a borehole pressure of 120 kPa (abs) the hydraulic conductivity decreased by another 20%. Gas contents measured at the beginning of phase (4) were twice as high as previously measured (1% v/v), suggesting that degassing may have caused the flow reduction. On the other hand, not enough testing was done above the bubble pressure to exclude the possibility that the observed flow reduction was caused by other changes in the system.

Step changes in flowrates coincided with blasts occurring at the 420 to 450 m levels below the test site. The magnitude of the changes was larger at lower borehole pressures. Pressure increases in monitoring well KA2511A also coincided with the blasts. Possible mechanisms of blasting effects on the flow system include changes in boundary conditions, effective stresses or deformation of fracture-lining materials. The flow fluctuations were not large enough to affect the hydraulic conductivity estimates; however, they illustrate how tunnel activities can affect the flow system and complicate the interpretation of test results.

Volumetric gas contents measured in other boreholes were variable and higher than in KA2512A, ranging from 1 to 3% v/v. More information regarding the composition of the dissolved gases in the groundwater at Äspö is required to understand the observed variability, however there is evidence from other researchers that biological activity in the near borehole region in the SELECT project boreholes, which may produce gas, has increased following drilling. A quantitative laboratory analysis of water samples from KA2512A, KA2511A.1, and KA3010A, obtained during test phase (4), indicated a total dissolved gas content of approximately 4% (v/v @ STP). Approximately half this value would be dissolved in water at atmospheric pressures. KA2511A.1 and KA2512A have elevated $C0_2$ and CH_4 concentrations relative to KA3010A but nitrogen represents over

70%. of the total gas content. The nitrogen/argon ratios analyzed for water samples from KA2512A.1 and KA3010A indicate that the nitrogen is of atmospheric origin. Both samples contain excess ^4He relative to the abundance in air which is radiogenic.

We recommend that the pilot hole test be repeated in a borehole with higher gas contents and that the equipment configuration ensure that the groundwater pressure can be reduced to values below the bubble pressure. The sampling for gas content measurement must be cognizant of the spatial and temporal variation indicated by the data in this report. Ideally, the dissolved gas contents in a potential test hole should approach the values measured at Stripa. In addition, injection-withdrawal tests using gas-saturated water should be considered to demonstrate the occurrence of flow reduction for higher gas contents than present in the native groundwater. Single-hole and cross-hole air injection-resaturation tests are recommended to obtain two-phase flow parameters necessary to model two-phase flow effects on hydrologic characterization from drifts and the performance of the repository following closure.

ACKNOWLEDGMENTS

This work was carried out under U. S. Department of Energy Contract No. DE-AC03-76SF00098, for the Director, Office of Civilian Radioactive Waste Management, Office of External Relations, administered by the Nevada Operations Office and under the Swedish Nuclear Fuel and Waste Management Company (SKB) Contract No 268070. We would like to gratefully acknowledge the assistance provided by the staff at the Äspö Hard Rock Laboratory Site Office. Olle Olsson of SKB, Gia Destouni of KTH, Kent Hansson of Geosigma and Jane Long, Christine Doughty and Stefan Finsterle of LBL contributed to the design of the pilot hole test and thoughtfully reviewed this report.

Paul Marschall of NAGRA and Anders Rasmuson of Chalmers University of Technology also provided useful comments. We are grateful to Mack Kennedy of LBNL and Bill Evans of the USGS for gas content analysis.

1. BACKGROUND AND OBJECTIVES

The investigation of potential underground nuclear waste repositories relies upon hydrologic testing from excavations, which provide access to the subsurface with the purpose of characterizing flow systems in undisturbed rock. Effects of the excavation on the hydrologic response of the system must be understood so that the measured behavior can be extrapolated to the rock away from the drift. Evidence from an investigation of excavation effects in the Stripa Mine in Sweden, a regionally saturated granitic rock formation, suggests that two-phase flow conditions evolved in the region of the drift, reducing flowrates by an order of magnitude compared to pre-excavation conditions (Olsson, 1992; Long *et al.,* 1992). The observation of gas bubbles in the water at Stripa led to the hypothesis that two-phase flow conditions can develop due to the depressurization of formation water, causing the dissolved gases to come out of solution.

A test plan entitled "The Degassing of Groundwater and Two-Phase Flow" was developed to investigate the occurrence of two-phase flow conditions in the near-drift region and their effects on hydrologic characterization. The test plan proposes a series of single hole, constant pressure, inflow tests to be performed at the Hard Rock Laboratory in Äspö, Sweden. For single phase conditions, Darcy's Law predicts that the inflow rate should be directly proportional to borehole pressure. A reduction in measured transmissivity at lower borehole pressures would indicate two-phase flow conditions. The presence of a gas phase may also cause flow fluctuations, hysteresis during pressure cycling and changes in compressibility. Because the magnitude of flow changes due to groundwater degassing is anticipated to be a function of fracture aperture, the test borehole will be packed off into as many as five sections to isolate fractures of varying transmissivities.

Equipment exists to drill a borehole while maintaining formation pressure. However, the development and construction of a packer system that could be installed without depressurization would be costly and its performance uncertain. It was decided to conduct a pilot hole test in a cased borehole drilled under pressure, without packers, which would eliminate uncertainty regarding the existence of single phase conditions when measuring the baseline flow tests above the bubble pressure. Hysteresis following borehole depressurization could then be examined and the need for the design and deployment of a packer system to be installed under pressure could be assessed. The pilot hole test also provided the opportunity to address other issues identified below before proceeding with the design and

implementation of the Degassing of Groundwater and Two-Phase Flow Experiments.

The objectives of the pilot hole test were as follows:

- Test whether degassing causes measurable changes in transmissivity and storativity at atmospheric borehole pressures.

- Evaluate the occurrences of hysteresis caused by borehole depressurization which would interfere with the interpretation of the degassing and two-phase flow tests.

- If gas evolves during depressurization, demonstrate whether the formation is re-saturated when background pressure is restored and what is the time required for resaturation.

- Obtain measurements of gas contents of the water to estimate bubble pressure.

- Determine whether two-phase flow effects can be distinguished from other possible causes of flow reduction at low borehole pressures such as effective stress changes, calcite precipitation and turbulence.

A series of constant pressure tests as a function of borehole pressure and pressure recovery tests were designed to meet the pilot hole test objectives. The test sequence and its rationale are described in the following section. The approach in these tests is to detect degassing effects from changes in transmissivity (T), or hydraulic conductivity (K), and storativity (S), or specific storage (S_s) at lower borehole pressures. Hydraulic conductivity should decrease and specific storage should increase in the presence of two-phase flow conditions. Calcite precipitation, the increase in effective stress, or turbulence may also cause a reduction in hydraulic conductivity at lower borehole pressures, however these effects may be distinguished from degassing effects because they should also cause a decrease in storativity. Hysteresis is evaluated by seeing if K and S_S values at higher borehole pressures are restored when the borehole is re-pressurized. One cause of hysteresis would be the slow dissolution of evolved gas when the borehole pressure is increased. Another cause is a change in the initial set of the fractures when the borehole is de-pressurized for the first time. These effects may be differentiated on the basis of changes in S_S. An increase in compressibility due to the presence of gas greatly increases the time for flowrates and pressures to reach a steady trend which may also be used to indicate degassing effects and hysteresis. Determination of S_S is inherently unreliable, however relative changes may be significant and useful even if the absolute value is unknown. Because changes in K and S_S, as opposed to their absolute values, will be used to indicate degassing effects, a thorough

characterization of the system above the estimated bubble pressure is essential.

2. PROCEDURES

2.1 TEST SEQUENCE

The pilot hole test sequence consists of the following four phases:

(1) characterize the flow system for single-phase conditions by a series of tests at borehole pressures above the estimated bubble pressure;

(2) allow two-phase flow conditions to develop by reducing the borehole pressure to atmospheric pressure and measure the change in transmissivity;

(3) repeat tests to observe any hysteresis as the flow system returned to single liquid phase conditions and measure the time required for resaturation;

(4) a long-term test at atmospheric borehole pressure to see if degassing effects evolve over time as water farther away from the borehole is sampled.

The timelines for borehole pressures and inflow rates for phases (1) through (3) are depicted in Figure 2-1a. Constant pressure tests (CPTs) and pressure recovery tests (PRTs) were conducted within each phase of the sequence. The bubble pressure is indicated by the heavy dashed line in the upper figure. Appendix I describes how the bubble pressure was estimated using previous gas content measurements in KA2511A and KA2598A. The fine dashed lines indicate the anticipated behavior for two-phase flow conditions. In the CPTs below the bubble pressure, flowrates are expected to drop off as the gas phase evolves and the time to reach steady-state conditions is expected to be much greater compared to single-phase conditions. The time to reach background pressure in a PRT is also expected to increase when a gas phase is present. If the formation does not completely re-saturate following well shut-in, flowrates during the subsequent CPTs of phase (3) may be lower than in phase (1).

Because the best evidence of two-phase flow conditions is in the deviation from single-phase behavior, it is critical to obtain the best characterization as practically possible above the bubble pressure. The test sequence was designed to allow the use of analytical solutions (type curves) to estimate values for hydraulic conductivity and storativity from both PRTs and CPTs. The PRTs were scheduled to provide quiescent conditions before a CPT to

allow use of the Jacob and Lohman (1952) solution to interpret the CPT. A long-term CPT was conducted before a PRT to establish a constant flowrate which is assumed in the Horner solution used to interpret the PRT. Other considerations in the design of the test sequence were to minimize the number of perturbations to the system, allow time for flowrates to achieve a recognizable trend and to complete the test cycle within the 2.5 week period available for testing.

Phase (4) was added to the test sequence upon the completion of phase (2), because no significant change in hydraulic conductivity had been observed and there was concern that two-phase flow effects might take a longer time to develop than the test schedule allowed for.

Table 2-1. Tests performed in KA2512A. CPT indicates constant pressure test, PRT indicates pressure recovery test. CPT 1 began after the well was shut-in overnight. Well was shut-in between CPT 9 and CPT 10, and between CPT 11 and CPT 12.

Test Phase	Test Number	Borehole Pressure (kPa abs)	Start Date and Time	Test Duration (min)
(1)	CPT 1	1500	12/01/94 15:59	1800
	PRT 1	3010**	12/02/94 20:58	1700
	CPT 2	1000	12/03/94 23:54	1300
	CPT 3	500	12/04/94 20:27	1500
(2)	CPT 4	120	12/05/94 23:30	4905
	CPT 5	300	12/09/94 10:51	1549
	PRT 2	3070**	12/10/94 12:42	1239
(3)	CPT 6	1500	12/11/94 09:21	1547
	CPT 7	1000	12/12/94 11:11	1425
	CPT 8	500	12/13/94 11:36	1887
	CPT 9	120	12/14/94 19:43	725
(4)	CPT 10	1500	01/09/95 19:03	819
	CPT 11*	120	01/10/95 08:42	11865
	CPT 12	120	01/24/95 16:05	19980

* Data only available from 01/10/95 13:58.
**Final borehole pressure.

The test sequence for phase (4) is shown in Figure 2-1b. Because of the need to use the borehole test equipment for other purposes, phase (4) was conducted 25 days after CPT 9, during which time the well was shut in. CPT 10 was conducted at a borehole pressure of 1500 kPa (abs) for comparison with phase (1) and (3) because there was concern that the system's response may change over the shut in period. The well was shut in for 8 days between CPT 11 and 12 to obtain water samples under pressure. The test numbers and their schedule are listed in Table 2-1.

2.2 BOREHOLE DESCRIPTION

Borehole KA2512A is located at 2512 m linear distance along the tunnel and extends in a direction 264° from North, outward from the tunnel spiral, dipping at a 2° angle from the horizontal. The map in Figure 2-2 shows the plan view of the tunnel and the orientation of KA2512A. The plan view indicates locations of fracture zones, which should be interpreted as indicating general trends, rather than precise locations because they were mapped using surface borehole data. The 85 mm diameter borehole was drilled while maintaining formation pressure above 1500 kPa. The borehole was drilled to a length of 37.27 m, when an inflow rate of 10.6 L/min was obtained at a borehole pressure of 1580 kPa. Almost all of the flow into the borehole occurred over the last 4 to 5 cm of drilling and the core log revealed an undulating, calcite-coated fracture at this location. During drilling, a pressure response was observed in all four packed-off sections along the approximately 300 m length of the nearby monitoring borehole KA2511A. (Lengths of sections are noted in Section 3.1.2.) Figure 2-2 shows that KA2511A crosses the line indicating the trend of NNW fractures. These observations suggest that the fracture encountered in KA2512A is hydraulically connected to a larger network of fractures. Water from borehole KA2598A was used for drilling. This water was dyed with uranine which was flushed from the borehole before testing. Detailed descriptions of the borehole drilling and the core log are provided in Gass and Ramqvist (1995) and Gass et al. (1995), respectively. Tests were conducted in the cased borehole without packers.

2.3 EQUIPMENT DESCRIPTION AND METHODS

2.3.1 Pressure and flow regulation

The experimental set-up is shown schematically in Figure 2-3. A Druck PTX 510-00 50 bar absolute pressure transducer monitored the borehole pressure and was connected to a back pressure controller (PC). A motor-

driven pressure regulating valve was used to control the borehole pressure. The time required for stabilizing borehole pressures at the set pressure was approximately 15 seconds. The regulating valve controlled pressures to within ± 2 kPa for pressures, down to a minimum pressure of 200 kPa (abs). The minimum borehole pressure achievable was 120 kPa (abs) due to head losses in valves and lines downstream of the casing. The pressure regulating valve was set to 120 kPa (abs) for these tests, however it could not actually regulate at this low pressure as the valve was completely open. A flowmeter (Fischer and Porter COPA-X D10D1165 volumetric flowmeter with a maximum range of 0 to 100L/min and a minimum range of 0 to 5 L/min) was installed upstream the pressure control valve. The accuracy of the flowmeter is ±1% of the real value. A Druck PTX 510-00 12 bar absolute pressure transducer was used to measure the barometric pressure. Figure 2-3 also shows the installation of the tube trap for gas content measurements described in section 2.3.3.

2.3.2 Data acquisition

The flowrate, the borehole pressure and the barometric pressure were continuously logged using BORRE datalogger version 2.2. During the first 30 seconds of the tests, data was logged each 4 seconds. During the subsequent two hours, sample rates decreased incrementally until they reached a rate of once every 15 minutes which was maintained throughout the rest of the test.

Data from the logger was transferred to a laptop PC every one to three days using the menu-driven SHELL program in WP-Lib, which is a part of the Äspö Hydro Monitoring System (see, e.g., Gentzschein, 1993). The SHELL program was also used to enter the calibration constants and transform the hexadecimal data to decimal format.

2.3.3 Gas contents

Volumetric gas contents were measured on-site by two methods: (1) trapping evolved gas over several liters of flowing water in a glass vessel at atmospheric pressure (referred to as a glass accumulator) and (2) measuring the evolved gas upon depressurization to atmospheric pressure of a known volume of water sampled under pressure in a stainless steel tube (referred to as a tube trap). Boreholes KA2512A, KA2598A, KA3010A and KA3067A were sampled by these methods which are described in more detail in the following paragraphs. Neither of these methods are suitable for obtaining gas samples for chemical composition analysis; however, they are useful for immediate estimations of gas contents of sampled water. Measurements by these methods should be interpreted as indications of

relative values because they have not been calibrated for known gas contents. Gas contents obtained by these on-site methods do not include the aqueous phase gas present at atmospheric pressure. In the laboratory analysis of gas contents, all of the gas is extracted from the aqueous phase by vacuum and therefore measures the total gas contents. Samples for the analytical determination of gas contents and chemical and isotopic composition were obtained from boreholes KA2511A, KA2512A, KA3010A, KA3067A and KA3105A and were analyzed by Bill Evans at the USGS in Menlo Park (gas composition) and by Mack Kennedy (noble gas analysis). These samples are acquired under pressure in a copper tubing which is clamped to effectively cold-weld the tubing and maintain the sample under pressure until analysis. The clamped seal is leak-proof to helium.

2.3.4 Glass accumulator

A sketch of the glass accumulator is shown in Figure 2-4. The inflow tube of the accumulator is connected downstream of a shutoff valve from the borehole and the outflow tube is directed to a 2 L graduated cylinder. The accumulator is filled with water until the meniscus reaches a gradation mark near the top of the cylindrical portion of the vessel, i.e. below the conical section. The shutoff valve is adjusted to achieve a flowrate of approximately 100 mL/min and the change in the level of the meniscus and the volume of water collected in the graduated cylinder are recorded with time. The gradation marks in the accumulator occur every 5 mL, so a minimum of 10 mL of gas must be collected to obtain a reliable reading. The gas contents are calculated as the percent volume of gas accumulated per volume of water collected in the graduated cylinder. In borehole KA2512A, the water is sampled upstream of the pressure control valve so that samples are obtained at several pressures (see Figure 2-3).

One limitation of this method is that the residence time of the water in the accumulator may be too short for all of the dissolved gas to come out solution. Bubbles were generally observed in the graduated cylinder downstream of the accumulator. Another problem is that dissolved gas may come out of solution in the tubing between the shut-off valve and the accumulator and become trapped upstream of the accumulator. For low gas contents, this could be a significant fraction of the evolved gas. Before taking a reading, the tubing was tapped to release any trapped gas. We observed that the amount of gas accumulated in the vessel was sensitive to flowrate and that approximately 100 mL/min was the optimum value. At significantly lower flowrates the volume of trapped gas decreased, perhaps because there was insufficient energy for gas nucleation. At much higher flowrates the volume of trapped gas decreased, presumably due to inadequate residence time.

2.3.5 Tube trap

The tube trap is shown in Figure 2-5 a and b. It consists of a section of stainless steel tube that has a volume of 187 mL and a section of 6 mm I.D. nylon tubing that has a volume of 31 mL. In borehole KA2512A the tube trap is installed upstream of the pressure control valve to allow sampling at the set pressure (see Figure 2-3). The tube is installed with valves a and d closed. Valves a, b, c and d are then opened and valve e is partially closed to drive flow through the sample tube. The tube trap is flushed for 15 minutes, during which time the tube is tapped and the translucent tubing checked to ensure that no gas bubbles are present. After flushing, valves a, b, c and d are closed, valve e is fully opened and the tube trap is removed by disconnecting the swagelok fittings between valves a and b and between valves c and d.

The installation of the tube trap for the other boreholes is shown in Figure 2-5 a. The trap is flushed by fully opening valves a, b and c and adjusting the flowrate with valve d. Then valve d is almost closed to maintain pressure in the tube trap while allowing a small outflow to continue flushing the tube. When approximately 2 L of water have been flushed through the tube, valve d is closed first to allow the pressure to build up in the tube, then valves c, b and a are closed, in that order, and the trap is removed by disconnecting the swagelok fittings between valves a and b.

The pressure in the tube trap is relieved by hanging it vertically, as shown in Figure 2-5 b. Valves b and c are initially closed. A water-saturated filter is connected to the end of valve c and submerged in water. The filter allows the outflow of water only, while trapping the evolved gas. Valve c is slowly opened to relieve pressure. After an equilibration period of 2 to 24 hours, the stainless steel tube is vigorously tapped to allow the gas to accumulate in the nylon tube section. The gas volume is calculated from the length of the trapped gas bubble multiplied by the cross-sectional area of the nylon tube.

The uncertainties of this method have to do with the potential for gas diffusion through the nylon tubing. Approximately 85% of the trapped water is held in the impermeable stainless steel tubing, although gas diffusion could affect the remaining 15% of water contained in the nylon tube. The manufacturer's specifications list the following values of gas permeability through the nylon tubing:

Table 2- 1. Gas permeability through nylon tubing

Gas	Permeability at 25°C {cm^3-mm/(s-cm^2-cm Hg)}x 10^{-10}
CO_2	9.1–20
H_2	19
O_2	2.0–5.4
N_2	0.2–1.1

No data is available for some of the other gases that might be in the water, such as methane. The amount of gas diffusion through the tube will depend upon the gas composition and the difference between the partial pressures of the gases in the tube and in the atmosphere. A sample calculation for worst case conditions assumes that after relieving tube pressure, the trapped gas phase consists of the most permeable gas, either H_2 or CO_2, using the high permeability value, and neglects the partial pressure of these gases in the atmosphere. This would result in a loss of 0.03 cm^3/hr through the nylon tubing, or a total of 0.8 cm^3 loss over 24 hours, which is equivalent to 0.33% v/v gas at STP per volume of water in the tube trap. Previous analyses of gas composition indicate that most of the gas volume is nitrogen. Because the atmosphere contains 79% nitrogen, there would be little driving force for diffusion of nitrogen through the tubing.

TEST SEQUENCE: Phases (1) - (3)

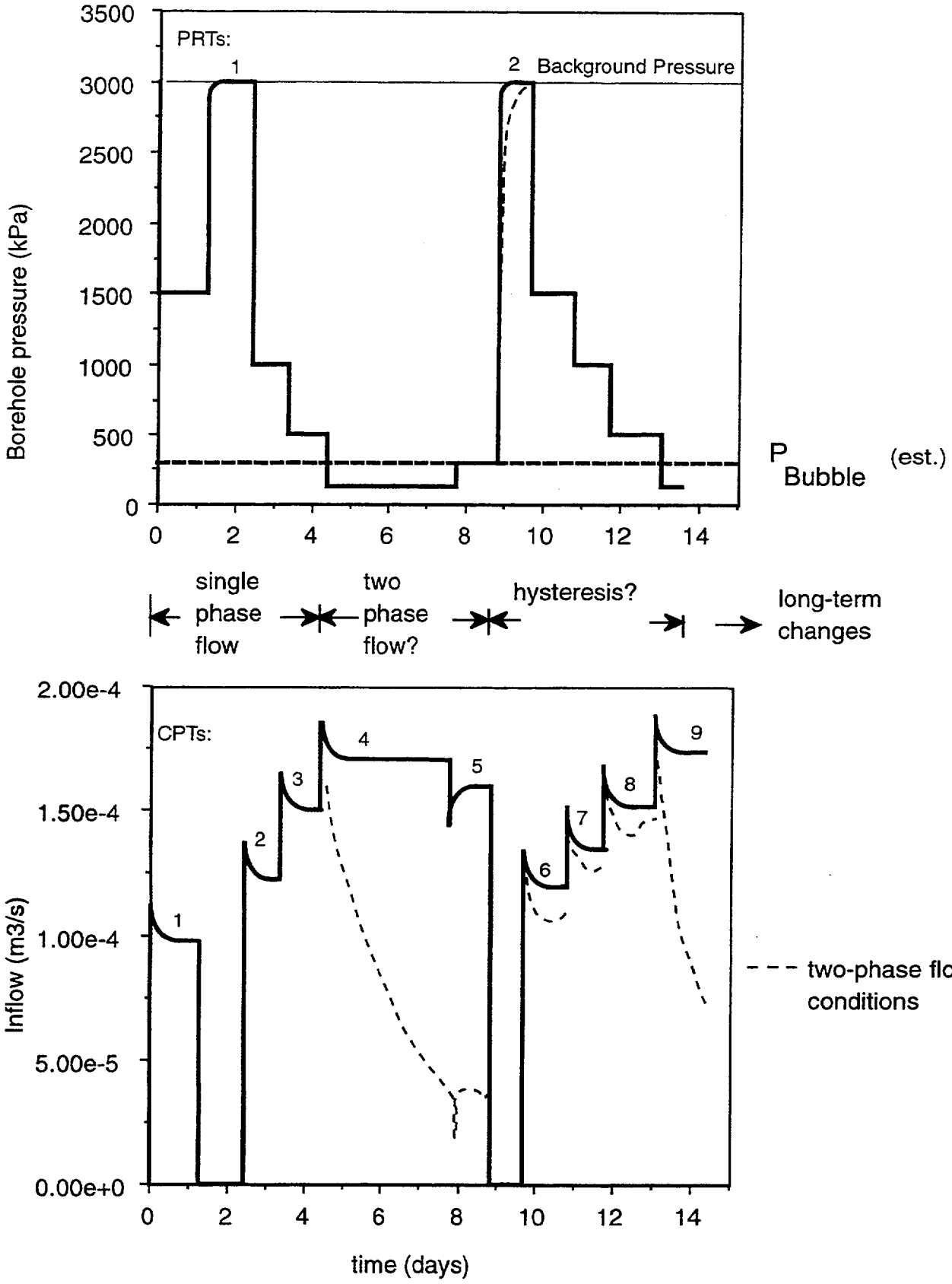

Fig. 2-1

TEST SEQUENCE: Phase (4)

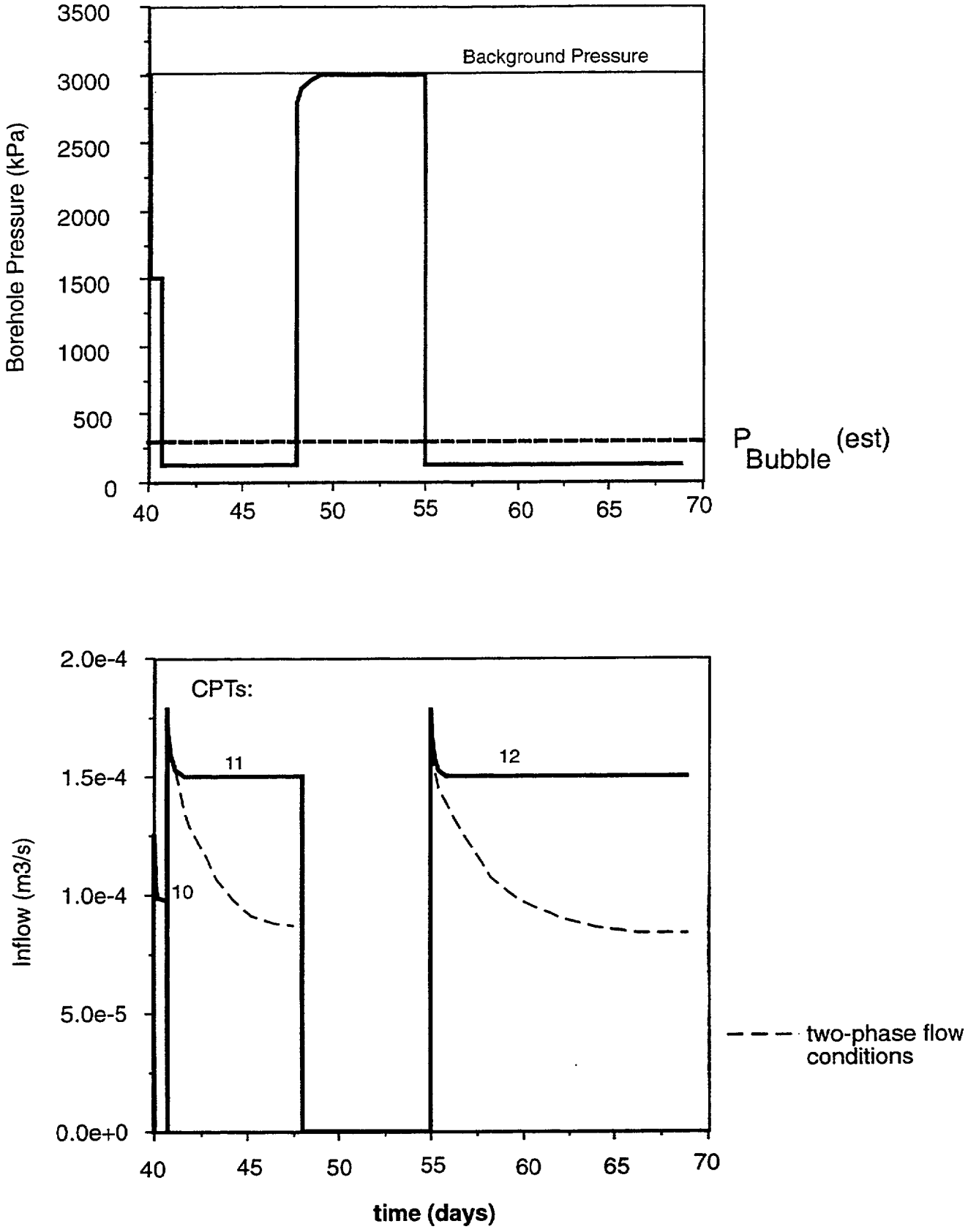

Fig. 2-2

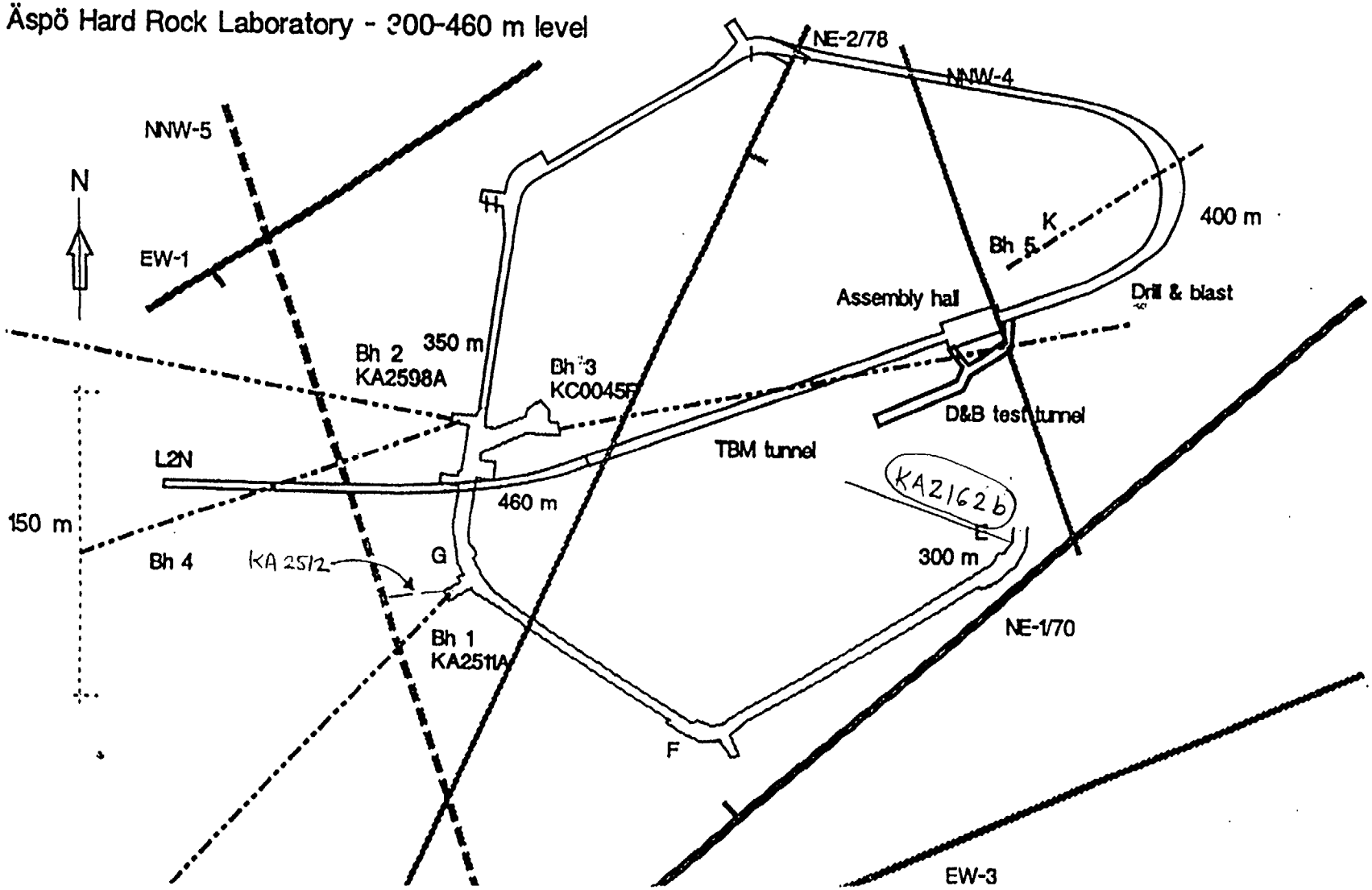
Äspö Hard Rock Laboratory - 300-460 m level
NE-2/78
NNW-4
NNW-5
N
EW-1
400 m
K
Bh 5
Assembly hall
Drill & blast
350 m
Bh 2
KA2598A
Bh 3
KC0045F
D&B test tunnel
TBM tunnel
L2N
460 m
KA2162b
E
150 m
Bh 4
KA 2512
G
300 m
NE-1/70
Bh 1
KA2511A
F
EW-3

Fig(-3

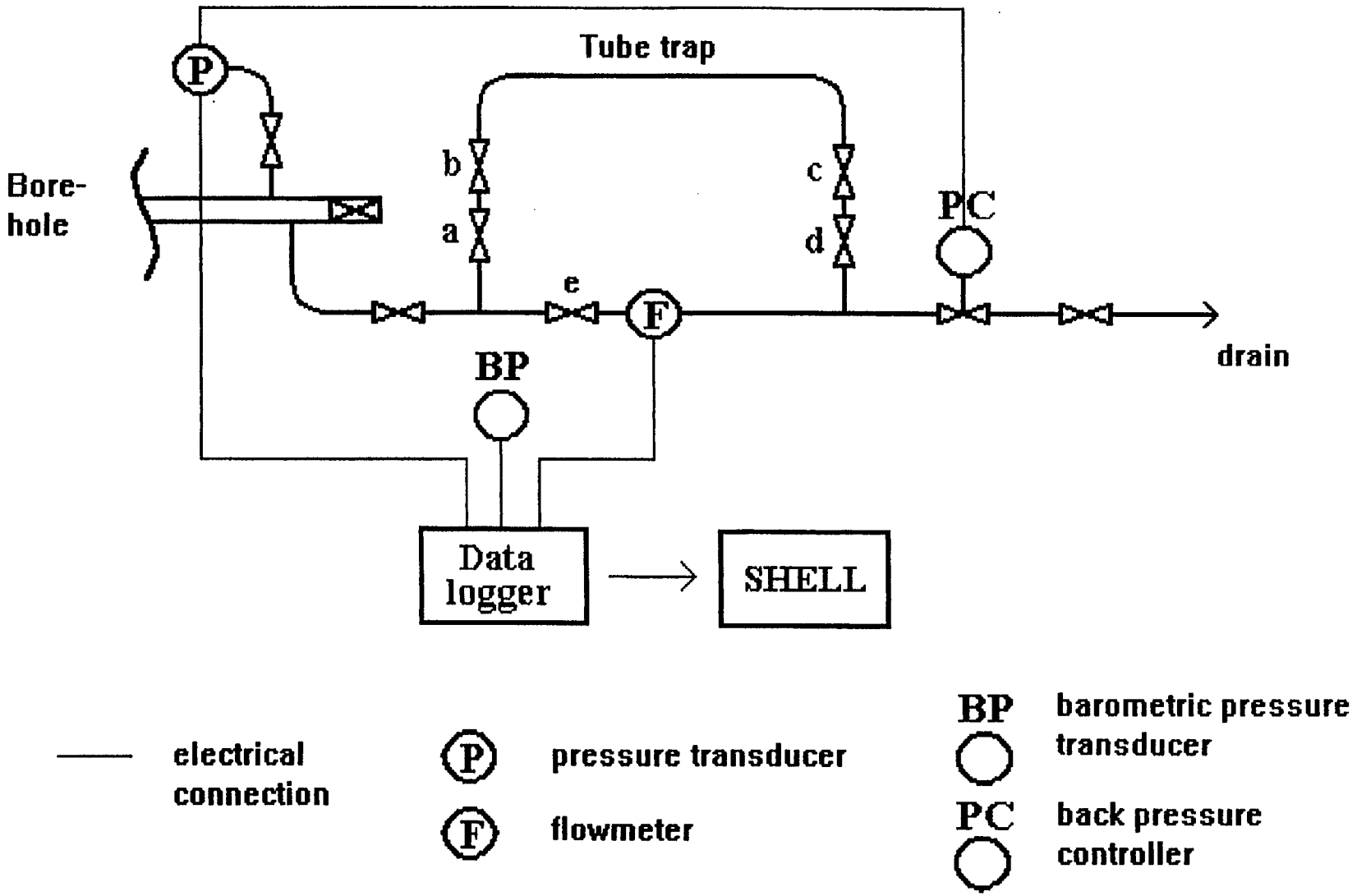
Tube trap
P
Bore-
hole
b
a
c
d
PC
e
F
drain
BP
Data
logger
SHELL
electrical
connection
P
pressure transducer
F
flowmeter
BP
barometric pressure
transducer
PC
back pressure
controller

Fig. 2-4

Glass Accumulator for Measurement of Volumetric Gas Contents

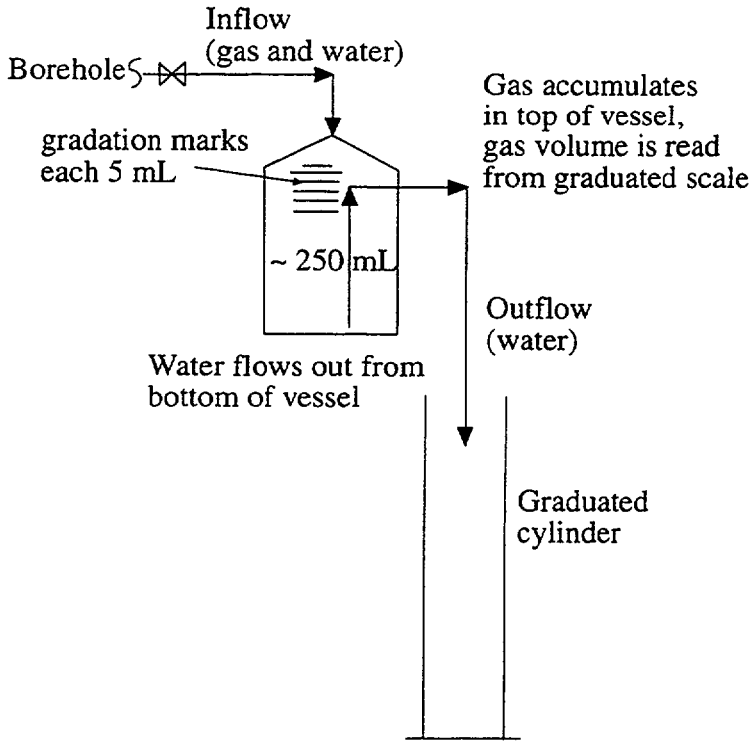

Fig. 2-5

Tube Trap for Measurement of Volumetric Gas Contents

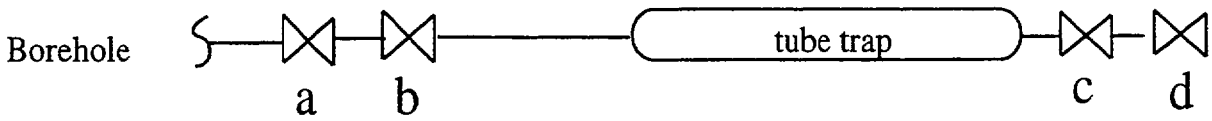

Tube trap installation

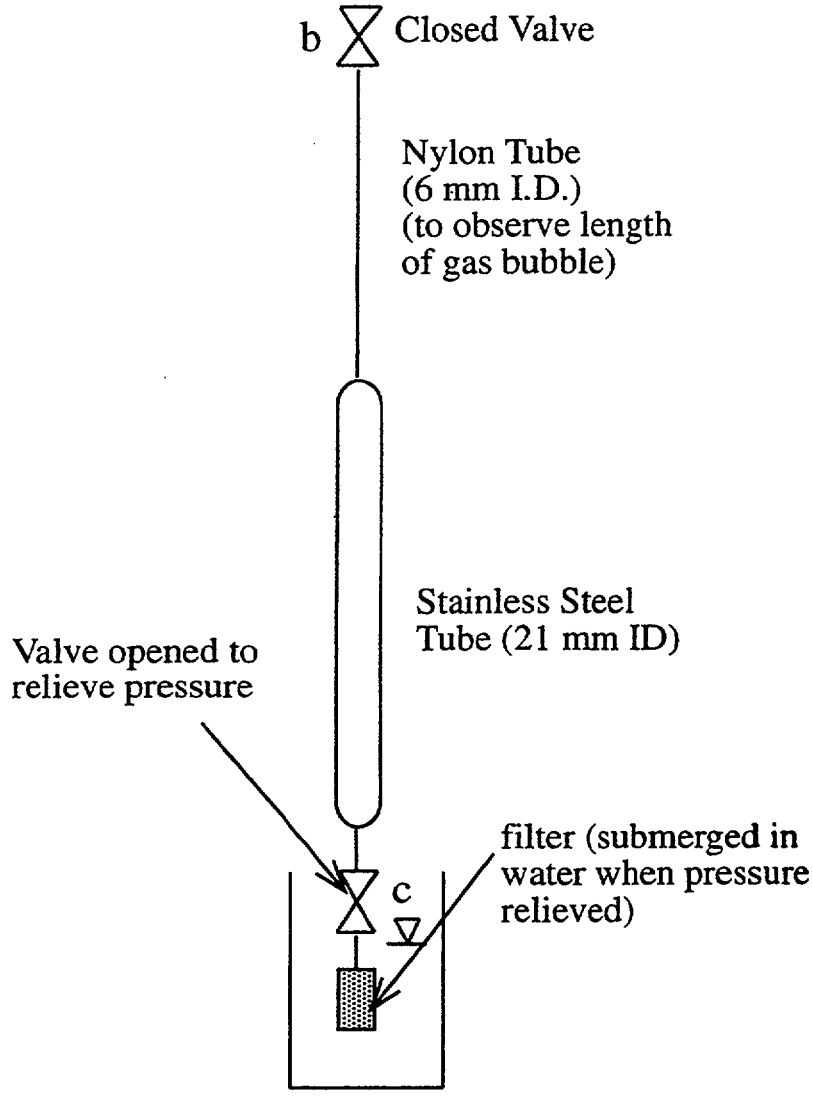

Orientation to relieve pressure and measure evolved gas

Fig. 2-6

3. RESULTS

3.1 TEST DATA AND AMBIENT CONDITIONS

3.1.1 Measurements in KA2512A

The measured flowrates as a function of time for CPT 1 throughout CPT 12 are shown in Figures 3-1 to 3-6. CPTs 1-9 correspond to phases (1)-(3) of the pilot hole test sequence; CPTs 1-3 are conducted above the bubble pressure (Figure 3-1), CPTs 4 and 5 correspond to the conditions below the bubble pressure (Figure 3-2) and CPTs 6-9 are repeat tests (Figures 3-3 and 3-4). CPTs 10-12 (Figures 3-4 and 3-5) correspond to phase (4) of the pilot hole test sequence. CPTs 10 through 12 were conducted in January 1995, after the well had been shut-in for 25 days. Two pressure recovery tests were performed (Figure 3-7): PRT 1 followed a constant pressure test of 1500 kPa (abs) and PRT 2 followed a constant pressure test of 300 kPa (abs).

Flowrates responded quickly to changes in borehole pressure; however, significant fluctuations in the flowrate occurred, as seen in CPTs 3 and 4 (Figures 3-1 and 3-2). Flowrates over the first 400 minutes of CPT 3 and over the first 500 minutes of CPT 4 have a "sawtooth" pattern, consisting of a series of sloping declines and step increases. The behavior also occurred in the first hour of CPTs 1 and 2, although it is not discernible in the scale of the plots. Such fluctuations did not occur in CPTs 6 through 8.

Some step changes in flowrates coincide with blasts at tunnel length 3370-3505 m (see section 3.1.2). The direction of change appears to be random. The times of the blasts are indicated with vertical arrows in the plots of the flowrates versus time (Figures 3-1 to 3-4). Blasting activities in the tunnel also affected the flowrates of repeat tests CPT 7 and 8, although to a lesser extent. There were no blasts during CPT 1, 2, 5 and 6. The cause of the step-increase in flowrate during CPT 8 at t = 1420 minutes is unknown. No corresponding changes were observed in KA2511A. In CPT 3 a flowrate decline proceeds a blast, at t = 1160 minutes by approximately 40 minutes. Similarly, a flow rate decline proceeds the blast at t =600 minutes by 80 minutes in CPT 4. These time intervals are longer than possible discrepancies between the data-logger clock and the blasting records. Flowrates during CPT 11 (Figure 3-5) are quite constant with the exception of blast-correlated step changes. However, the first 27 hours of data were lost. During CPT 12, the frequency of blasting was two to three times a day, which was much higher than in the other tests. Not all of the flowrate

fluctuations in CPT 12 coincide with blasts and not all the blasts caused a response in flowrate. Figure 3-6 shows the borehole pressures during CPTs 11 and 12. Borehole pressures during CPT 11 are slightly less than 120 kPa (abs), while during CPT 12 they are slightly higher than 120 kPa (abs). Disregarding the effect of the blasts on the CPT-curves and the initial perturbations seen in CPT 3 and 4, flowrates seem to stabilize within the first hour of the test. Beyond this time, flowrates decline very slowly.

The data for the pressure recovery tests are shown in Figure 3-7. Pressures went up to 99% of the background pressure within the first few seconds of the test, and then it took about 8 hours to reach the full background pressure. Subsequent changes in pressure trends appear to be in response to changing far-field conditions. In the second half of PRT 1, pressures leveled off and then declined slightly. In PRT 2, pressures did not level off as they did in PRT 1, probably due to the increase in background pressure observed in other boreholes (see section 3.1.2).

3.1.2 Response in monitoring wells

Pressures in borehole KA2511A (location shown in Figures 3-8 and 3-9) responded to the tests in borehole KA2512A, indicating hydraulic communication between the two boreholes. KA2511A is divided into four sections with packers separating each section. Figure 3-12 shows the pressures in KA2511A, sections 1-4, at the time of the hydraulic testing of KA2512A. The linear distance along the borehole from the drift wall for each section are as follows: section 4 extends 6 to 30 m, section 3 extends 31 to 80 m, section 2 extends 81 to 170 m and section 1 extends 171 to 293 m. Pressure changes in sections 1-4 correlate well with the start times of the hydraulic tests (indicated with horizontal arrows in Figure 3-12). Section 4 of KA2511A (i.e., the section next to the tunnel) is spatially closer to KA2512A as compared with section 1, due to differences in dip of the two boreholes. The pressures in section 4 (squares in Figure 3-12) also show a bigger response to the test sequence compared to section 1 (circles in Figure 3-12). The incremental increase in pressure in each section reflects the regional water table drawdown caused by the presence of the drift.

A trend of pressure increase occurs in KA2511A in addition to the response to the testing in KA2512A. Pressures in KA2511A, section 4, increase by almost 65 kPa over the seven days between the end of PRT 1 and the end of PRT 2. This is in agreement with the observed difference of 62 kPa between the pressures in KA2512A measured at the end PRT 1 and PRT 2. Figure 3-12 shows that this pressure increase begins at the end of CPT 3 and continues while the pressure in KA2512A is constant at 120 kPa during CPT 4. The times of blasts at tunnel length 3370-3505 m (Appendix II) are

indicated with vertical arrows in Figure 3-12 and coincide with step increases in background pressure.

The pressure record of KA2162B (see Figure 3-8 and 3-9 for the locations of boreholes), is shown in Figure 3-13. There is no obvious influence of the hydraulic tests in KA2512A on the pressures in KA2162B, but the step increases in pressures that were observed in KA2511A, starting at the end of CPT 3 (12/05/94, 5 p.m.), is also very pronounced in the first section (circles in Figure 3-13) of KA2162B. In sections 2 (+) and 3 (x) the pressure increase is less pronounced but still visible, and in section 4 (squares) there is practically no pressure increase.

In KA1754A (Figure 3-14), the general pressure increase starting at about 5 p.m. 12/05/94 coincides with increases in KA2511A and KA2562B. Although these boreholes show similar responses, pressure records from other boreholes show that this is not a general behavior. For instance, in KA2555A (no figure shown) a pressure increase can be observed during this period, but the changes in pressure with time are different. Furthermore, there was precipitation during this period of time which also could affect pressures in these boreholes. Nevertheless, there are some indications that the blasts at the end of CPT 3 and throughout CPT 4 affected the fracture system, changing the pressure conditions in several boreholes at various depths.

3.1.3 Blasting activities

Blasting occurred at the 430 to 450 m level of the laboratory during the course of the experiment. A record of the times and locations of the blasts appear in Tables II-1 and II-2 of Appendix II. The times of blasts are also indicated in the plots of the CPTs in section 3.1.

An accelerometer was installed in the KA2512A niche to get a measure of stress changes resulting from the blasts. The results are summarized in Table 3-1. Each blast contained about 175-180 kg of explosives, but only 5 to 6 kg are detonated at the same time. The distance to the blast is 145 m. The results indicate a dominating frequency of about 300 Hz.

A rough estimate of the stress change due to the blasts can be obtained from the measurements in Table 3-1 where

stress = elastic modulus x ground velocity / wave velocity. (3-1)

A compressional wave velocity of 6 km s^{-1} gives a dilatational stress of about 30 kPa. Uncertainties in the type of stress would change this estimate by no more than a factor of 2. Only the first of the blasts for which ground motion measurement was made occurred during a CPT (CPT 11). The other two measurements were made during the time KA2512A was shut-in. The blasts in January were shot further down the tunnel than the blasts in December and the first blast in Table 3-1 did not cause a measurable flowrate change during CPT 11. Other blasts did occur during CPT 11 and CPT 12 which caused step changes in flowrates, although not all blasts resulted in a response. Without ground motion measurements that coincide with the December blasts, or with a significant flowrate change during the measurements of ground motion, it is difficult to arrive at any conclusions regarding the effect of the blasts. However, the observed pressure and flow response to the blasts suggest that the blasts changed conditions in the formation, including perhaps far-field boundary conditions, effective stresses, or deformation of softer fracture-lining materials. The blasts may open or close hydraulic connections to different parts of the system which could change both boundary conditions and water chemistry.

Table 3-1. Vibration monitoring of rounds at level 450m (UVS 1201 Vibration Monitor, Nitro Consult UVS standard geophone vertical orientation)

Date	Time	Velocity (mm/s)	Acceleration (g)	Displacement (microns)
01/17/95	09:59	2.6	0.55	2
01/17/95	19:47	3.9	0.78	2
01/18/95	10:45	2.8	0.61	1

3.1.4 Precipitation, barometric pressure and temperature

The water level in one of the vertical percussion boreholes located on the Äspö island (HAS13:2) rose 6.8 meters (Figure 3-15) between 5pm 12/05/94 and 12/07/94, i.e., the same time period as the observed pressure increase in boreholes KA2511A, KA2562B and KA1754A. It has previously been observed that rain may cause a large and rapid increase of the water level in this borehole (Nyberg et al., 1994). Typically, the water levels in HAS13:2 fluctuated between 0.5 and 10 meters below the surface level during the Autumn of 1994. If the fracture intersecting KA2512A is connected to a larger fracture network, this could explain the correlation

between pressure changes in KA2512A with pressure changes in more distant boreholes, and even surface boreholes.

Precipitation appears to have caused the observed increase in background pressures. Figure 3-16 shows precipitation data for the time period 12/01/94 to 12/15/94, obtained from the SMHI weather stations located in Västervik (light bars) and northern-most Öland (dark bars). The precipitation events during this period begin just before the water level increase in HA213 and in background pressures in boreholes described above.

The measured barometric pressure in the tunnel at KA2512A (Figure 3-17) was also lower during the period when precipitation occurred. During the first 5 days of the test sequence, the pressure continuously decreased from 106.5 kPa to 103 kPa, and thereafter the pressure fluctuated between a lowest value of 102 kPa and a highest value of 104 kPa. The discontinuities of the curve for $6000 < t < 8000$ and $t = 13500$ can be explained by the switching of data loggers at these times.

The temperature of the air in the ventilation shaft at the 70 m tunnel length is shown in Figure 3-18 and varied between +5°C and +12°C during the time of the test sequence.

3.1.5 Gas contents

Gas content measurements using the methods described in Section 2.3.3 are summarized in Tables 3-2 through 3-4. The values for evolved gas on-site at P_{atm} represent the volume of gas evolving from a sample when the liquid pressure is reduced from the line pressure to atmospheric. The values measured at vacuum represent the total gas contents of the water which includes dissolved gases at atmospheric pressure. Previous measurements of total gas contents by Arvidsson (1994) and Lif (1993) are listed in the tables for comparison. Evolved gas contents in KA2512A (Table 3-2) range from 0.1 to 0.5%, while values in the other boreholes (Table 3-3) range from 1 to 3%. In KA2512A, evolved gas contents were sampled at different borehole pressures. Gas contents are generally greater at the higher borehole pressures, with the exception of the low gas contents measured at 1000 kPa during CPT 7. During CPT 10, which was conducted after the borehole was shut-in for 25 days, an evolved gas content of 1.2% was measured. The total gas content of KA2512A water reported in Table 3-2 is 3.9%. The gas composition analysis in Table 3-4 shows that the gas consists mainly of nitrogen. Assuming that the evolved gas at atmospheric pressure is mostly nitrogen, the evolved gas contents should be approximately equal to the difference between the total gas contents and the

aqueous solubility of nitrogen (approximately 1.9% v/v @ STP in 10°C distilled water at atmospheric pressure).

One hypothesis for the increase in evolved gas content in KA2512A in CPT 10 is that dissolved gas concentrations may be higher in the water near the borehole, compared to water farther into the formation. Measurements during CPT 4 in KA2512A were made after eight days of constant pressure flow tests, so one may assume that formation water originating at some distance from the borehole was sampled. The CPT 10 measurement, however, was made 3 hours after CPT 10 had begun; previous to CPT 10, the well had been shut-in for 25 days. The other boreholes were only opened for sampling, and although they were flushed beforehand, the water sampled must have been from the near-borehole region.

Table 3-3 summarizes gas content measurements in other boreholes. KA2598A, which was used as a supply of drilling water for KA2512A, was sampled at the end of a line near KA2512A. All the other boreholes were sampled at the cover of the casing. Higher gas contents were obtained in the tube sampler compared to the glass accumulator in KA2512A and in KA2598A, but this was not observed in KA3010A. The highest evolved gas content was measured in KA3067A. Pressure and flow oscillations during the drilling of KA3067A, which was drilled at a small over-pressure, but lower than in KA2512A, suggested the presence of a significant amount of gas. The difference between the total gas contents and the evolved gas contents is on the order of the aqueous solubility of nitrogen at atmospheric pressure for the higher values obtained in on-site evolved gas measurements.

Equilibration times for reading gas contents in the tube trap varied from 2 to 24 hours. If gas was lost through the nylon tubing, one would expect much lower gas contents for longer equilibration times and significantly lower gas contents compared to the gas accumulator. In KA2511A, longer equilibration times were used, and gas contents were comparable between the two methods. In KA2598A, gas contents measured with the tube trap with a 2-hour equilibration time were twice as high as measured in the accumulator. This was also true in KA3010A. It appears that some gas was lost through the tubing during the longer equilibration times; however, the calculation in Section 2.3.3 indicates that the loss would not be more than 0.33% of the total gas contents. Given the uncertainties in the sampling method, there may be some error in the absolute values of the gas contents reported here. Nonetheless, conclusions can be made regarding the relative values of the measurements.

The variability in gas contents raises interesting questions regarding the origin of the gas, why gas contents in KA2512A would be lower than in the other boreholes and why they differ from earlier measurements in

KA2511A, which is hydraulically connected to KA2512A. Gas composition analysis of sampled waters shown in Table 3-4, as well as in surface boreholes show that over 70% of the gas is nitrogen, with the next largest components being CO_2, CH_4 and He. Because the deep groundwater is anaerobic, the presence of O_2 indicates contamination during sampling. The nitrogen-argon ratios indicate that the gases are of atmospheric origin. This is consistent with the noble gas data for samples from KA2512A and KA3010A (Kennedy, 1995). The noble gas analysis indicated that these samples contained an excess of ^4He, where $^4He/^{36}Ar$ ratios are approximately 1000 times the ratio in air, or 5000 times the ratio in air-saturated water. The ^3He /^4He ratio is approximately $7 \cdot 10^{-8}$ indicating that the excess He is radiogenic, i.e. derived from the decay of U and Th.

The boreholes sampled were drilled with different methods, which may impact the near-borehole, biologically-produced gas. KA2598A and KA2511A were drilled with standard techniques. To minimize contamination in the SELECT boreholes, the drilling equipment was washed before use.

Pedersen (1995) has detected the presence of sulfate and sulfur-reducing bacteria as well as methane producing bacteria in groundwater extracted from the SELECT boreholes. They hypothesize that the these bacteria are indigenous and that their metabolic activity was increased following drilling. However, elevated CH_4 and CO_2 concentrations in the borehole region due to biological activity were not observed in KA3010A. In addition, the calculated bubble pressures of CO_2 and CH_4 in water sampled from KA2512A and KA3010A (Table 3-5) are well below atmospheric pressure. Consequently these gases are not likely to evolve at atmospheric pressures if they are present in the amounts reported in Tables 3-2 through 3-4. Therefore, another mechanism may be responsible for the differences in measured gas contents between wells that are in hydraulic communication, such as KA2511A and KA2512A, as well as for the observations of temporal variability.

Table 3-2. Summary of volumetric gas contents measured in KA2512A

When sampled	P_{bore} (kPa)	Gas Contents (%v/v @ STP) Evolved gas on-site (P_{atm})	Total Gas Contents (Meas. @ vacuum)	Source/ Method
CPT 4	120	0.07	--	glass accum (220 mL/min)
CPT 6	1500	0.46	--	tube trap (equilib 25 hrs)
		0.23	--	glass accum (120 mL/min)
CPT 7	1000	0.06	--	tube trap (equilib 22 hrs)
CPT 8	500	0.07		glass accum (200 mL/min)
CPT 10*	1500	1.19	--	tube trap (equilib 10 hrs)
after end of	3000	--	3.9	Evans, USGS (composition in
CPT 12**				Table 3-4)

* after borehole shut-in for 25 days
** sampled 2/16/95, after borehole shut-in for 7 days

Table 3-3. Summary of volumetric gas content measurements

Borehole	Date sampled	Gas contents (%v/v@STP) Evolved gas on-site (P_{atm})	Total gas contents meas. @ vacuum	Source/Method
KA2511A	3-23-94	--	3.2	Arvidsson (1994)
KA2511A.1	2-95	--	4.3	Evans, USGS
KA2598A	12-07-93	--	3.8	Lif (1993)
	3-23-94	--	4.0	Arvidsson (1994)
	12-07-94	0.93	--	glass accum (50 mL/min)*
	12-13-94	1.18	--	glass accum (142 mL/min)
	12-14-94	2.19	--	tube trap (equilib 2.3 hrs)**
KA3010A	12-14-94	1.58	--	glass accum (68 mL/min)
	12-14-94	1.72	--	glass accum (127 mL/min)
	12-14-94	1.06	--	tube trap (equilib 12 hrs)
	1/09/95	1.06	--	tube trap (equilib 2.3 hrs)
	2-95	--	4.0	Evans, USGS
KA3067A	12-14-94	2.82	--	glass accum (98 mL/min)
KA3067A.2	5-95	2.5	--	tube trap & glass accum

* flowrate during measurement
** time period of sample equilibration with atmospheric pressure

Table 3-4. Composition of gas contents

Borehole	Date sampled	Gas composition (% fraction) N_2	O_2	Ar	He	CO_2	CH_4	Source
KA2512A	2-16-95	69.1	0.05	1.6	n.r.	14.2	15.1	Evans, USGS
*								
KA2511A	3-23-94	69.2	3.8	n.r.	0.08	17.5	9.5	Arvidsson (1994)
KA2511A.1	2-16-95	65.3	0.07	1.4	n.r.	21.9	11.3	Evans, USGS
KA2598A	12-07-93	79.6	2.0	n.r.	4.7	13.4	0.3	Lif (1993)
	3-23-94	97.8	1.4	n.r.	0.3	0.4	0.2	Arvidsson (1994)
KA3010A*	2-16-95	87.9	0.04	1.9	n.r.	6.8	3.4	Evans, USGS
Henry's Law Constant (kPa/mole-fraction)		6.8E6	3.3E6	2.3E6	1.3E7	1.0E5	3.0E6	

n.r. = not reported
* Noble gas analysis conducted by Mack Kennedy, LBNL

Table 3-5. Calculation of bubble pressure for dissolved gases in sampled water

Borehole	Date Sampled	Bubble Pressure* (kPa abs) N_2	Ar	CO_2	CH_4
KA2512A	2-16-95	175	1	0.5	14
KA3010A	2-16-95	229	2	0.3	3

*Bubble pressure = Henry's law constant x mole fraction of dissolved gas

3.2 DATA ANALYSIS

3.2.1 Steady-state data (flowrates as a function of borehole pressure)

The final steady-state flowrates as a function of borehole pressure for CPT 1 through CPT 12 are plotted in Figure 3-10, indicated by filled circles. The number next to each data point refers to the CPT and an asterisk indicates that blasting occurred during that CPT. Flowrate fluctuations are indicated by maximum and minimum values for the specific CPT. The data for CPT 1 through CPT 9 are linear over the entire range of borehole pressures. There is a slight shift in the points of phase 3 (CPT 6 through CPT 9) compared to the points of phase 1 and 2 (CPT 1 through CPT 5), which may be related to the change in background pressure (see Section 3.1.2); however, the change in slope is insignificant. The trend indicated by phase 4, (CPT 10 through CPT 12 which began after the well was shut in for 25 days) is unclear. The steady-state flowrate for CPT 11 is 30% lower than in phases 1 through 3; however, the value for CPT 12 approaches the trend exhibited by

the previous phases. Most of the significant flow fluctuations occurred at the times of blasting (see CPT data in section 3.1.1) and the magnitude of the fluctuations is greater at the lower borehole pressures.

Several processes may induce changes in transmissivity at low borehole pressures in addition to groundwater degassing; however, effects of these processes were not observed in the results of CPT 1 through CPT 9. The groundwater has been reported to be super-saturated with respect to calcite. Calcite precipitation can occur quickly upon depressurization, with a subsequently slow dissolution upon pressure increase. Precipitation of calcite could block flow paths and decrease transmissivity at the lower borehole pressures. The actual degree of supersaturation in KA2512A will be computed when the water chemistry data is available; however, the fact that the flowrates increased from CPT 11 to CPT 12 is inconsistent with the occurrence of calcite precipitation. The increase of effective stress as a result of decreasing borehole pressure did not appear to affect transmissivity, although the flow fluctuations observed in the first part of the tests in phases 1 and 2 discussed in the previous section may indeed be related to effective stress changes. Effects of turbulence causing flow reductions at the higher flowrates were also not observed.

In Figure 3-11, the steady-state flowrates for test phases 1, 2 and 3 are plotted as a function of borehole pressure and transmissivity is determined from the slope of the data, using the following equation for steady-state radial flow conditions:

$$Q = -\frac{2\pi T}{\rho g}\ln\left(\frac{r}{R_w}\right)\left[P_{borehole} - P(r)\right] \tag{3-2}$$

where Q is the inflow rate to the borehole, ρ is the density of water, g is the acceleration of gravity, r is radial distance away from the center of the borehole, R_w is the radius of the borehole and $P(r)$ is the formation pressure distance r away from the borehole. Transmissivity is then equal to

$$T = m\left[\frac{\mathrm{m^3/s}}{\mathrm{kPa}}\right]\ln(R_w / r)\frac{\rho g}{2\pi}\left[\frac{\mathrm{Pa}}{\mathrm{m}}\right]\mathrm{x}10^{-3}\left[\frac{\mathrm{kPa}}{\mathrm{Pa}}\right] \tag{3-3}$$

where m is the slope computed from the regression, listed in Table 3-2. The x intercepts at zero flow, shown in Figure 3-11, represent the background pressure at the end of the test phase and are included in the regression. A separate regression was done for CPT 1 through CPT 5 and for CPT 6 through CPT 9. Table 3-6 lists the regression results and the

computed transmissivity for r=250 m. The computation is relatively insensitive to the value of r, which was selected based upon distances to wells that responded to testing in KA2512A.

Table 3-6. Linear regression results for CPT 1 through CPT 9 and transmissivity for steady-state radial flow.

	CPT 1 through 5	CPT 6 through 9
slope ($\Delta Q/\Delta P_b$) ($m^3\ s^{-1}\ kPa^{-1}$)	-5.8×10^{-8}	-6.3×10^{-8}
Y intercept ($m^3\ s^{-1}$)	1.8×10^{-4}	$2. \times 10^{-4}$
r^2	0.994	0.987
Predicted background pressure (kPa)	3066	3166
T ($m^2\ s^{-1}$)	8.02×10^{-7}	8.74×10^{-7}

The r^2 values on the order of 0.99 indicate that the flowrate is indeed linear with borehole pressure over the tested range and the fit with the x intercept at background pressure is good. The difference in transmissivities between the two test phases is insignificant.

3.2.2 Single-well analysis of constant pressure tests (CPTs)

The theory for interpretation of single-well constant rate flow tests (e.g. Theis, 1935; Earlougher, 1977 and Barker, 1988) can be extended to develop diagnostic methods and interpretative equations for analyzing constant-head test data. We will in the following consider the conceptual flow models that have been developed for linear ($n=1$), radial ($n=2$) and spherical ($n=3$) flow geometries. The expressions yielding the flow response for the periods of time at which outer boundary effects do not influence the system, are (Carslaw and Jaeger, 1959; Jacob and Loman, 1952):

$$\frac{\Delta H}{q(t)} = \frac{1}{A}\sqrt{\frac{\pi t}{KS_s}} \qquad \text{for } n=1 \qquad (3\text{-}4)$$

$$\frac{\Delta H}{q(t)} = \frac{1}{4\pi K b}\ln\left(\frac{9}{16}\frac{t}{t_{diff}}\right) \qquad \text{for } n=2 \qquad (3\text{-}5)$$

$$\frac{\Delta H}{q(t)} = \frac{1}{4\pi K r_w\left(1+\sqrt{\frac{4}{\pi}\cdot\frac{t_{diff}}{t}}\right)} \qquad \text{for } n=3 \qquad (3\text{-}6)$$

where the diffusion time t_{diff} [T] is defined as:

$$t_{diff} = \frac{r_w^2 S_s}{4K} \qquad (3\text{-}7)$$

and ΔH is the drawdown head at the well [L], $q(t)$ is the flow response [L^3/T] as a function time, A is the linear well area [L^2] which equals $2bw_a$ where w_a is the aperture width, K is the hydraulic conductivity [L/T], S_s is the specific storage [1/L], t is the time [T], b is the height of the cross-sectional area perpendicular to the flow direction [L] , w_a is the fracture aperture width and r_w is the radius of the borehole [L]. For radial flow geometry, the transmissivity T equals Kb, and the storativity S equals $S_s b$. Equation (3-5) is a long-term approximation of the exact solution. However, for times relevant to the present set of data, this approximation coincided with the exact solution.

Field data is typically matched with the analytical solutions (Equations 3-4 through 3-6), for $\Delta H/q(t)$ in order to determine the flow geometry of the system and estimate the values of K and S_s. In Figures 3-19 to 3-31, flow data from the constant pressure tests (CPTs 1-4 and 6-12) are matched with analytical solutions for radial and spherical flow geometries. CPT 5 was preceded by a CPT at a lower borehole pressure and is therefore excluded from the comparison. The drawdown head ΔH was calculated as $(P_f - P_w)/g\rho$, i.e. the formation (or background) pressure minus the constant pressure maintained in the well (or the borehole pressure). A P_f value of 3010 kPa (abs) was used for CPTs 1-4, and for CPTs 6-11, a P_f value of 3070 kPa (abs) was used. Curve matching was done on an Excel spreadsheet after Doughty (1995), adjusting values of K and S_s until the best match was obtained.

The match of the CPT data to the type curves representing spherical flow geometry is shown in Figures 3-19 to 3-29. Flow perturbations during the first hours of CPTs 1-4 (note the logarithmic time-scale of the plot) makes it hard to match the data with the type curve, despite the fact that for CPT 1 and 2, these perturbations were small enough not to be visible in the plots of flow versus (normal) time (Figure 3-1). These fluctuations might be due to changes in rock stresses (due to the lowering of water pressures) causing plastic deformation of the rock and affecting the hydraulic properties of the fracture, a hypothesis which is supported by the fact these flow fluctuations were greater during CPT 3, when also the borehole pressure was lower in comparison with CPT 2. In addition, these early flow fluctuations cannot be observed at all during the repeat tests (CPT 6 to 10), which fit better to the type curves.

Changes in specific storage shift the type curves in the x-direction, and therefore, the determination of S_s requires a bend in the field data curves in order to get an unique match. Because of the flatness of the field data curves, the match between the type curves and the field data is not very sensitive to S_s, whereas the hydraulic conductivity can be more precisely determined because changes in K shift the curves in the y-direction. However, the first parts of the curves for CPT 6 through 10, corresponding to early time data, are not as flat as for CPT 1 through 4, which result in a better fit of the data to the type curves.

Equations (3-1) to (3-3) were developed under the assumption that the constant pressure period is preceded by a period of no-flow conditions. This was only the case for CPT 1, which was performed after a well shut-in overnight, and CPT 2 and 6, which were preceded by PRTs 1 and 2, respectively. A strict analysis of the other CPTs would require that the flow perturbations induced by previous constant pressure tests be superimposed on the solution for the flow versus time, as in Mishra (1992). However, the data shown in Figures 3-19 to 3-29 suggest that for the present flow conditions, these perturbations do not significantly change the goodness of fit of the field data to the type curves, nor the result of the fit in terms of obtained K and S_s values.

The match of two representative CPTs (number 2 and 6) to the type curves for radial flow geometry is shown in Figures 3-30 and 3-31. The fit is not as good as for the spherical case, suggesting that the flow field around the borehole show more similarities with the spherical geometry rather than the radial. A match between the field data and the $n=2$ curves based upon the first part of the field data curves results in a bad fit for the last part. For $n=1$ (linear flow geometry), no agreement at all can be observed between the $n=1$ curve and the field data.

Table 3-7. Values of K and S_S obtained through matching field data with $n = 2$ and $n = 3$ type curves.

CPT #	n	K * (m/s)	S_s (1/m)	Comments
1	3	$1.2 \cdot 10^{-6}$	(1)	(2)
2	3	$1.1 \cdot 10^{-6}$	(1)	(2)
3	3	$1.1 \cdot 10^{-6}$	(1)	(2)
4	3	$1.0 \cdot 10^{-6}$	(1)	(2)
6	3	$1.4 \cdot 10^{-6}$	$3.0 \cdot 10^{-4}$	(3)
7	3	$1.2 \cdot 10^{-6}$	$3.0 \cdot 10^{-4}$	(3) First data point was not accounted for in fit
8	3	$1.1 \cdot 10^{-6}$	$6.0 \cdot 10^{-5}$	(3) The lower Ss-value is due to differences in the two first data points as compared to CPT 6,7 & 9
9	3	$1.2 \cdot 10^{-6}$	$1.0 \cdot 10^{-4}$	(3) First data point was not accounted for in fit
10	3	$1.05 \cdot 10^{-6}$	$3.0 \cdot 10^{-4}$	(3)
11	3	$0.80 \cdot 10^{-6}$	(1)	Fit not sensitive to S_s due to missing early time data
12	3	$1.0 \cdot 10^{-6}$	(1)	Fit not sensitive to S_s due to missing early time data
2	2	$1.1 \cdot 10^{-6}$	$1.0 \cdot 10^{-7}$	Poor fit
6	2	$0.90 \cdot 10^{-6}$	$1.0 \cdot 10^{-7}$	Poor fit

*Tabulated K-values for $n = 2$ were obtained with $b = 1$ m, and are thus identical to corresponding T-values.

Notes for Table 3-7:
(1) indeterminate
(2) Early time flow fluctuations impeded analysis of S_s
(3) Fair fit, but S_s determined from very early time data

The K and S_s values derived from the type curve fits are tabulated in Table 3-7. The K values do not show any significant changes for CPTs at different borehole pressures. The mean value and standard deviation of the K values obtained in CPTs 1 - 9 for n=3 was $1.15 \cdot 10^{-6} \pm 0.12 \cdot 10^{-6}$ m/s. The K values for CPTs 10 and 12 are within about one standard deviation of the mean hydraulic conductivity measured for CPTs 1 through 9. In CPT 11, K

is three standard deviations, or about 30%, lower than the mean. This decrease in K might be due to degassing but could also be due to other changes in the system during the period in which the well was shut in between CPT 9 and CPT 10.

3.2.3 Cross-well analysis of constant pressure tests (CPTs)

The pressure responses to the CPTs as a function of time in the four packed-off sections of the monitoring well KA2511A were matched to the following analytical expressions (Carslaw and Jaeger, 1959):

$$\frac{\Delta h(t, r_{tw})}{\Delta h_0} = \text{erfc}\sqrt{\frac{r_{tw}^2 S}{4Kt}} \qquad \text{for n=1} \qquad (3\text{-}8)$$

$$\frac{\Delta h(t, r_{tw})}{\Delta h_0} = \frac{r_{ed}}{r_{tw}}\text{erfc}\sqrt{\frac{r_{tw}^2 S}{4Kt}} \qquad \text{for n=3} \qquad (3\text{-}9)$$

where $\Delta h(t,r_{tw})$ is the drawdown head in the monitoring well, Δh_0 is the constant drawdown head held in the test hole, r_{ed} is an effective radius within which the drawdown equals Δh_0, r_{tw} is the distance between the monitoring well and the test hole and the rest of the parameters are as in Equations (3-4) through (3-6). No simple analytical expression exists for the n=2 case.

The match of CPT field data to single-well CPT type curves was found to be relatively insensitive to S_s (Section 3.2.2). However, the analysis provided unambiguous results for K. Since Equations (3-8) and (3-9) contain the ratio of these two parameters, K was fixed to $1.2 \cdot 10^{-6}$ m/s, which is the mean value of K for CPTs 1-9 (see Table 3-7), while S_s was allowed to vary during the curve-fitting procedure. The second unknown parameter r_{ed}, which by definition is equal to or greater than the test hole radius, is also determined through the curve-fitting procedure. The distance r_{tw} was set equal to the distance between the end of borehole KA2512A (where the borehole intersects the water bearing fracture) and the center of the four packed-off sections in borehole KA2511A.

Table 3-8. Values of r_{ed} and S_S obtained through matching KA2511A pressure response data to Equation (3-9).

CPT#	KA2511A section#	r_{tw} (m)	Background pressure (kPa)	r_{ed} (m)	S_s (1/m)
1	1	242	3123	1.2	$1.0 \cdot 10^{-7}$
1	2	122	3086	0.7	$1.5 \cdot 10^{-7}$
1	3	47	3043	0.38	$1.1 \cdot 10^{-6}$
1	4	29	3016	0.36	$1.1 \cdot 10^{-6}$
6	1	242	3154	1.3	$2.0 \cdot 10^{-7}$
6	2	122	3123	0.75	$3.5 \cdot 10^{-7}$
6	3	47	3091	0.38	$1.1 \cdot 10^{-6}$
6	4	29	3072	0.36	$1.1 \cdot 10^{-6}$

The n=3 fits (Table 3-8) produce S_s values of 10^{-7} to 10^{-6} 1/m with negligible changes between CPT 1 and 6. This is considerably lower than the values of 10^{-4} 1/m, resulting from the single-well analysis of the CPTs (section 3.2.2). However, two facts made the S_S determination in the single-well analysis uncertain, namely that the field data curves in general were flat and horizontal, which resulted in non-unique fits, and that the bent curves only had their characteristic shape for very early time data, which might cause the fit to reflect the specific storage of the borehole region rather than the specific storage of the fracture. The comparison of results strongly suggests that the storativity of the region around KA2512A cannot be estimated on the basis of single-well tests alone.

Provided that K was properly quantified in section 3.2.2, the above mentioned problems with the determination of S_s are eliminated by the cross-well analysis. Changes in the specific storage shift the inclined part of the type curves, which correspond to the pressure response breakthrough, in the x-direction (see Figures 3-32 to 3-35). This enables a unique match with corresponding parts of the field data curves. Although the unknown value of r_{ed} also affects the match between the type-curve and the field data, it can be seen from Equation (3-9) that different values of r_{ed} only affect the magnitude of the pressure response (or drawdown) and not the breakthrough time. Thus, r_{ed} is determined separately by fitting the type curves to the maximum drawdown observed in the field. Table 3-8 shows that, for both CPT 1 and CPT 6, the specific storage values vary somewhat for the different sections of KA2511A.

Errors in the S_s estimates of Table 3-8 are likely to stem from the simplifying assumption of spherical flow geometry. The magnitude of pressure response in a spherical flow field is proportional to r_{ed}/r_{tw}

(Equation 3-9) which accounts for the attenuation of the response with distance from the source due to geometric spreading. The decrease in fitted r_{ed} values with decreasing distance from the test well (Table 3-8) suggests that the actual attenuation in pressure response due to geometric spreading is less than predicted for spherical geometry. On the other hand, Equation (3-8) shows that $\Delta h/\Delta h_0$ approaches unity after the pressure response breakthrough due to the absence of geometric spreading for the linear flow case. Figures (3-32) to (3-35) exhibit a decrease in $\Delta h/\Delta h_0$ after breakthrough with increasing distance from the test hole indicating that geometric spreading occurs and that the field flow geometry lies between the two above-mentioned extremes.

Some uncertainty in the r_{ed} and S_s estimates is associated with uncertainties in values of the distance r_{tw}. For instance, if the distance between KA2512A and section 4 of KA2511A in reality were two times the distance given in Table 3-8, the S_s value corresponding to the best fit would be $2 \cdot 10^{-7}$ 1/m, i.e. 18% of the value given in Table 3-8. Changes in the boundary conditions can also be a source of errors. Specifically, the last parts of CPTs 1 and 6 were disregarded because changes in the background pressure caused the section pressures to decrease somewhat in the last parts of the tests for both CPTs 1 and 6. However, the agreement between S_s values obtained from analysis of these CPTs indicate that the changing boundary conditions did not affect the overall results of the analysis.

Relatively few values have previously been reported for crystalline rock, but the magnitude of S_s values of 10^{-7} to 10^{-6} 1/m is in agreement with the results of Almén et al. (1986), who reported S_s values in the range of 10^{-10} to 10^{-6} 1/m for bulk, crystalline rock in single-well tests and values ranging from 10^{-6} to 10^{-4} 1/m for fracture zones in cross-well tests.

3.2.4 Single-well analysis of pressure recovery tests (PRTs)

Applying the method of Horner (1951), the pressure head as a function of time when the well is shut in after a time period t_1 of constant flow, can be derived by superimposing the effects of a well flowing at a rate q for time $(t_1 + t)$ and a well flowing at rate $-q$ for time t, where t is the time from the well shut-in. The long-term solution for radial flow and the general solution for spherical flow yield:

$$\frac{\Delta h(t)}{q} = \frac{1}{4\pi Kb}\ln\left(\frac{t_1+t}{t}\right) \qquad \text{for } n=2 \qquad (3\text{-}10)$$

$$\frac{\Delta h(t)}{q} = \frac{1}{4\pi Kr_w}\left(\text{erfc}\left(\sqrt{\frac{t_{diff}}{t+t_1}}\right) - \text{erfc}\left(\sqrt{\frac{t_{diff}}{t}}\right)\right) \qquad \text{for } n=3 \qquad (3\text{-}11)$$

where Δh is the drawdown head in the well, q is the flow rate during t_1, and the rest of the parameters are as in Equations (3-4) through (3-6). For the times relevant to the present set of data, Equation (3-10) coincides with the exact solution.

Generally, the field data did not match the type-curves very well. Equation (3-10) predicts that for n=2, $\Delta h/q$ versus $(t_1+t)/t$ should be linear when plotted on a lin-log scale. The linearity of the field data in Figure 3-36 indicates a closer match to the n=2 Horner solution (Equation 3-10) rather than the n=3 solution (Equation 3-11). The bend of the early-time part of the curve for PRT 1 could be due to skin effects and / or well borehole storage. However, the first part of PRT 2 shows no signs of such effects. The analysis of skin effects is not within the scope of this report. The bend of the late-time portion of the PRT 1 curve reflects the decrease in background pressure. Figures 3-27 and 3-28 are plots of $\Delta h/q$ versus $\log((t_1+t)/t)$ for PRT 1 and 2, where K can be determined from the slope of the linear parts of the field data curves. The type curve for n=2 is also included in the plots and it can be seen that $\Delta h/q$ should go to zero as $(t_1+t)/t$ goes to one, i.e. as time approaches infinity. The data for PRT 1 deviate from the type-curve at later times due to the increase in background pressures, therefore this part of the curve is disregarded. The obtained K values for n=2 were $3.0\cdot10^{-5}$ m/s for PRT 1 and $3.5\cdot10^{-5}$ m/s for PRT 2. These values are one order of magnitude higher than the K values obtained from the CPTs (see Table 3-7). The reported K value for PRT 2 corresponds to the slope of the later-time data, but the result changes by less than a factor two when other parts of the curve are used for determining K. Note that S_s cannot be evaluated assuming n=2 since this parameter is not included in Equation (3-10).

Figures 3-39 and 3-40 show the fit of data from PRT 1 and PRT 2 to the Horner curve representing spherical flow geometry ($n=3$). Disregarding the left part of the PRT 1 field data, which was affected by decreasing background pressures, it can be seen that the fit of the field data to the n=3 type-curve is non-unique due to the lack of characteristic shape of the field data (Figure 3-39). It can also be seen from Figure 3-40 that the field data from PRT 2 crosses the type-curve using the K and S_s values obtained from

the curve match with CPT 8. Similar results are obtained using the K and S_s pairs that were determined from CPTs 6, 7 and 9.

3.2.5 Cross-well analysis of pressure recovery tests (PRTs)

The single-well analysis of the PRTs (Section 3.2.4) indicated a better agreement between the field data and the type curves for n=2 than n=3. In order to further investigate this observation, cross-well analysis was used to evaluate the pressure response to PRT 1 and 2 in the four packed-off sections in the monitoring borehole KA2511A (Table 3-9). The Horner solutions (Equations 3-10 and 3-11), were used for the analysis, substituting the distance between the test hole and the monitoring well, r_{tw}, for the well radius, r_w. Although the field data was matched to the long term approximation of the Horner solution (Equation 3-10), which does not include r_w, it was found that for the distances and conductivities shown in Table 3-9, the exact Horner solution for n=2, which includes r_w, did not differ significantly from Equation (3-10). This may be a consequence of the fast travel times of the pressure pulse for the high hydraulic conductivity of the formation.

Table 3-9. Values of K obtained from matching pressure response data from borehole KA2511A with n=2 type-curves.

PRT#	n	KA2511A section#	r_{tw} (m)	Background pressure (kPa)	K (m/s)
1	2	1	242	3125	$2.2 \cdot 10^{-5}$
1	2	2	122	3085	$2.8 \cdot 10^{-5}$
1	2	3	47	3045	$2.2 \cdot 10^{-5}$
1	2	4	29	3015	$2.9 \cdot 10^{-5}$
2	2	1	242	3155	$4.2 \cdot 10^{-5}$
2	2	2	122	3125	$3.4 \cdot 10^{-5}$
2	2	3	47	3095	$3.0 \cdot 10^{-5}$
2	2	4	29	3080	$2.6 \cdot 10^{-5}$

The K values presented in Table 3-9 are similar to those obtained in the single-well PRT analysis for radial geometry, where K equals to $3.0 \cdot 10^{-5}$ and $3.5 \cdot 10^{-5}$ m/s for PRTs 1 and 2, respectively. The K and S_s values assuming a spherical geometry were indeterminate due to non-unique fits in the cross-well as well as in the single-well analysis of the PRTs. Generally, the analysis of the pressure response in the monitoring well is consistent with the single-well analysis.

3.2.6 Discussion

In test phases (1) through (3), the relationship between borehole pressure and inflow rate was linear over borehole pressures ranging from 1500 kPa (abs) down to 120 kPa (abs), and a mean hydraulic conductivity of $1.15 \cdot 10^{-6} \pm 0.12 \cdot 10^{-6}$ m/s was obtained through fitting constant pressure test data to n=3 type curves. The results show no measurable effects of other processes that might reduce transmissivity at low borehole pressures, such as calcite precipitation, increase in effective stress or turbulence. The low gas contents measured in KA2512A (0.5% v/v STP) indicate that during phase (2), water pressures below the bubble pressure may not have been achieved with the equipment configuration used. The estimated bubble pressure for these gas contents, assuming that the gas is nitrogen and a Henry's Law constant of $8.14 \cdot 10^{6}$ kPa/(mole fraction), is 134 kPa (abs). From the 2^{o} dip of the borehole, the end of the borehole where the water-flowing fracture was intersected is approximately 1.3 m below the elevation of the borehole casing where pressure was measured. During phase (2), the borehole pressure was 120 kPa (abs), resulting in a pressure at the end of the borehole of approximately 133 kPa (abs).

In CPT 11 (phase (4)), the hydraulic conductivity decreased from a value of $1.05 \cdot 10^{-6}$ m/s at a borehole pressure of 1500 kPa (abs) to a value of $0.8 \cdot 10^{-6}$ m/s. Gas contents measured at the beginning of phase (4) were twice as high as previously measured (1% v/v), which gives an estimated bubble pressure of 167 kPa (abs). In this case, the groundwater pressure in the formation may have been less than the bubble pressure, suggesting that degassing may have caused the flow reduction. This suggestion must be qualified by the fact that not enough testing was done above the bubble pressure to exclude the possibility that the observed flow reduction was caused by a change in boundary conditions or blast-induced effects.

CPTs 1-4 did not match the type curves as well as CPTs 6-10 mainly because of irregularities in the curves, which might have been caused by changes in rock stresses during the initial lowering of water pressure, which then can affect the hydraulic properties of the fracture. Before starting the test cycle, it would thus be preferable to lower the pressure as much as possible and cycle pressures up and down, in order to observe if effective stress changes cause hysteresis, particularly in the first cycle.

Due to the fast response of the system, only the very first part of CPTs 1-6 showed an inclined shape that could be matched with the type curves for single-well analysis. This particularly decreased the sensitivity of the analysis with respect to the S_S values. More frequent data sampling during the first 10-30 seconds, preferably several times per second, might provide better sets of data for fractures with this yield. However, this may not be practical because the backpressure controller cannot ensure constant

pressures during the first 15 seconds of the test. The cross-well analysis showed that a much lower S_s value than obtained in the single-well analysis was required to match the arrival of the pressure response in the monitoring well KA2511A. Since the S_s-values in the single-well analysis were derived from very early-time data, they may be biased by the specific storage of the borehole region and it is likely that they do not reflect the specific storage of the fracture region.

The field CPT data fitted best to the type curves representing spherical flow geometry, while the field PRT data fitted better to radial flow geometry for both single-well and cross-well solutions. The occurrence of these idealized flow geometries in fractured rock is questionable. For instance, a borehole intersecting a fracture zone might represent a geometry that, in reality, is in between radial and spherical, so that neither the conditions for n=2 nor the conditions for n=3 are fulfilled. Thus, a fit of field data to a curve representing n=3 does not necessarily imply that the flow field is spherical but rather that the flow field under certain conditions shows similarities to the spherical flow case. Generally, if one assumes spherical flow geometry around the borehole, the cross-sectional area perpendicular to the direction of flow is greater than the corresponding area available for flow per meter borehole length for the radial case (when radial distances exceed 0.5 meters). This implies that the calculated conductivities for a borehole should be lower if making the spherical geometry assumption than the radial geometry assumption. This was also the case for KA2512A (with calculated K values on the order of 10^{-6} m/s for the spherical case (section 3.2.2) and 10^{-5} m/s for the radial case (sections 3.2.4 and 3.2.5)). Therefore, if the flow geometry in the field lies between these two cases, the hydraulic conductivity should be between 10^{-6} and 10^{-5} m/s.

Increasing amounts of gas phase in the borehole would be observed as an apparent increase in the specific storage obtained through matching field data to Equations 3-2, 3-3 and 3-6, since S_s is linearly proportional to the fluid compressibility, which increases by several orders of magnitude when a gas phase is present. Furthermore, a higher gas phase saturation in the fracture could reduce the hydraulic conductivity due to two-phase flow effects. The solutions for constant pressure tests are a function of the hydraulic diffusivity which is the ratio of hydraulic conductivity and specific storage. Two-phase conditions should cause a decrease in hydraulic conductivity and an increase in specific storage, resulting in a large overall decrease in hydraulic diffusivity. Consequently, the change in these parameters relative to single-phase conditions should be readily detectable, even if an absolute value of storativity cannot be measured with confidence. Studies have shown that absolute values of K and S_s might differ by orders of magnitude depending on which test method is chosen (e.g. Almén et al. (1986)); therefore, it is important to conduct similar tests to evaluate changes in K and S_s. No decrease in K was measured throughout the test

sequence in KA2512A, and it is likely that changes in S_s would have been much more obvious if degassing had been significant compared to those resulting from uncertainty in the type-curve matching.

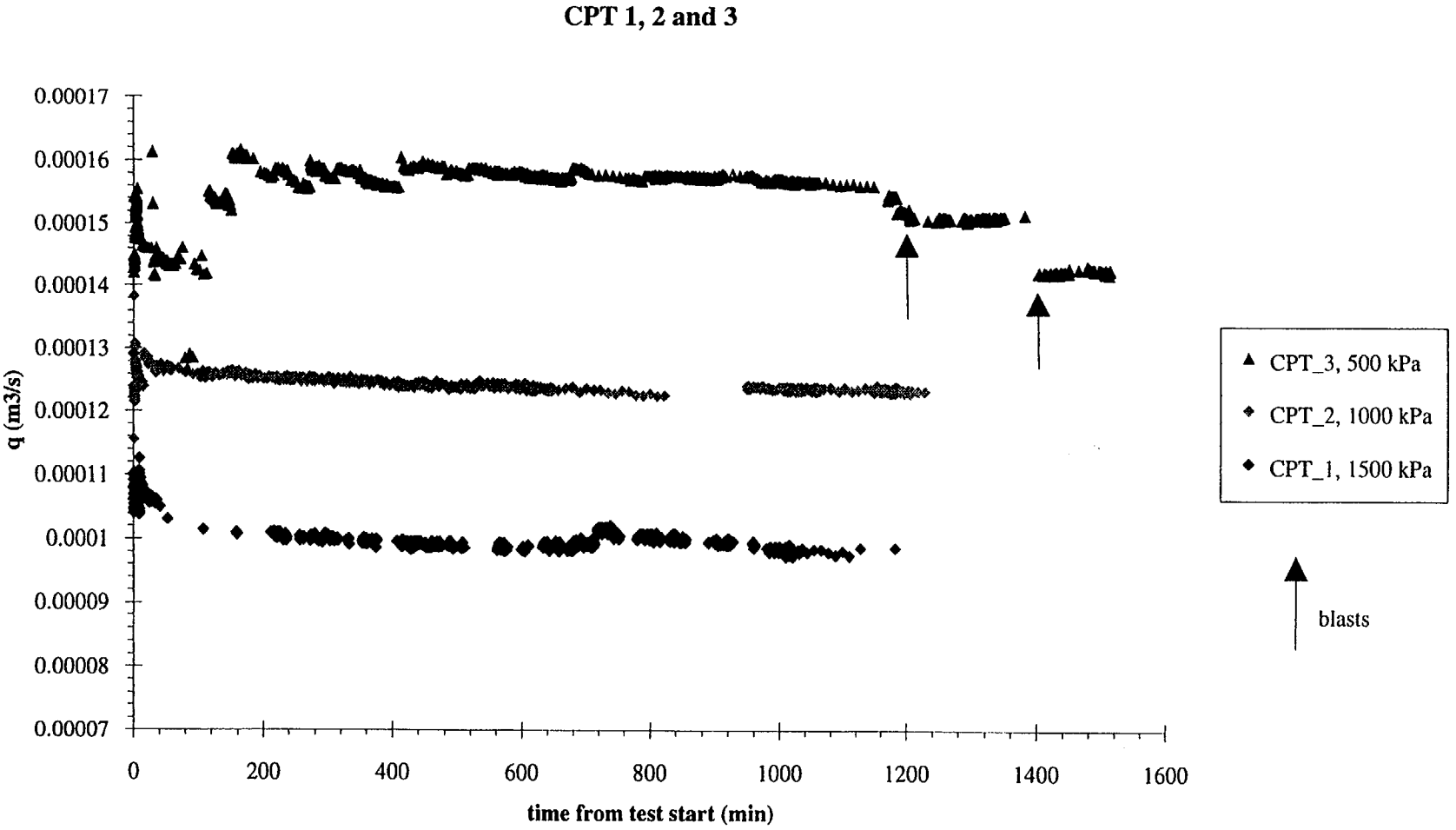
CPT 1, 2 and 3
0.00017
0.00016
0.00015
0.00014
0.00013
0.00012
0.00011
0.0001
0.00009
0.00008
0.00007
q (m3/s)
0
200
400
600
800
1000
1200
1400
1600
time from test start (min)
CPT_3, 500 kPa
CPT_2, 1000 kPa
CPT_1, 1500 kPa
blasts

Fig. 3-1

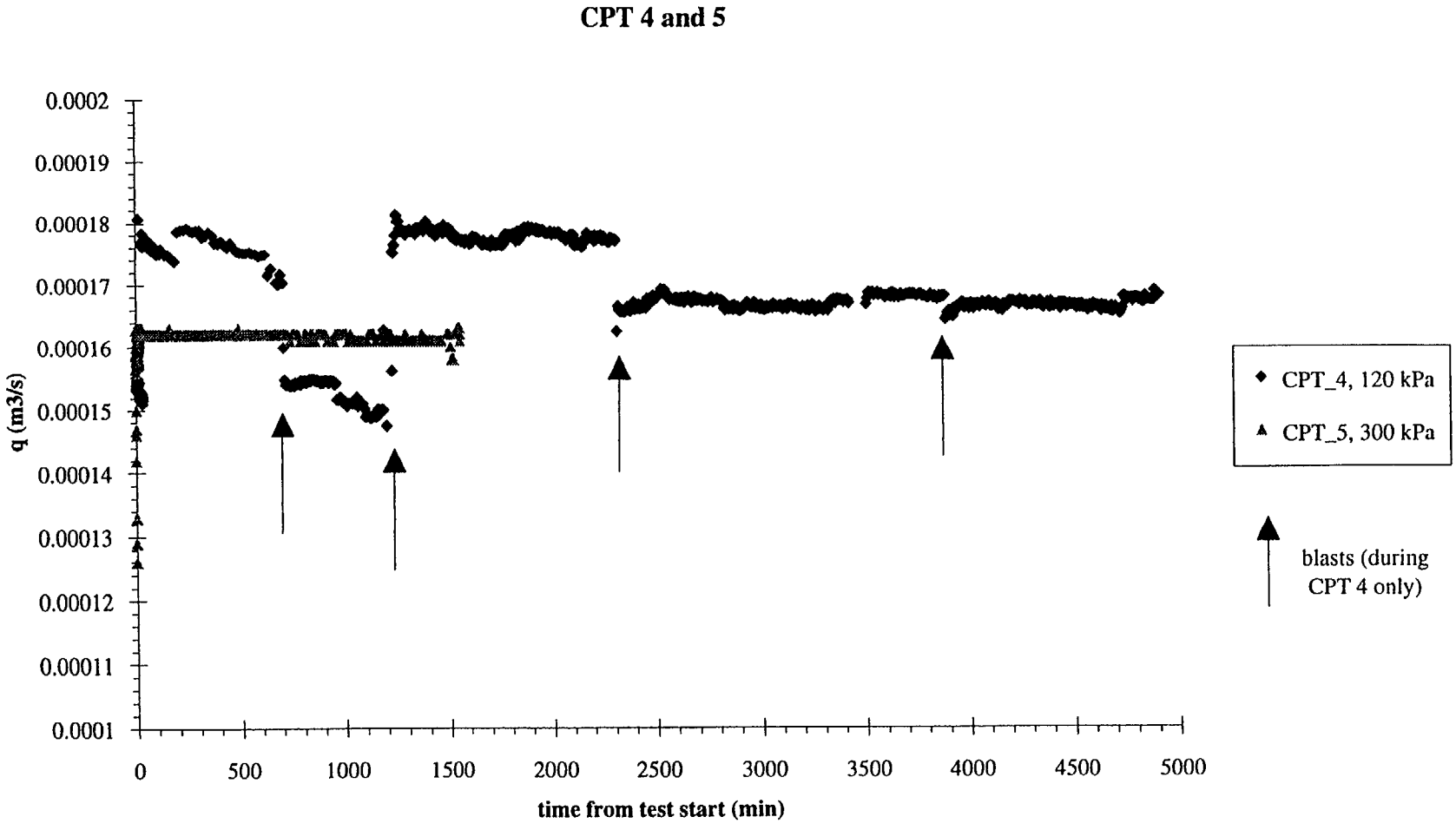
CPT 4 and 5
0.0002
0.00019
0.00018
0.00017
0.00016
0.00015
0.00014
0.00013
0.00012
0.00011
0.0001
q (m3/s)
0
500
1000
1500
2000
2500
3000
3500
4000
4500
5000
time from test start (min)
CPT_4, 120 kPa
CPT_5, 300 kPa
blasts (during CPT 4 only)

Fig. 3-2

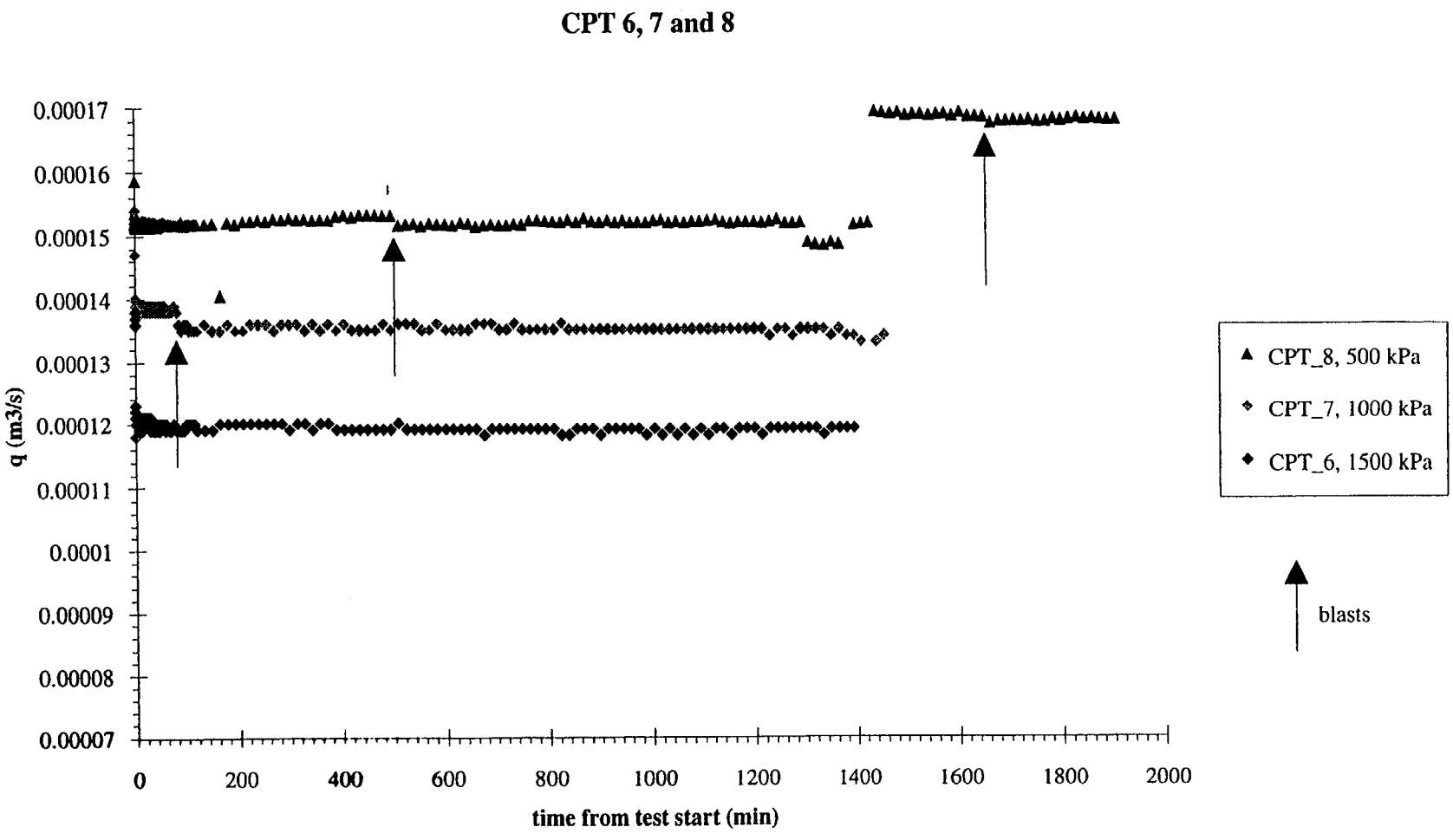
CPT 6, 7 and 8
0.00017
0.00016
0.00015
0.00014
0.00013
0.00012
0.00011
0.0001
0.00009
0.00008
0.00007
q (m3/s)
0
200
400
600
800
1000
1200
1400
1600
1800
2000
time from test start (min)
CPT_8, 500 kPa
CPT_7, 1000 kPa
CPT_6, 1500 kPa
blasts

Fig. 3-3

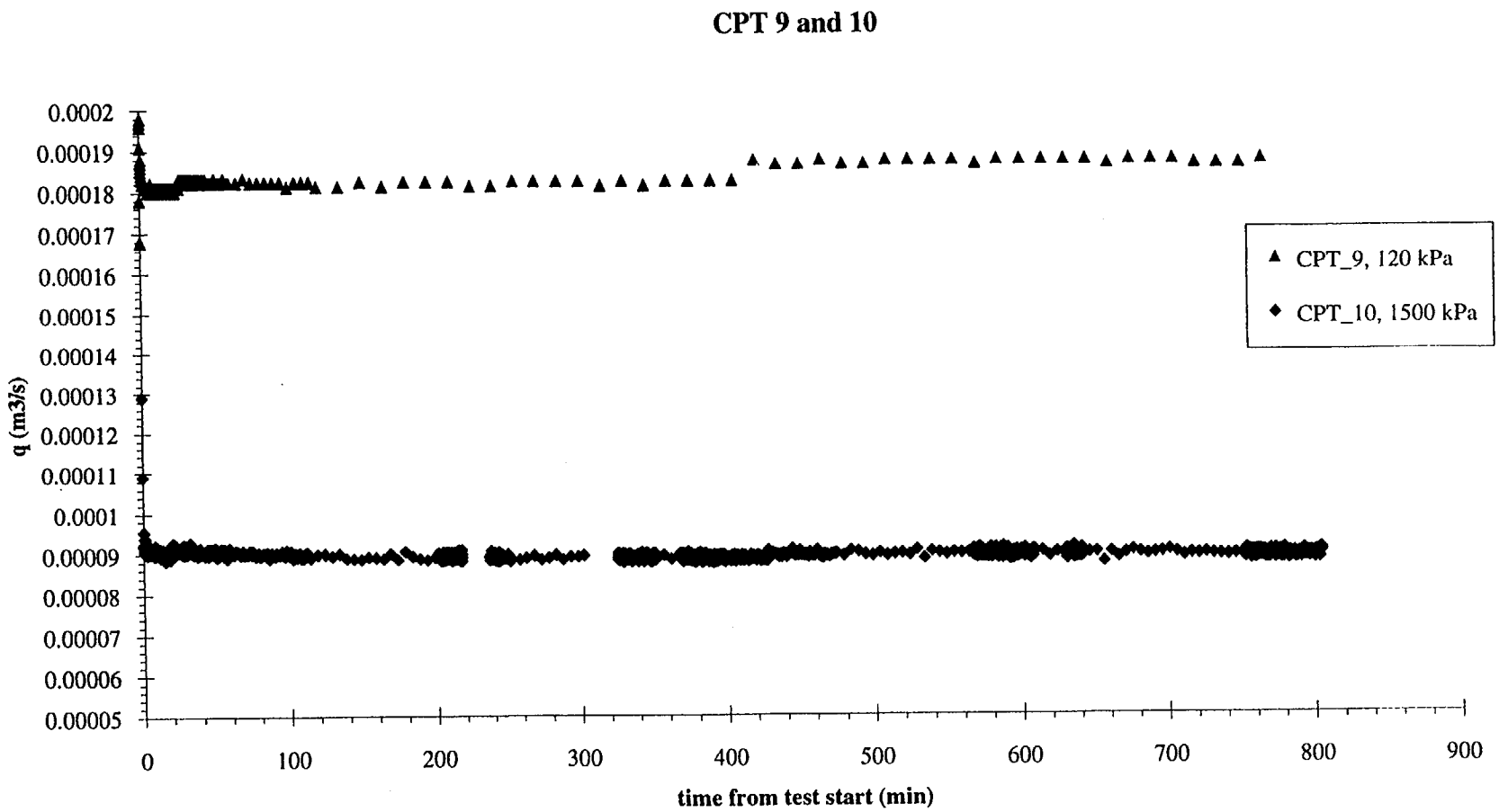
CPT 9 and 10
0.0002
0.00019
0.00018
0.00017
0.00016
0.00015
0.00014
0.00013
0.00012
0.00011
0.0001
0.00009
0.00008
0.00007
0.00006
0.00005
q (m3/s)
0
100
200
300
400
500
600
700
800
900
time from test start (min)
CPT_9, 120 kPa
CPT_10, 1500 kPa

Fig. 3-4

CPT 11 and 12

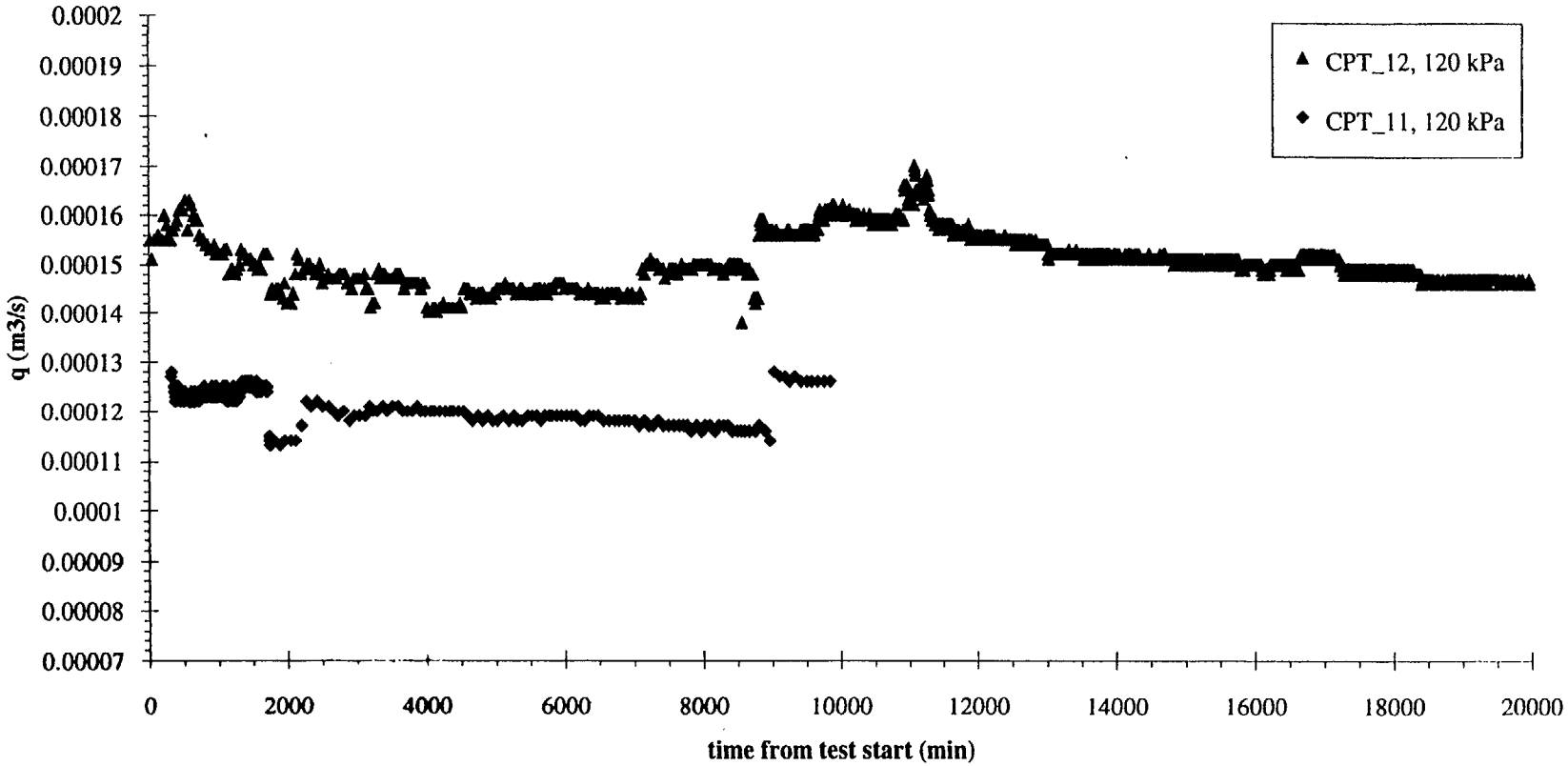

Fig. 3-5

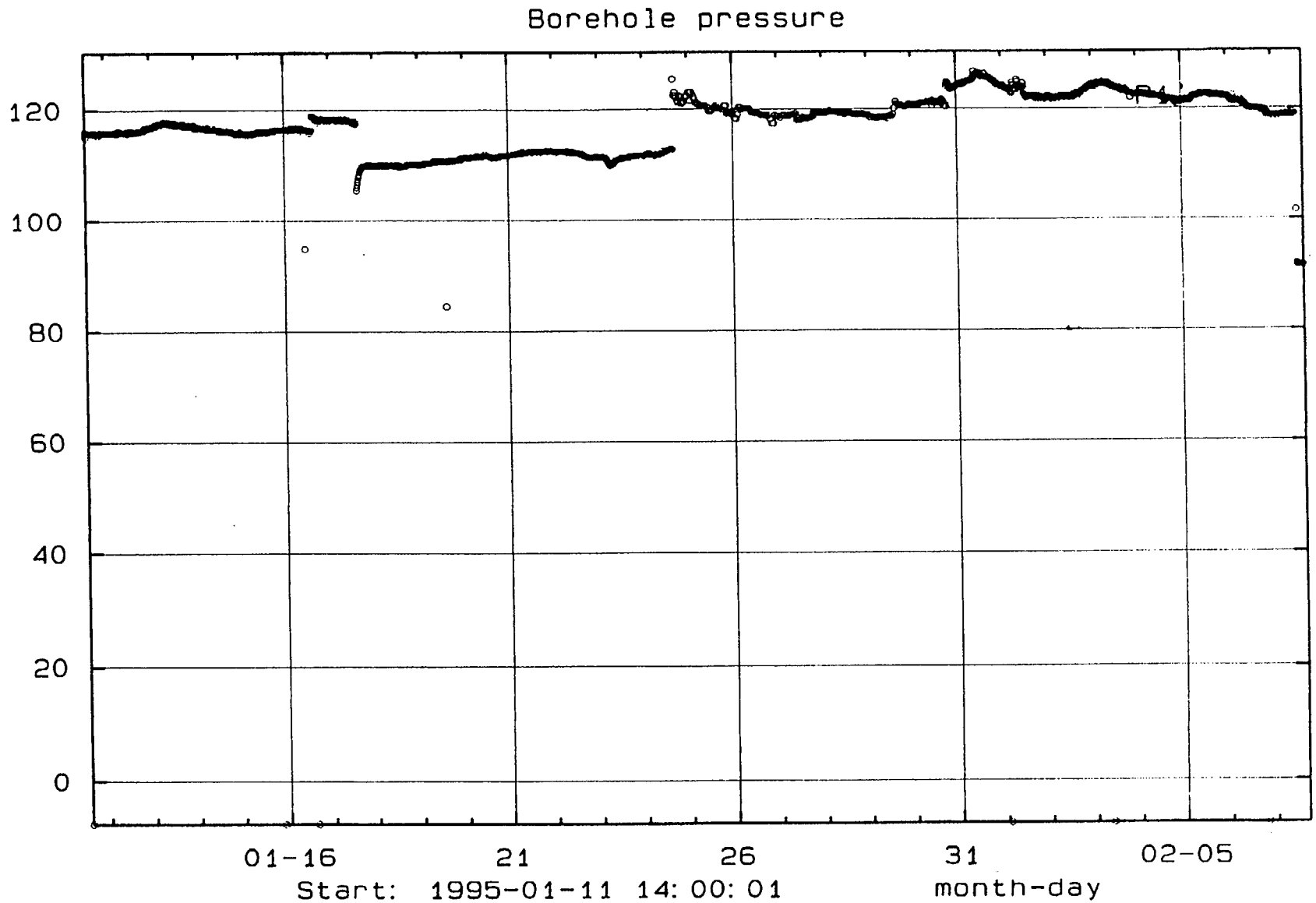
Borehole pressure
KPa
120
100
80
60
40
20
0
01-16
21
26
31
02-05
Start: 1995-01-11 14:00:01
month-day

Fig. 3-6

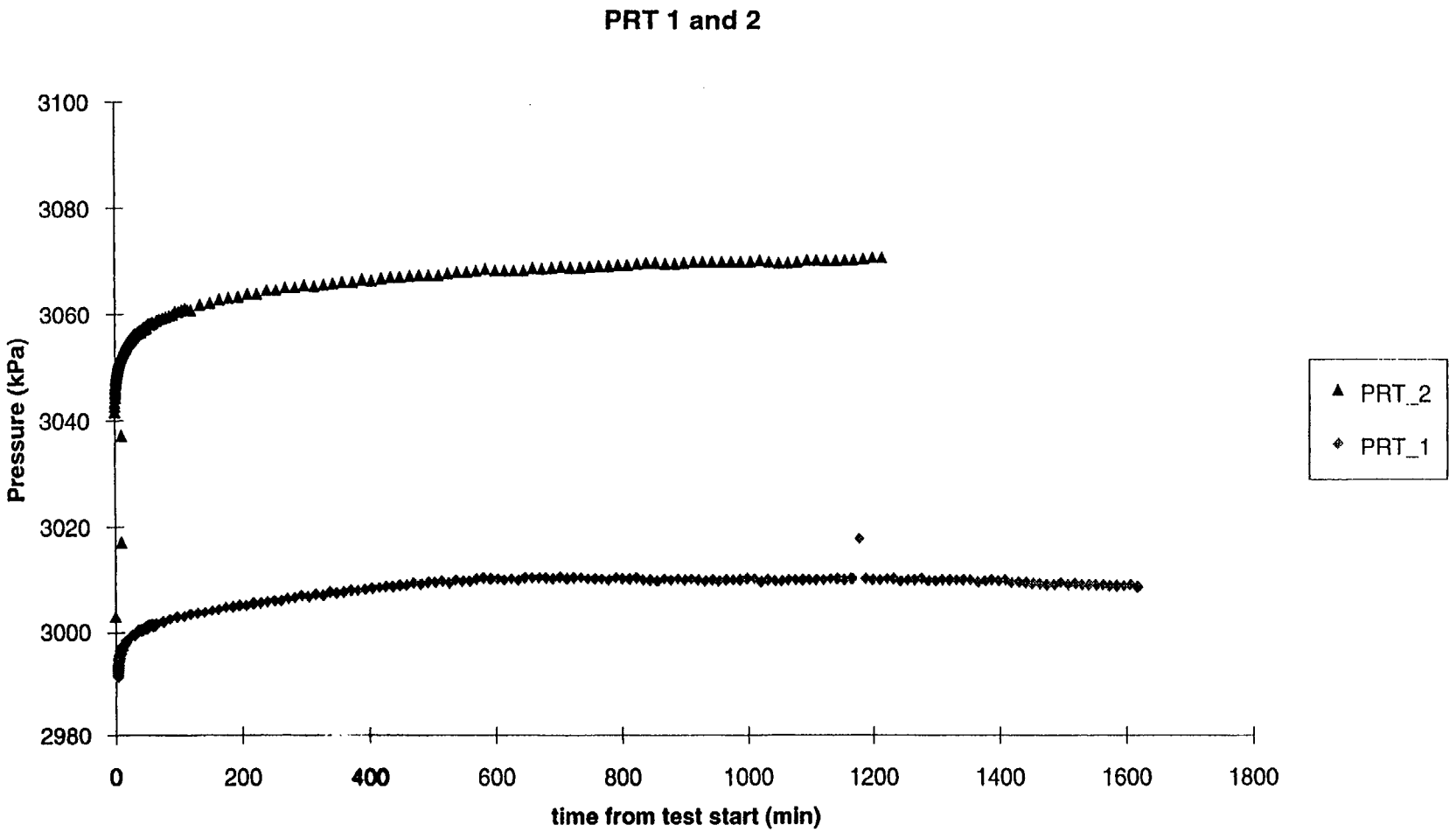
PRT 1 and 2
3100
3080
3060
3040
3020
3000
2980
Pressure (kPa)
0
200
400
600
800
1000
1200
1400
1600
1800
time from test start (min)
PRT_2
PRT_1

Fig. 3-7

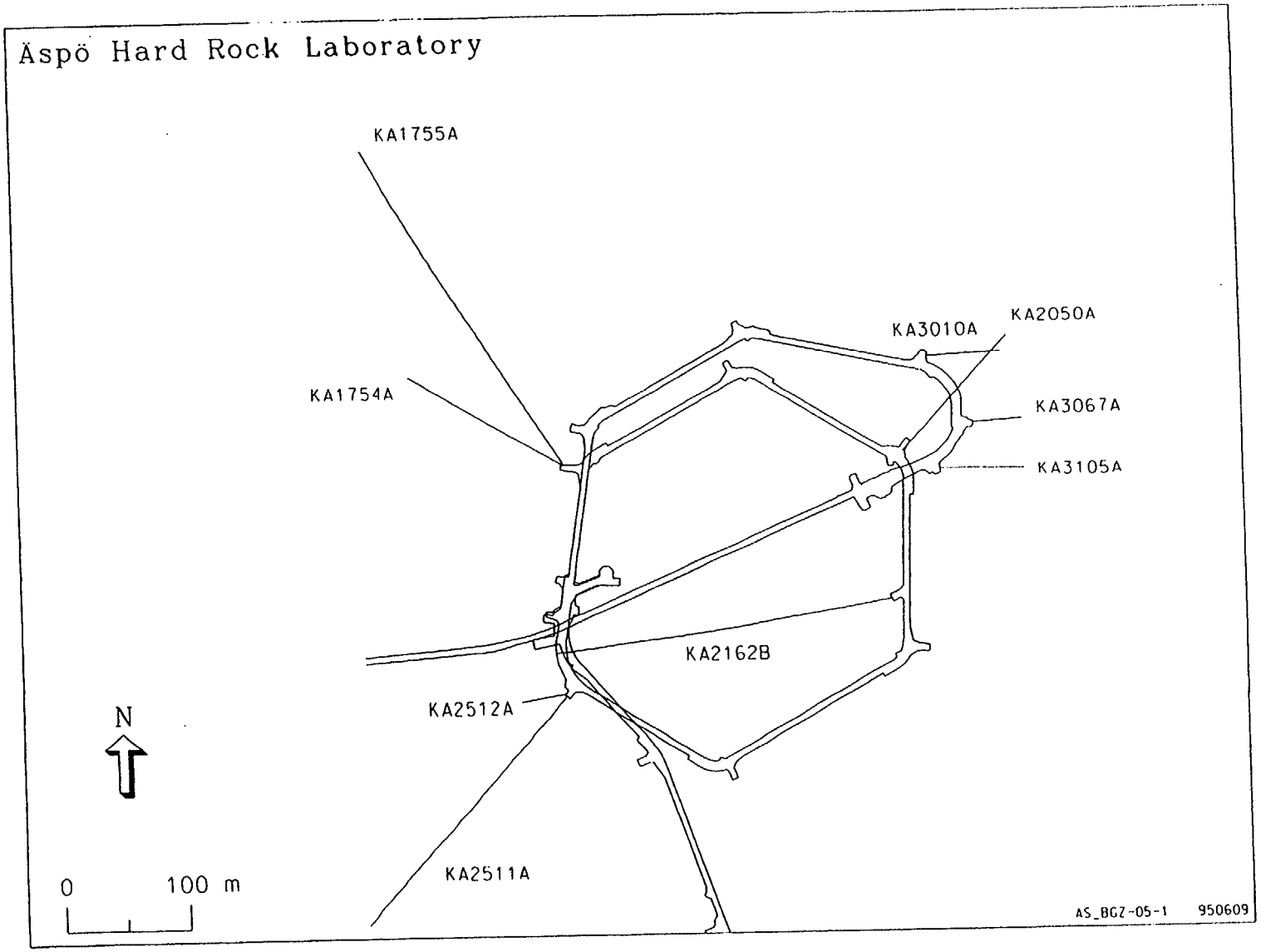
Äspö Hard Rock Laboratory
KA1755A
KA1754A
KA3010A
KA2050A
KA3067A
KA3105A
KA2162B
KA2512A
KA2511A
N
0
100 m
AS_BGZ-05-1
950609

Fig. 3-8

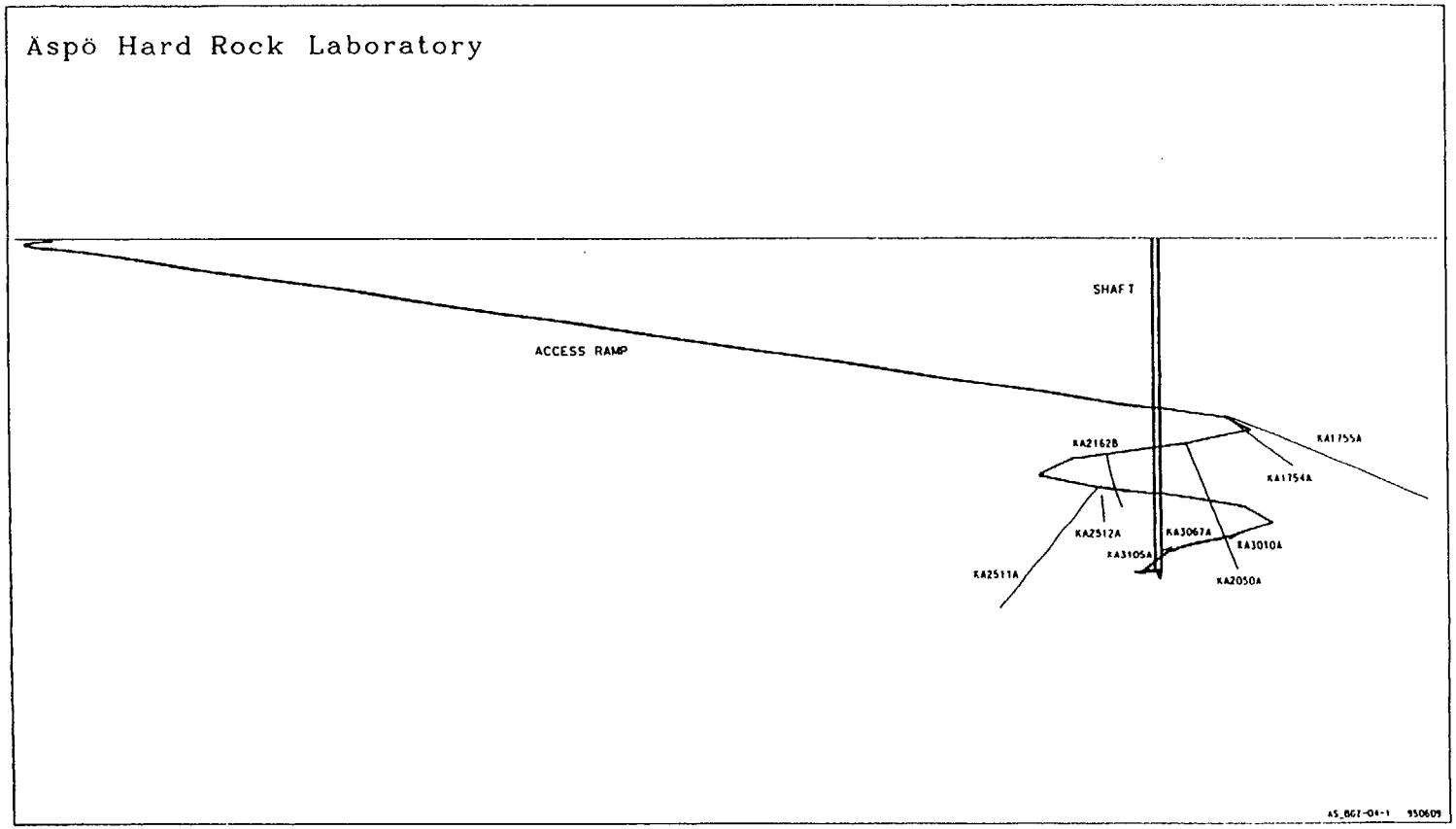
Äspö Hard Rock Laboratory
SHAFT
ACCESS RAMP
KA2162B
KA1755A
KA1754A
KA2512A
KA3067A
KA3105A
KA3010A
KA2511A
KA2050A

Fig. 3-9

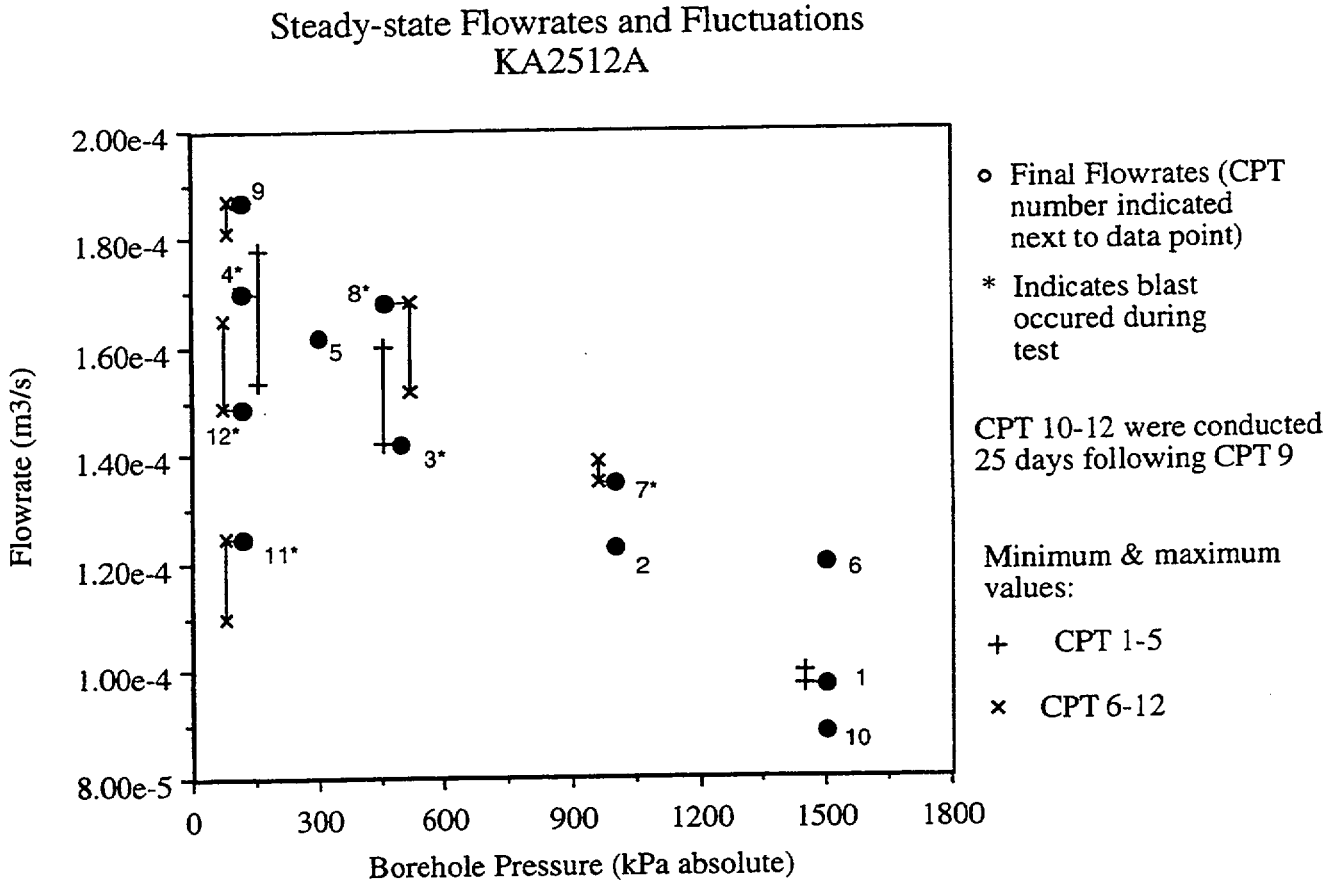
Steady-state Flowrates and Fluctuations
KA2512A
Flowrate (m3/s)
2.00e-4
1.80e-4
1.60e-4
1.40e-4
1.20e-4
1.00e-4
8.00e-5
0
300
600
900
1200
1500
1800
Borehole Pressure (kPa absolute)
9
4*
8*
5
12*
3*
7*
11*
2
6
1
10
o Final Flowrates (CPT number indicated next to data point)
* Indicates blast occured during test
CPT 10-12 were conducted 25 days following CPT 9
Minimum & maximum values:
+ CPT 1-5
× CPT 6-12

Fig. 3-10

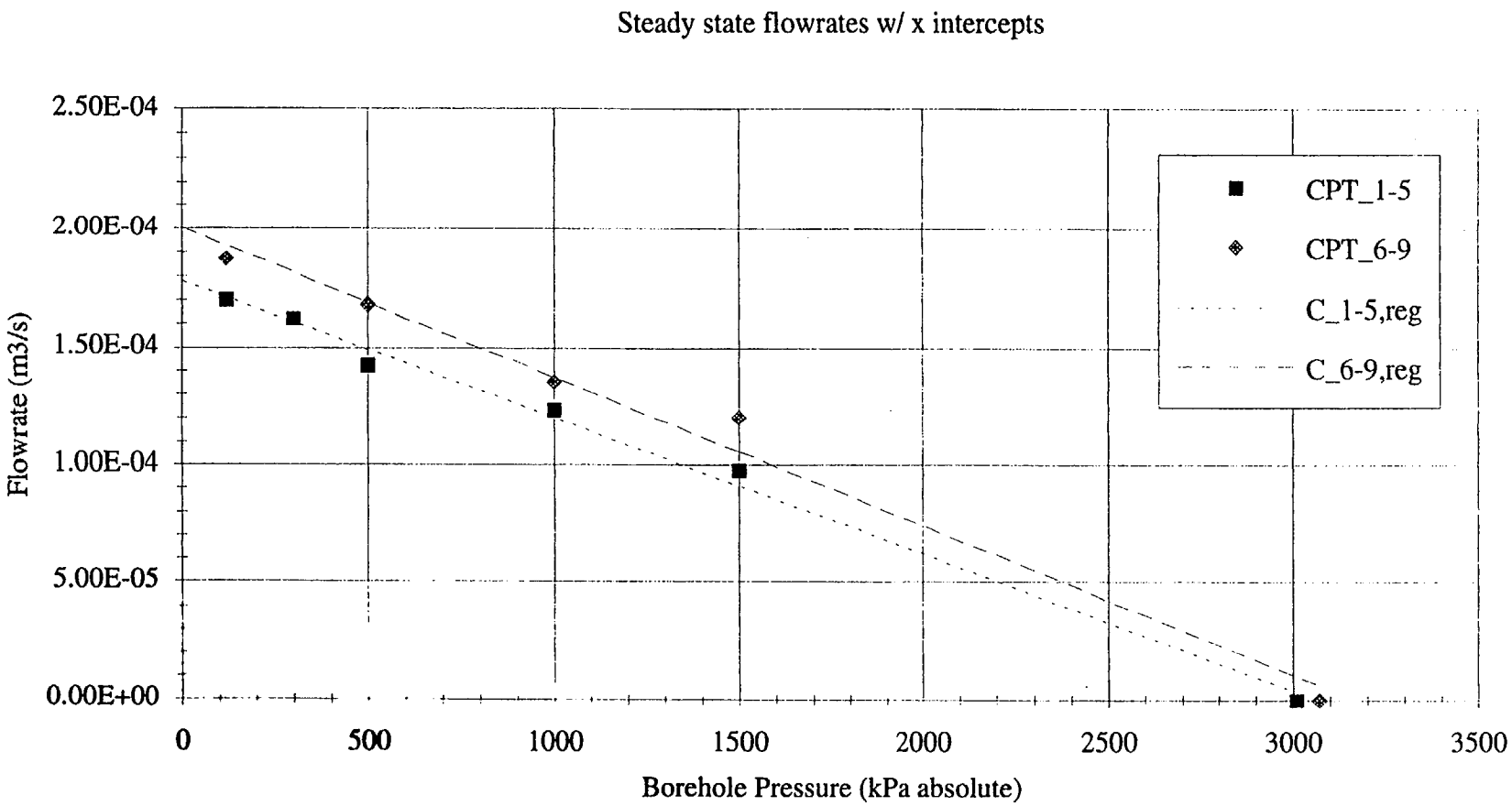
Steady state flowrates w/ x intercepts
2.50E-04
2.00E-04
1.50E-04
1.00E-04
5.00E-05
0.00E+00
Flowrate (m3/s)
0
500
1000
1500
2000
2500
3000
3500
Borehole Pressure (kPa absolute)
CPT_1-5
CPT_6-9
C_1-5,reg
C_6-9,reg

Fig. 3-11

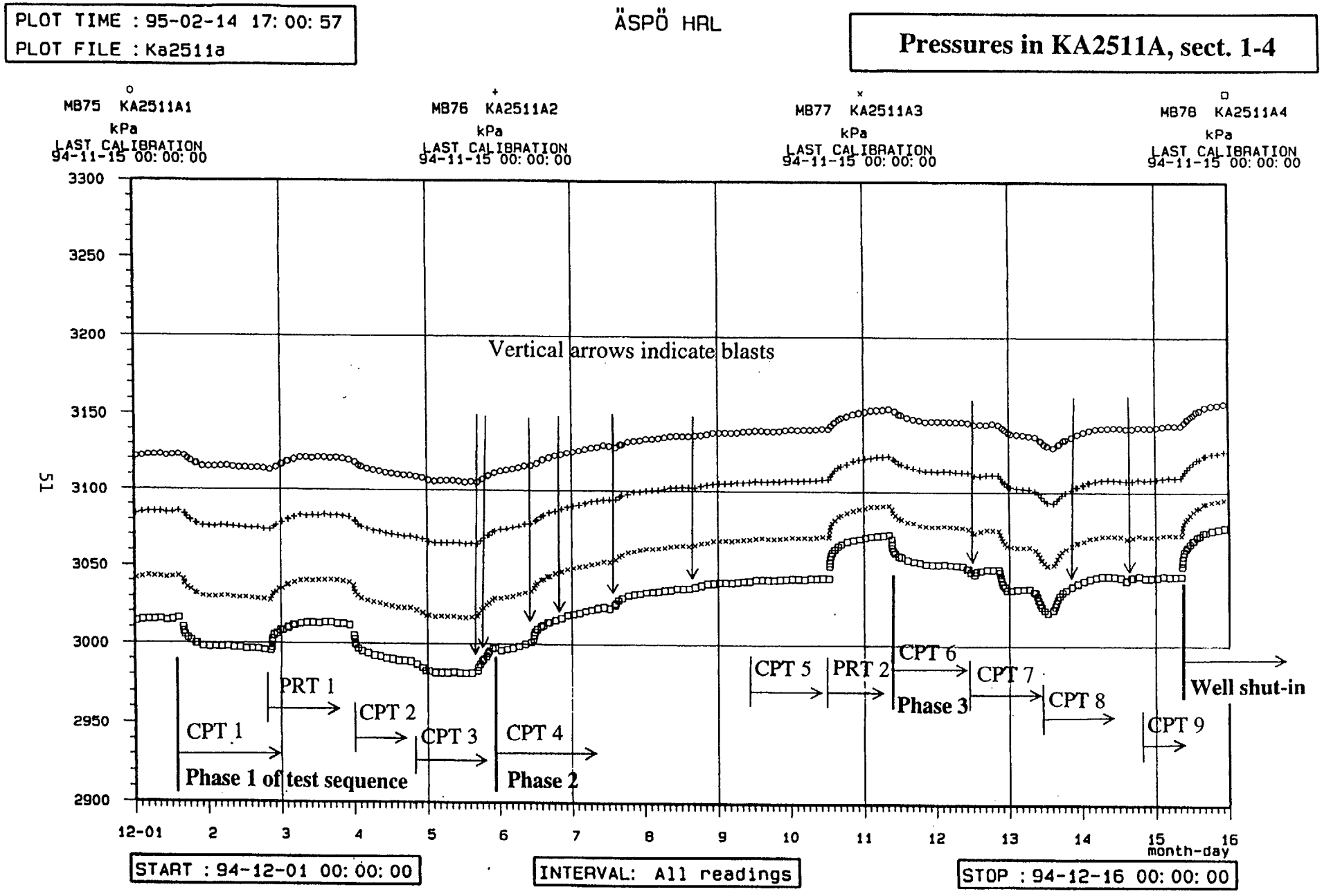
PLOT TIME : 95-02-14 17: 00: 57
PLOT FILE : Ka2511a
ÄSPÖ HRL
Pressures in KA2511A, sect. 1-4
o
MB75 KA2511A1
kPa
LAST CALIBRATION
94-11-15 00: 00: 00
+
MB76 KA2511A2
kPa
LAST CALIBRATION
94-11-15 00: 00: 00
x
MB77 KA2511A3
kPa
LAST CALIBRATION
94-11-15 00: 00: 00
□
MB78 KA2511A4
kPa
LAST CALIBRATION
94-11-15 00: 00: 00
3300
3250
3200
3150
3100
3050
3000
2950
2900
Vertical arrows indicate blasts
CPT 1
PRT 1
CPT 2
CPT 3
CPT 4
Phase 1 of test sequence
Phase 2
CPT 5
PRT 2
CPT 6
CPT 7
CPT 8
CPT 9
Phase 3
Well shut-in
12-01
2
3
4
5
6
7
8
9
10
11
12
13
14
15
16
month-day
START : 94-12-01 00: 00: 00
INTERVAL: All readings
STOP : 94-12-16 00: 00: 00

Fig. 3-12

PLOT TIME : 95-02-14 17: 03: 33
PLOT FILE : Ka2162b

ÄSPÖ HRL

Pressures in KA2162B, sect. 1-4

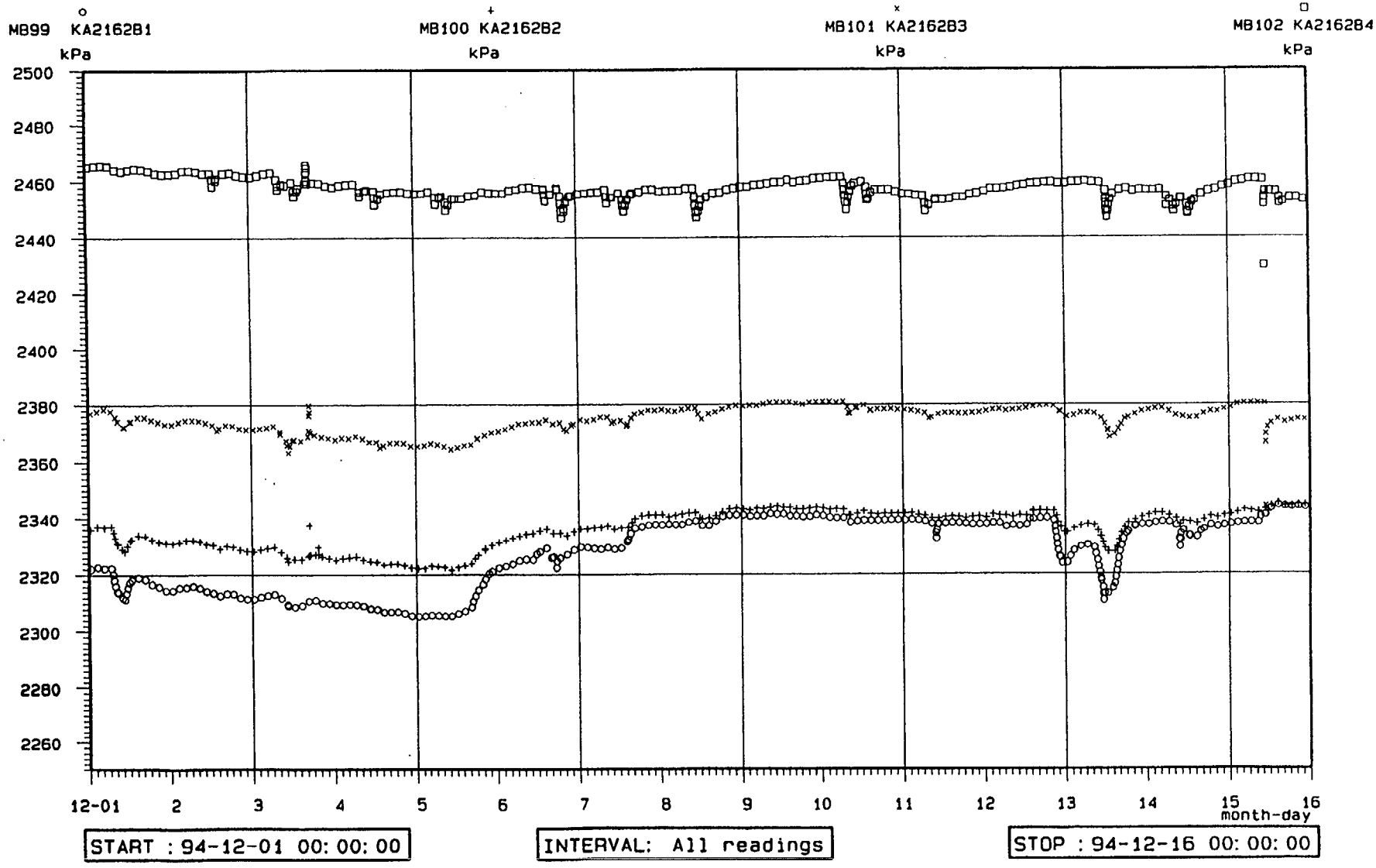

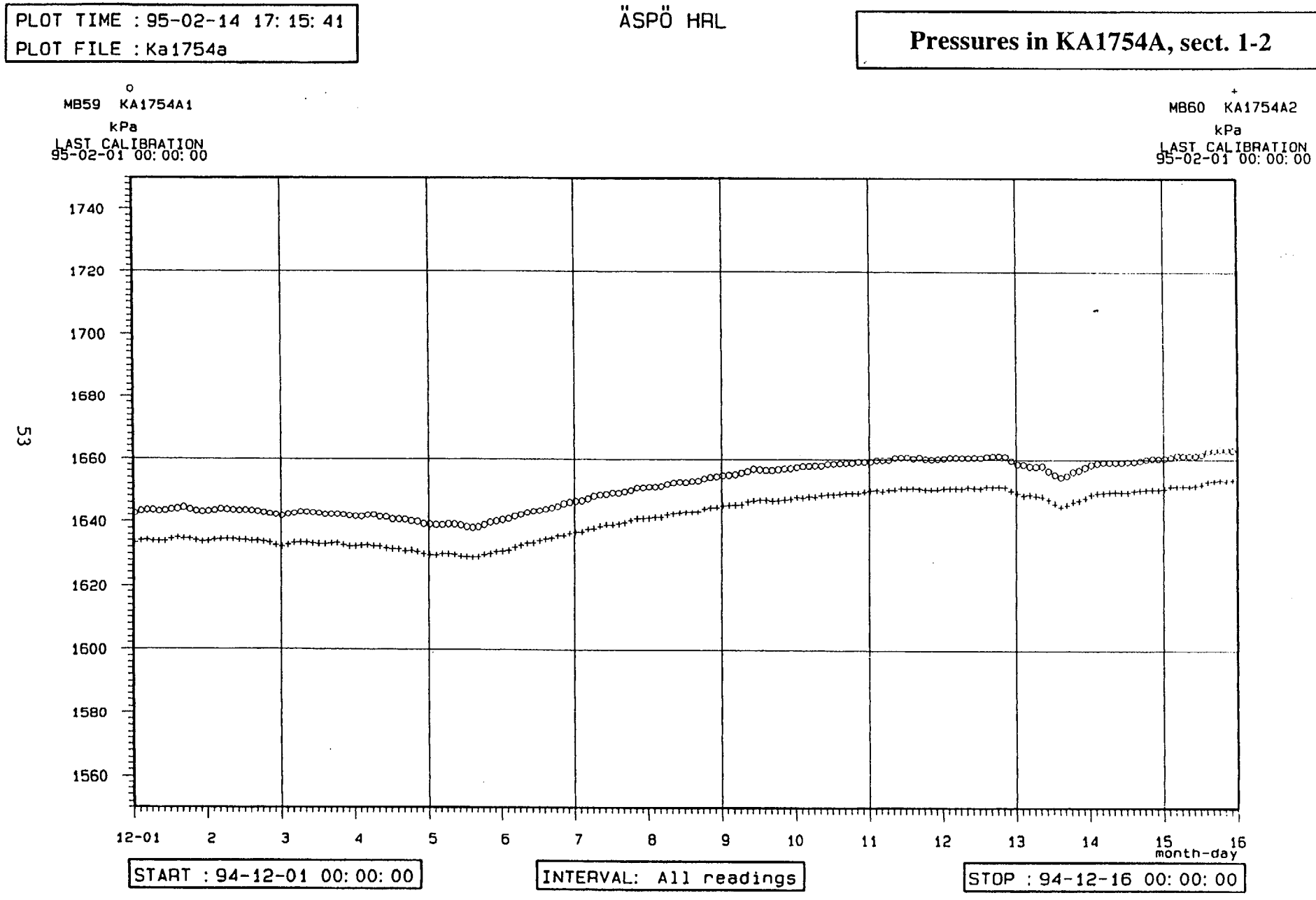
PLOT TIME : 95-02-14 17: 15: 41
PLOT FILE : Ka1754a
ÄSPÖ HRL
Pressures in KA1754A, sect. 1-2
o
MB59 KA1754A1
kPa
LAST CALIBRATION
95-02-01 00: 00: 00
+
MB60 KA1754A2
kPa
LAST CALIBRATION
95-02-01 00: 00: 00
1740
1720
1700
1680
1660
1640
1620
1600
1580
1560
12-01
2
3
4
5
6
7
8
9
10
11
12
13
14
15
16
month-day
START : 94-12-01 00: 00: 00
INTERVAL: All readings
STOP : 94-12-16 00: 00: 00

Fig. 3-14

PLOT TIME : 95-02-14 17: 35: 33
PLOT FILE : Has13

ÄSPÖ HRL

Pressures in HAS13, sect. 1-2

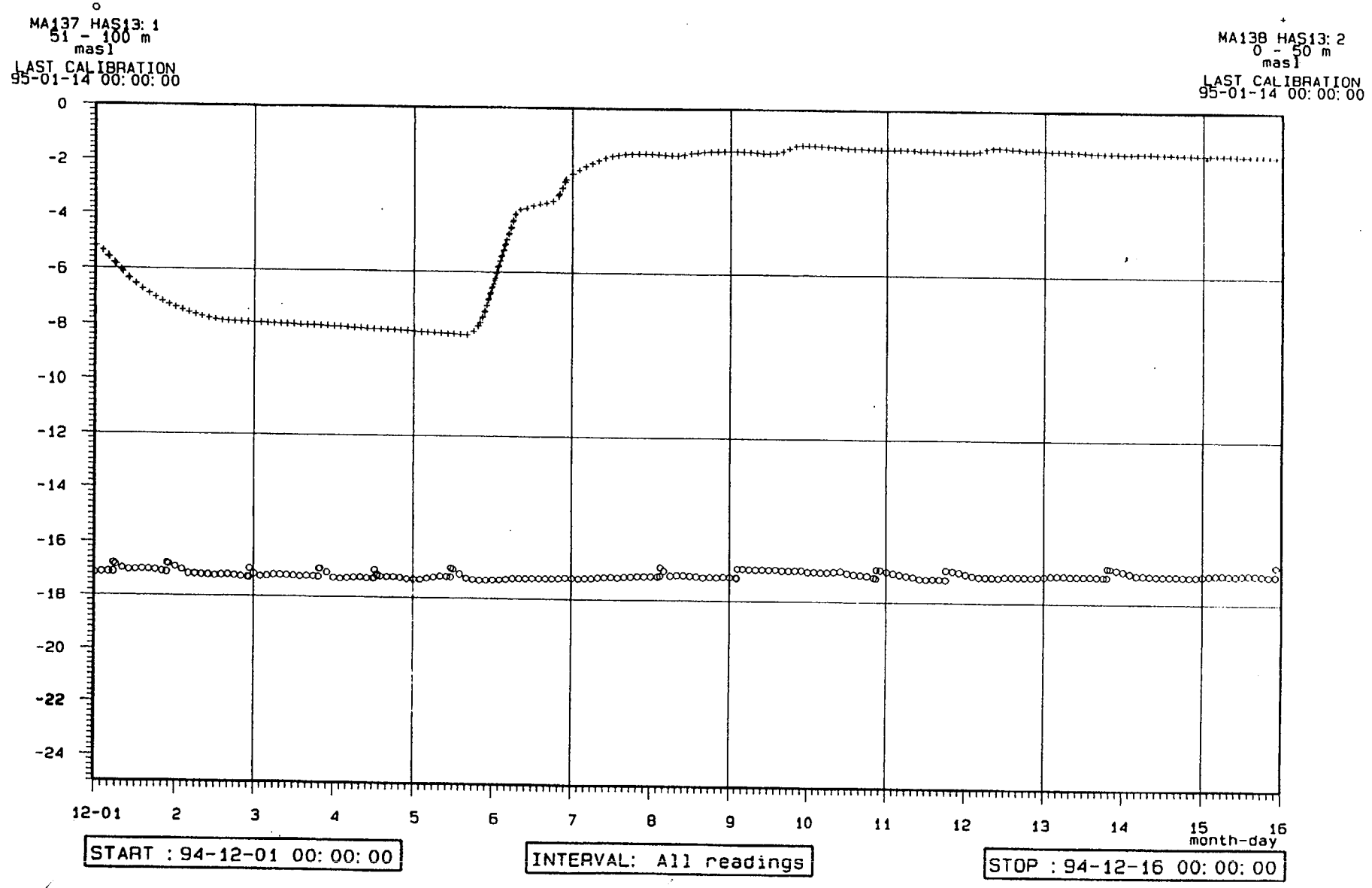

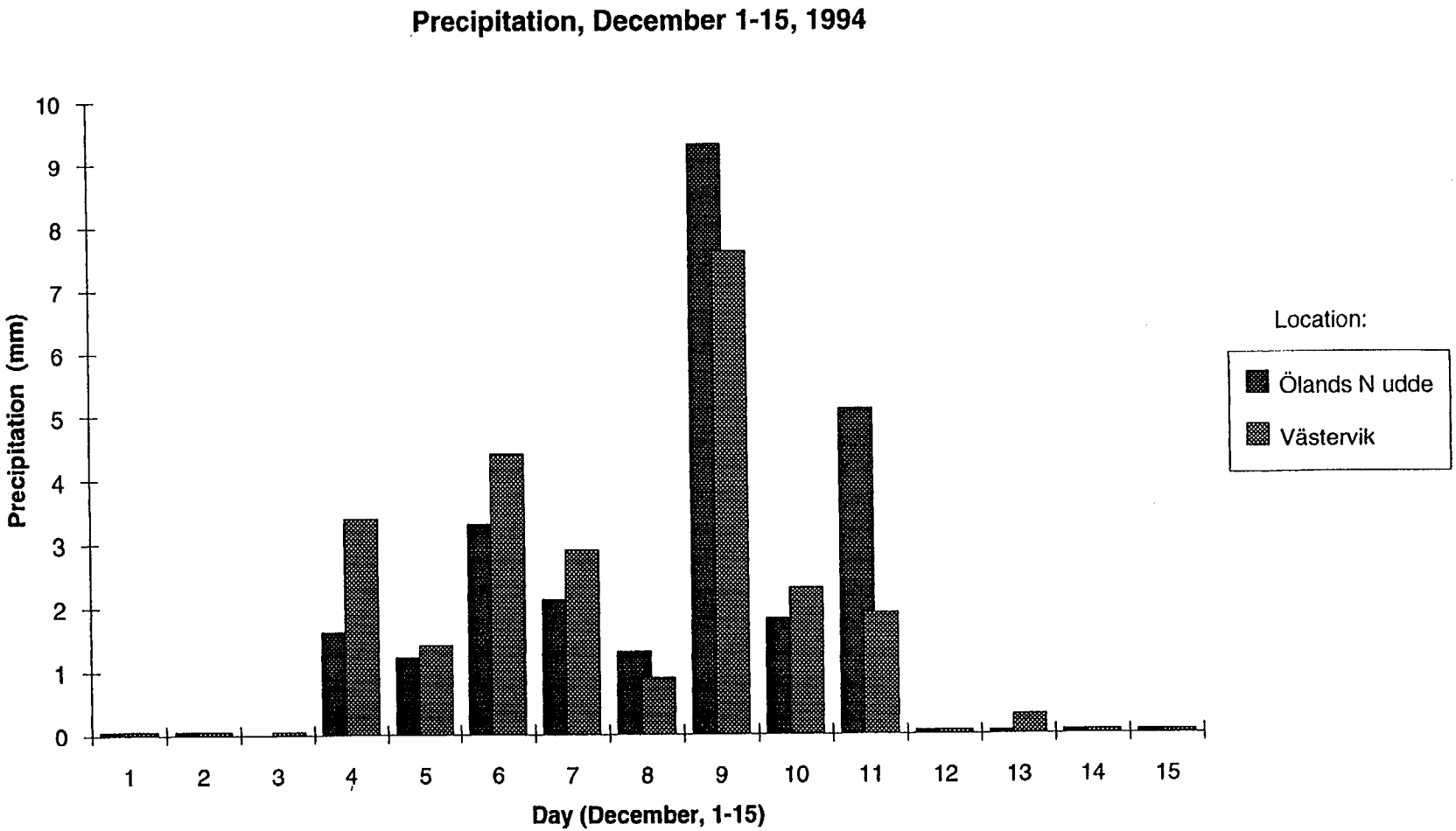
Precipitation, December 1-15, 1994
Precipitation (mm)
0
1
2
3
4
5
6
7
8
9
10
1
2
3
4
5
6
7
8
9
10
11
12
13
14
15
Day (December, 1-15)
Location:
Ölands N udde
Västervik

Fig. 3-16

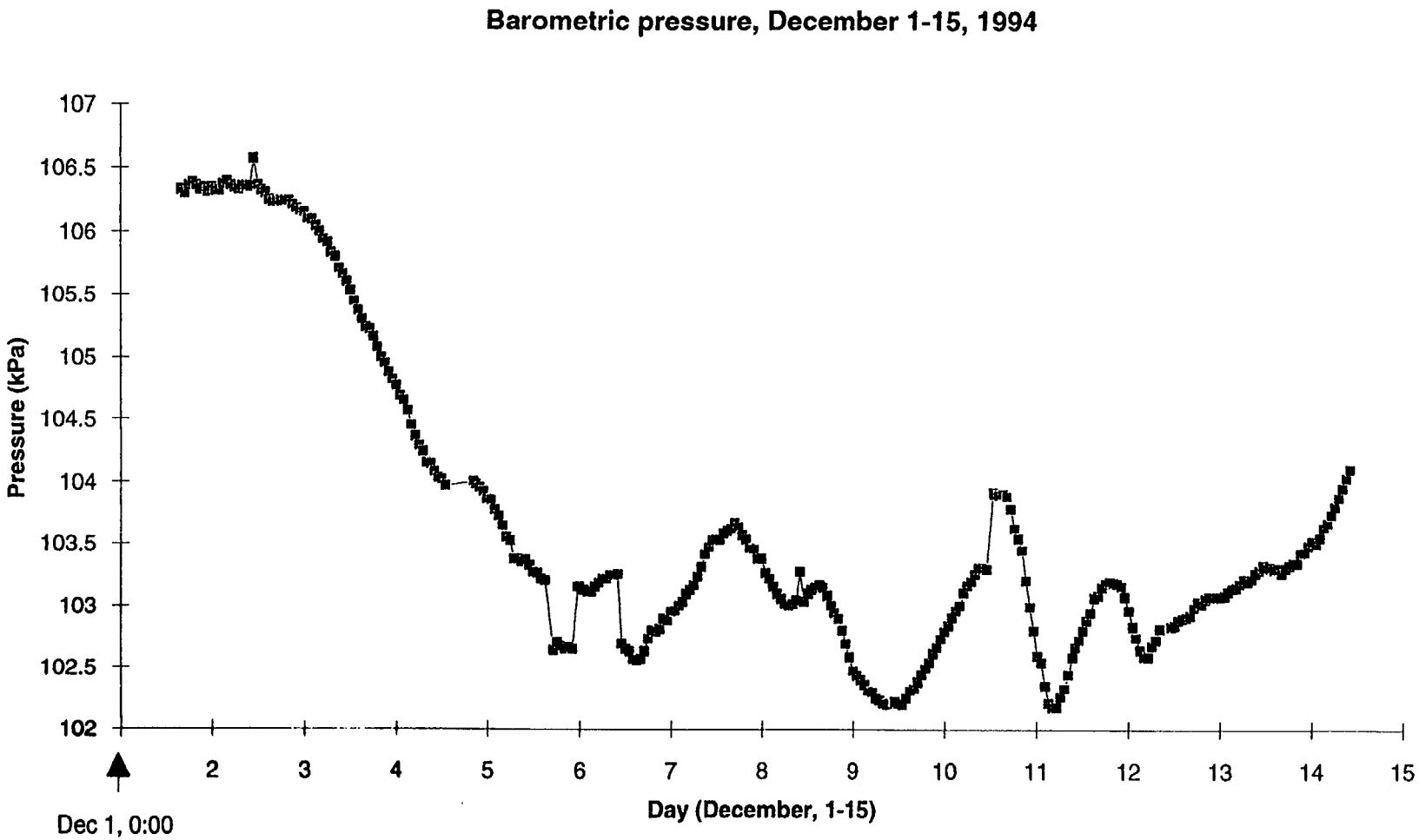
Barometric pressure, December 1-15, 1994
Pressure (kPa)
107
106.5
106
105.5
105
104.5
104
103.5
103
102.5
102
2
3
4
5
6
7
8
9
10
11
12
13
14
15
Day (December, 1-15)
Dec 1, 0:00

Fig. 3-17

PLOT TIME : 95-02-14 17: 44: 31
PLOT FILE : Tun_tempinout

ÄSPÖ HRL

Ventilation shaft temperature

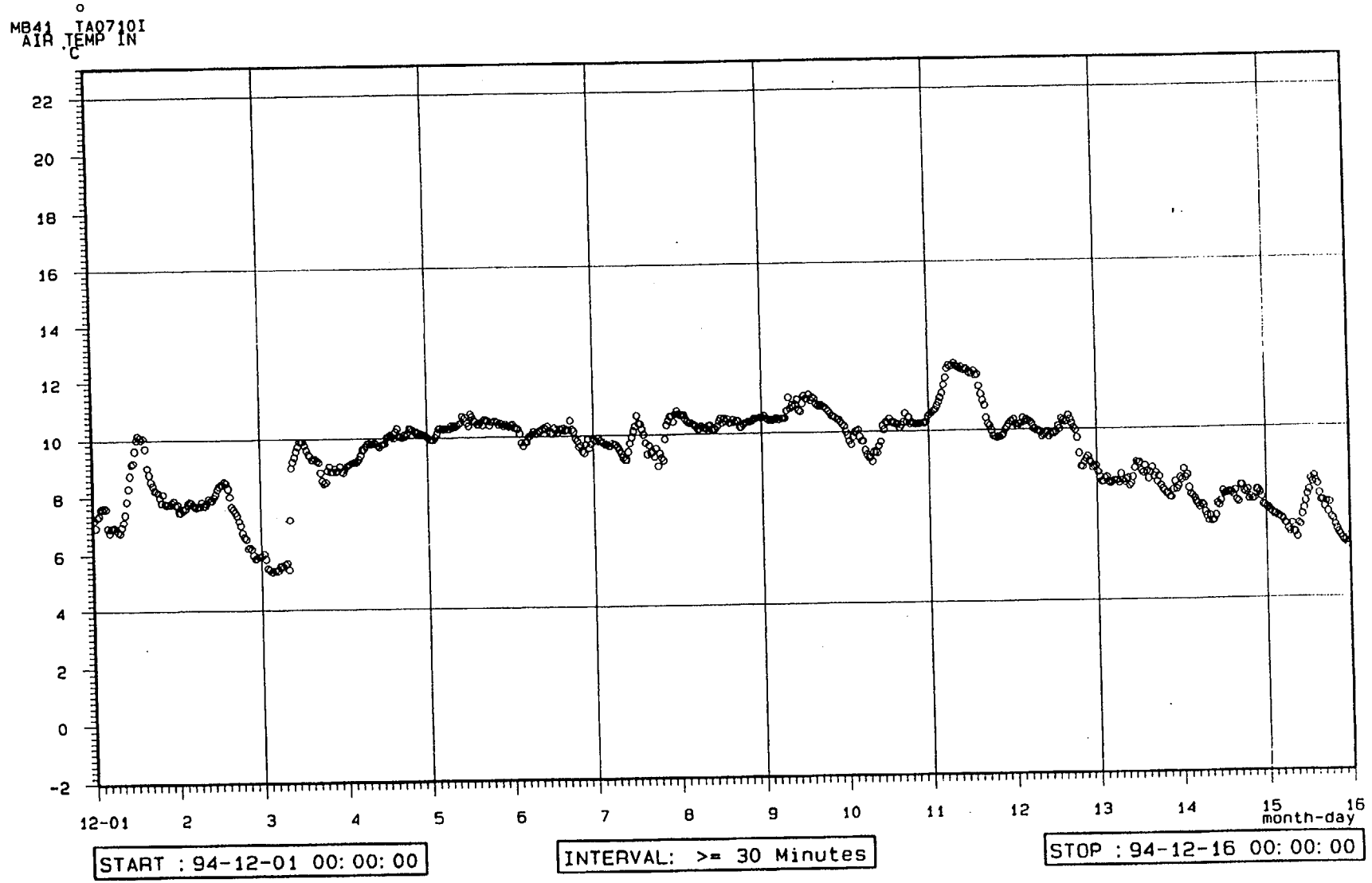

Fig. 3-18

C P T _ 1 , n = 3
K=1.2e-6 m/s, Ss=1.0e-3 1/m

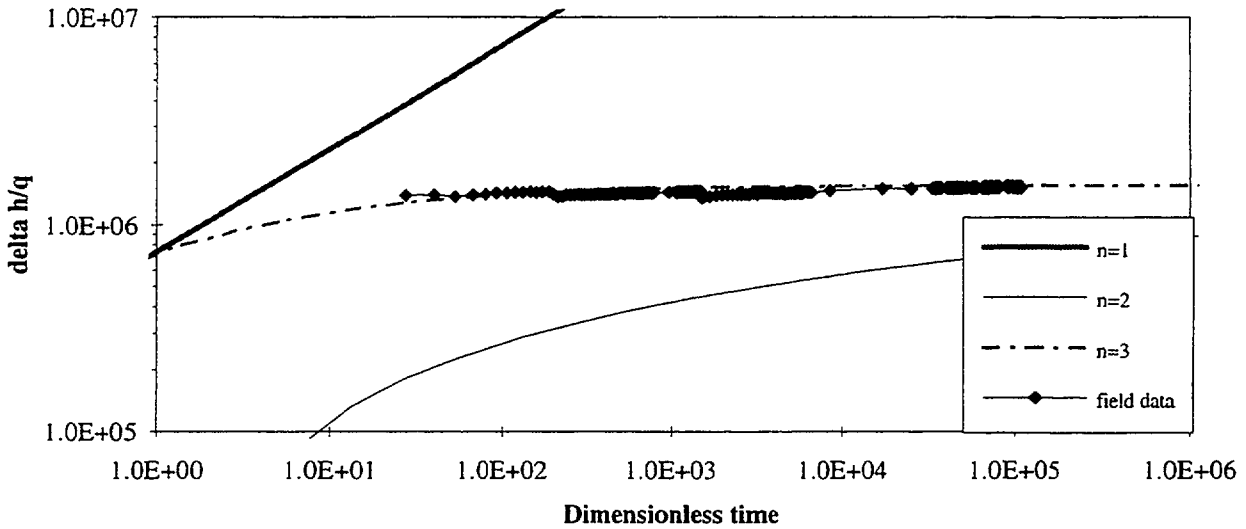

Fig. 3-19

C P T _ 2 , n = 3
K=1.1e-6 m/s, Ss=1.0e-3 1/m

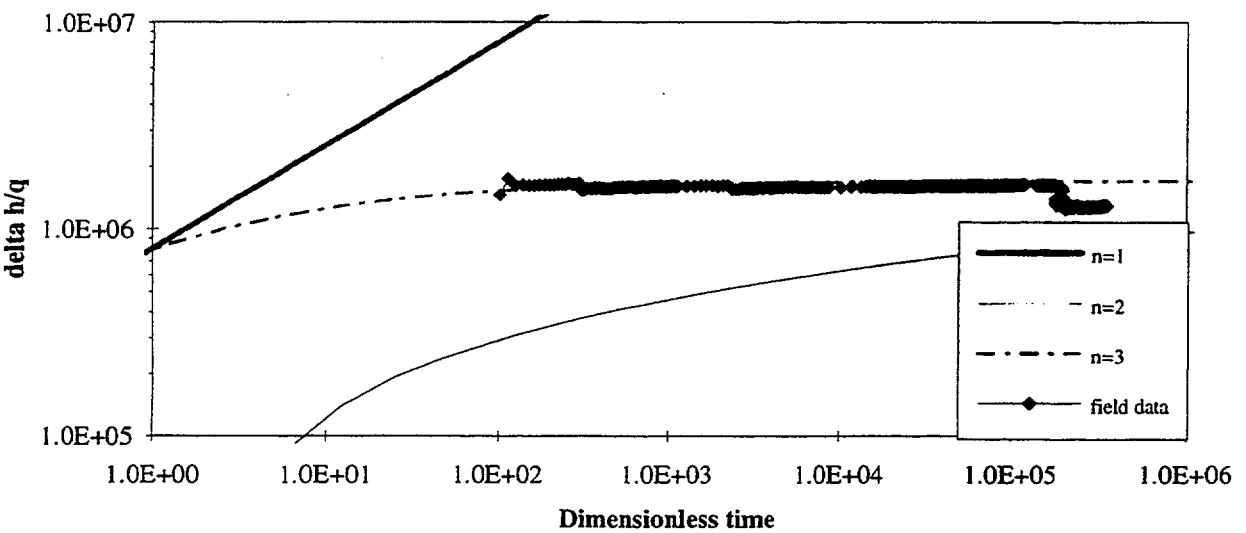

Fig. 3-20

C P T _ 3 , n = 3
K=1.1e-6 m/s, Ss=1.0e-3 1/m

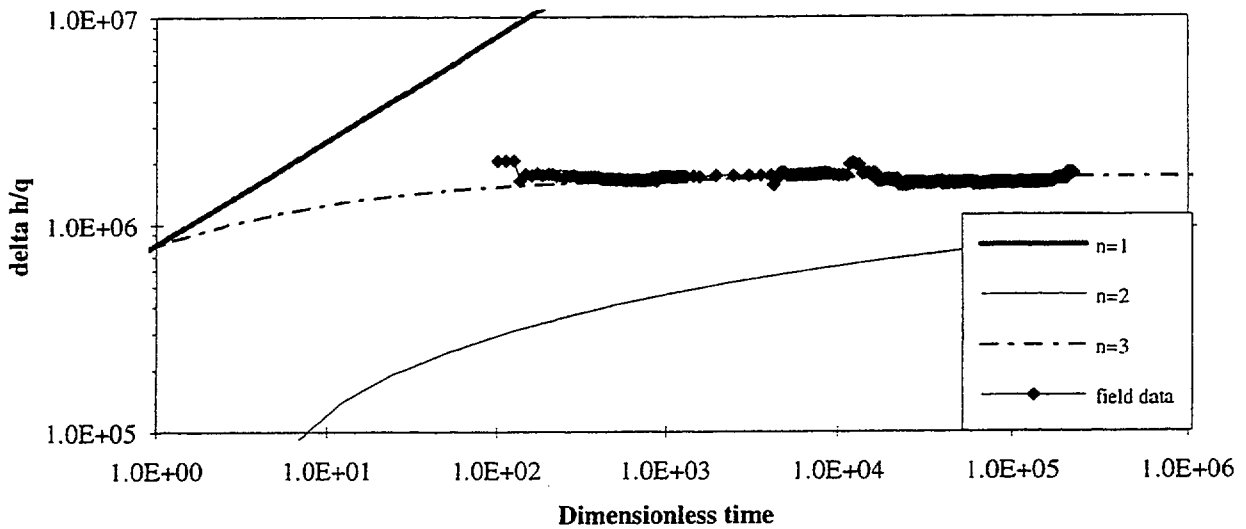

Fig. 3-21

C P T _ 4 , n = 3
K=1.0e-6 m/s, Ss=1.0e-3 1/m

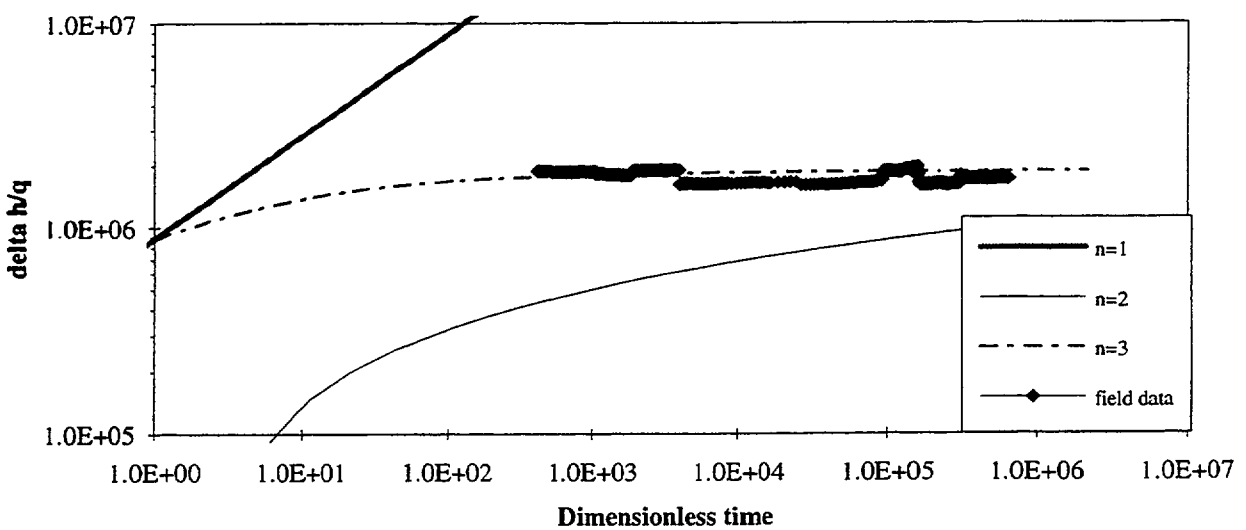

Fig. 3-22

C P T _ 6 , n = 3
K=1.4e-6 m/s, Ss=3.0e-4 1/m

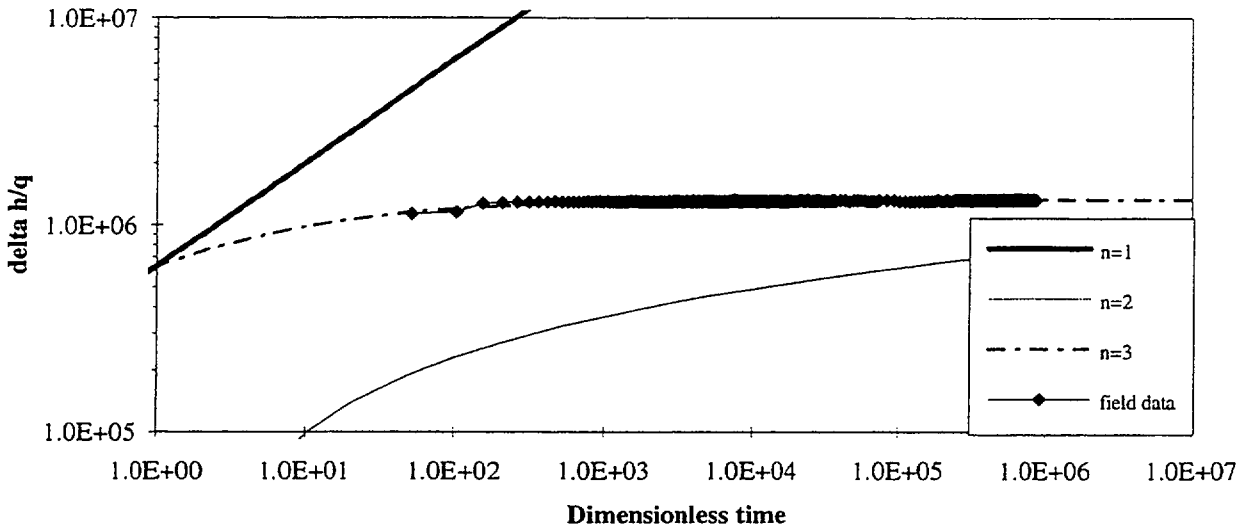

Fig. 3-23

C P T _ 7 , n = 3
K=1.2e-6 m/s, Ss=3.0e-4 1/m

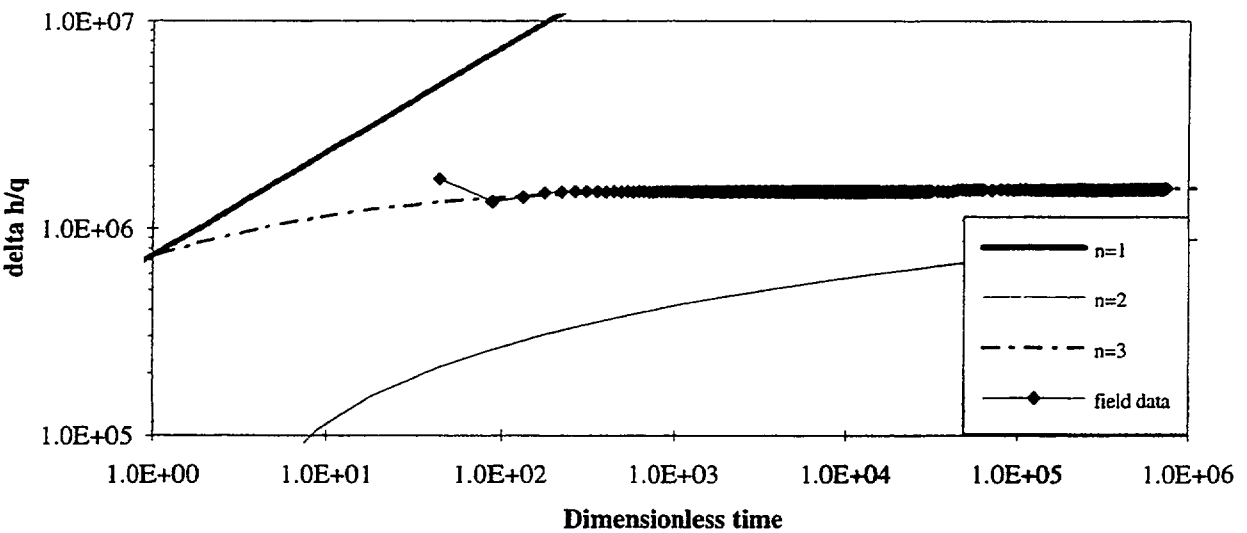

Fig. 3-24

C P T _ 8 , n = 3
K=1.1e-6 m/s, Ss=6.0e-5 1/m

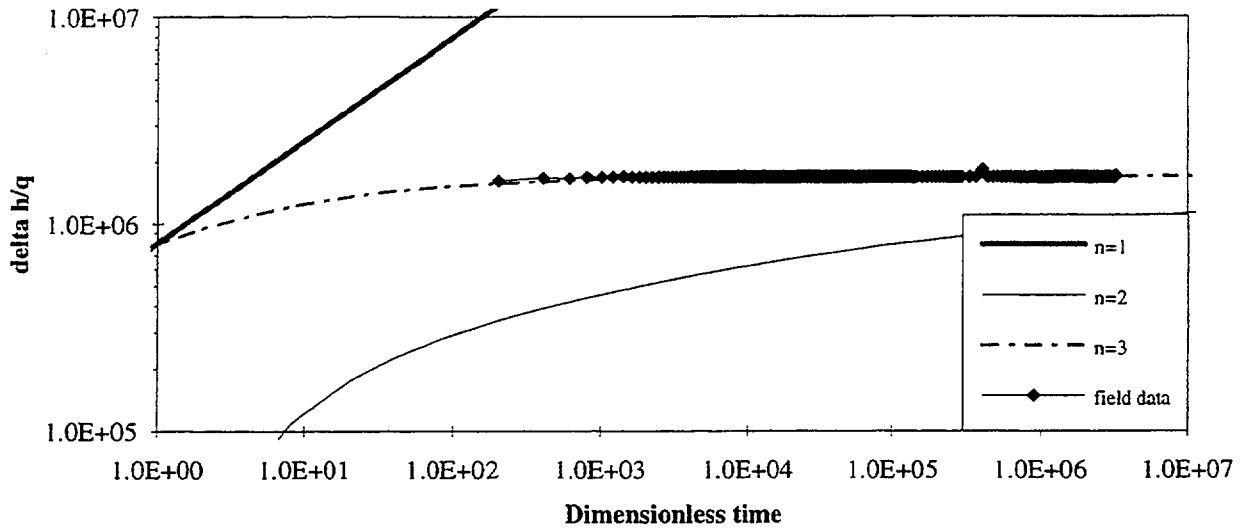

Fig. 3-25

C P T _ 9 , n = 3
K=1.2e-6 m/s, Ss=1.0e-4 1/m

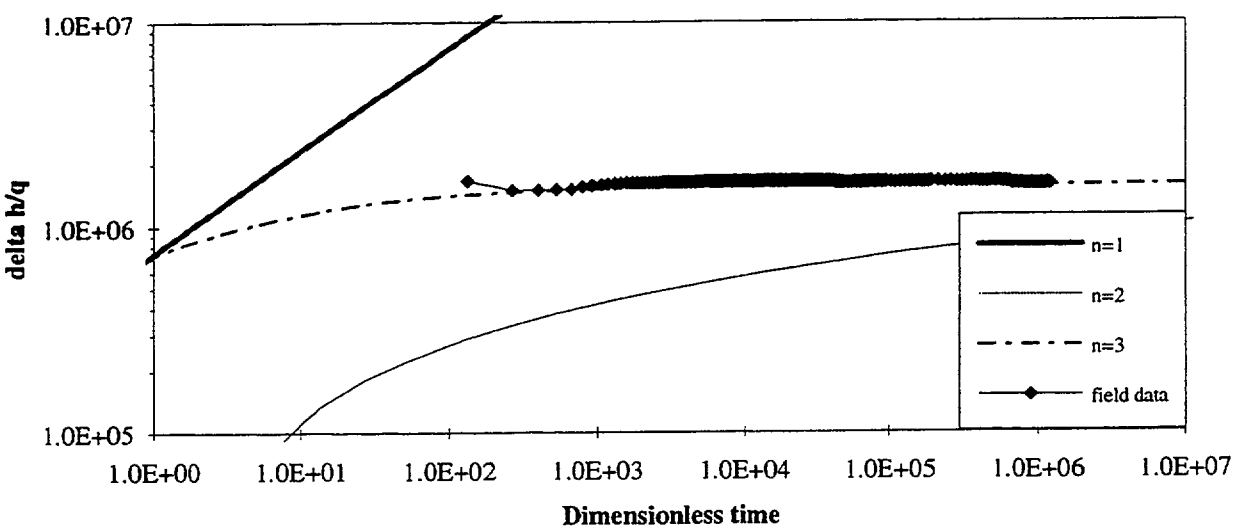

Fig. 3-26

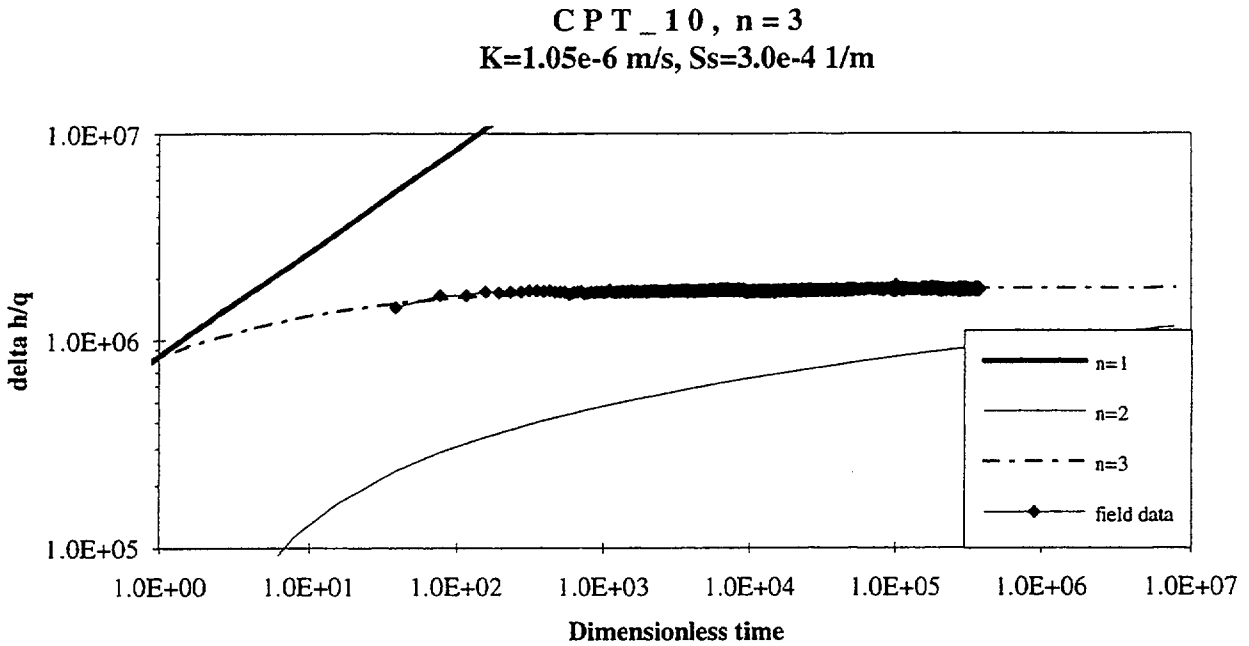

Fig. 3-27

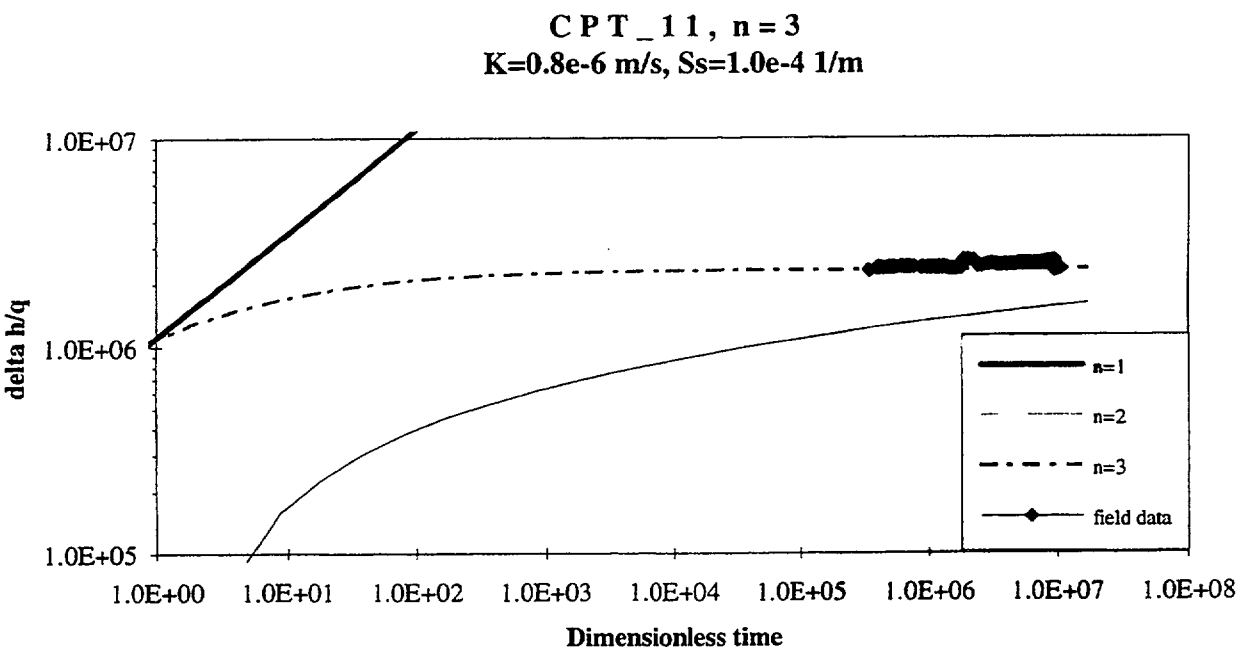

Fig. 3-28

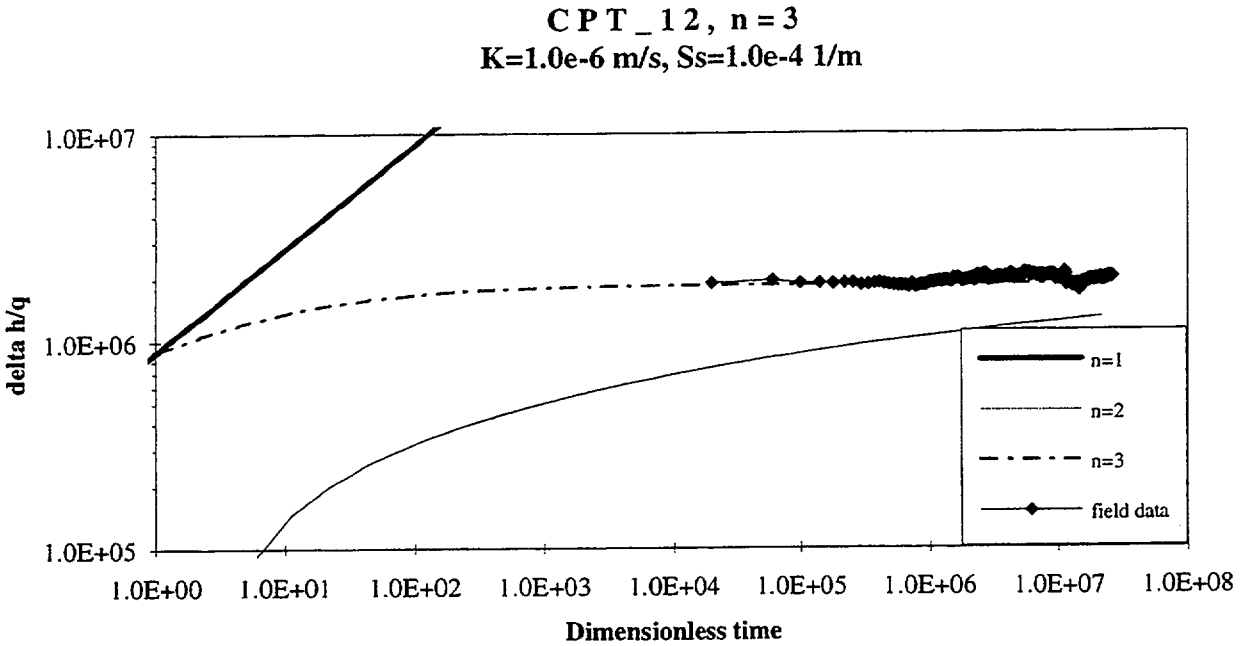

Fig. 3-29

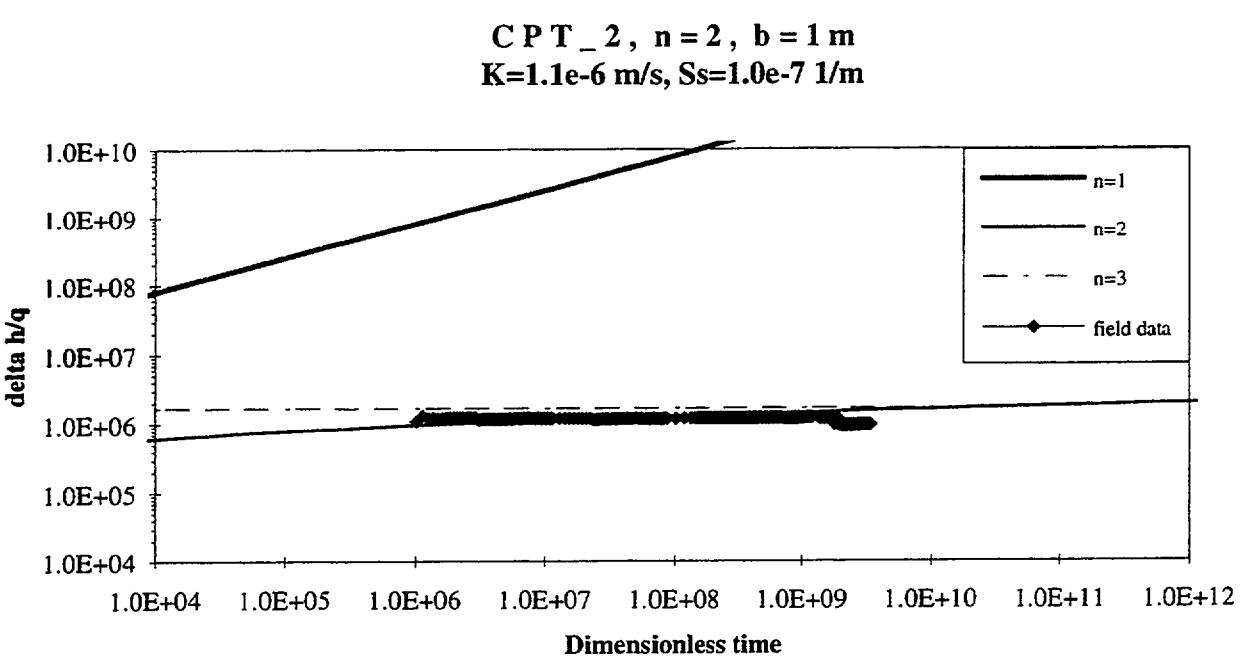

Fig. 3-30

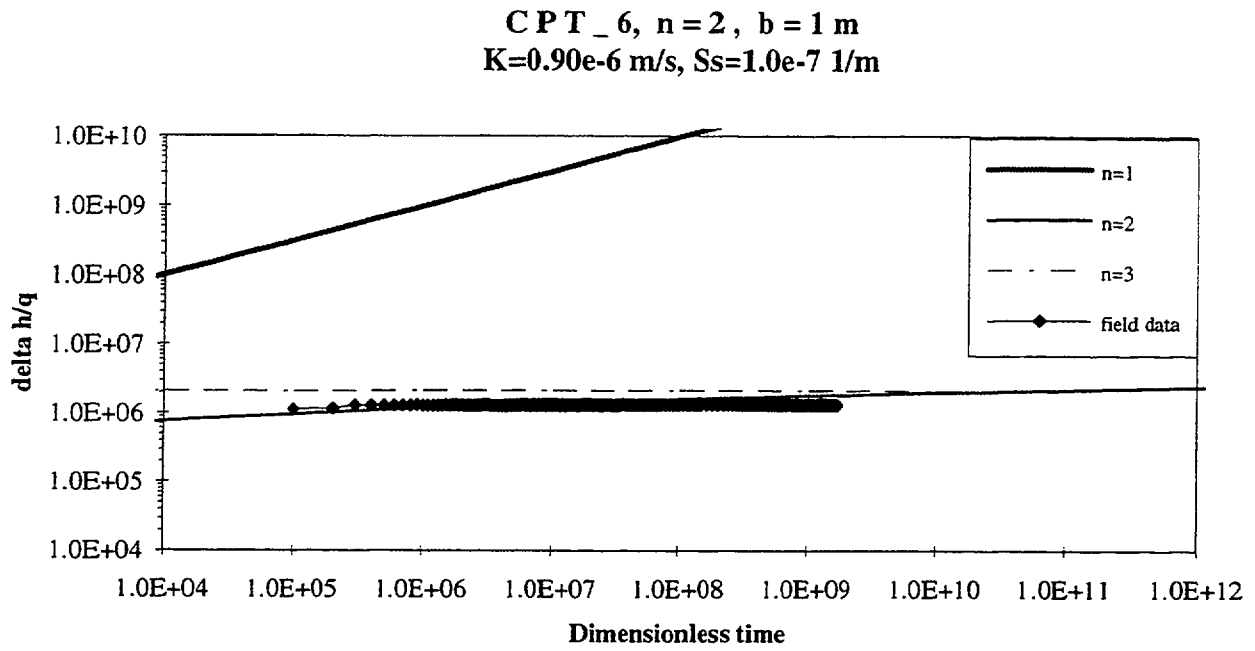

Fig. 3-31

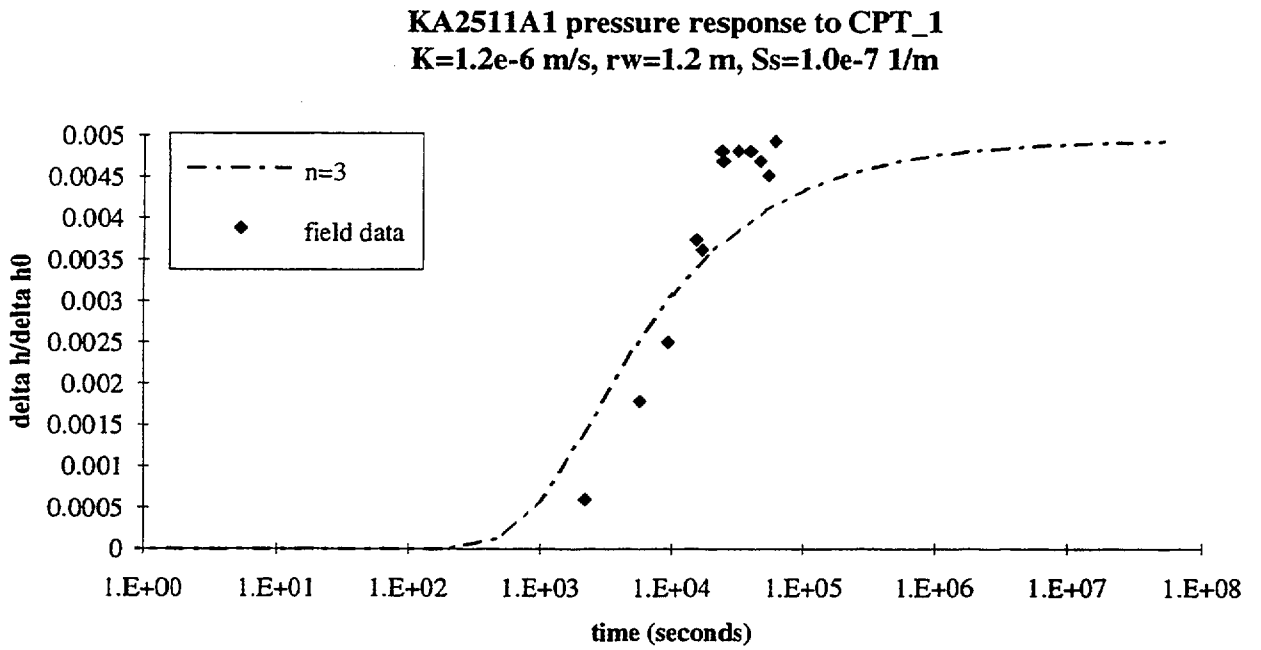

Fig. 3-32

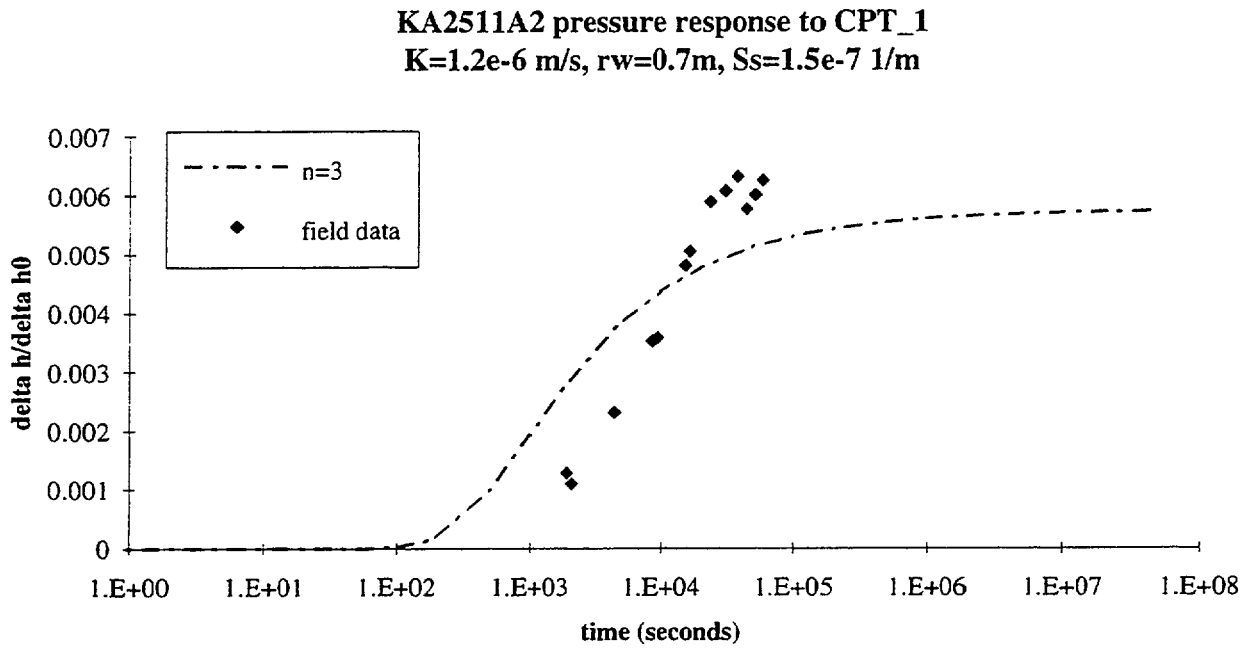

Fig. 3-33

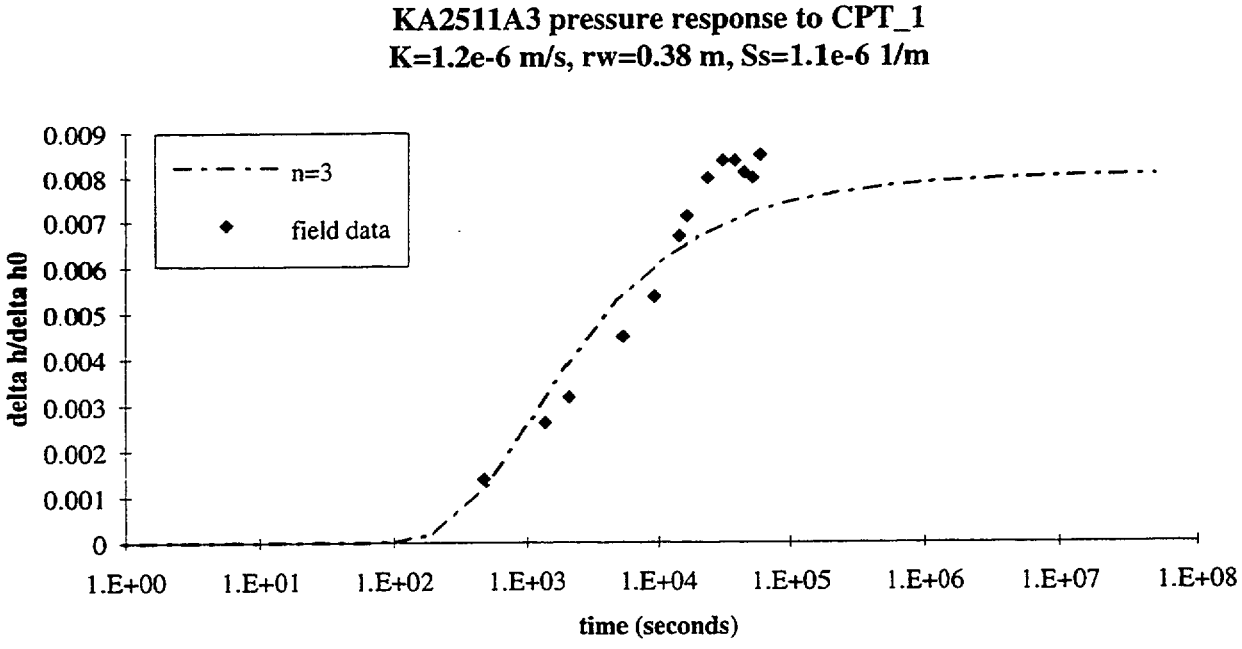

Fig. 3-34

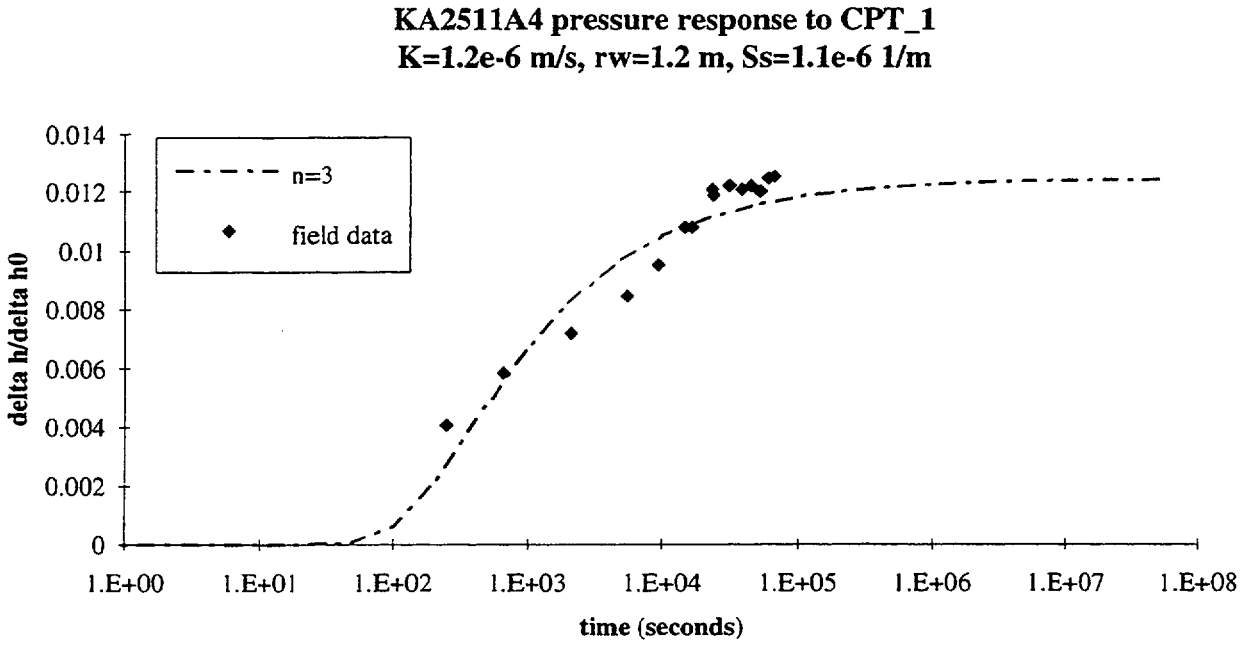
KA2511A4 pressure response to CPT_1
K=1.2e-6 m/s, rw=1.2 m, Ss=1.1e-6 1/m
n=3
field data
delta h/delta h0
0.014
0.012
0.01
0.008
0.006
0.004
0.002
0
1.E+00
1.E+01
1.E+02
1.E+03
1.E+04
1.E+05
1.E+06
1.E+07
1.E+08
time (seconds)

Fig. 3-35

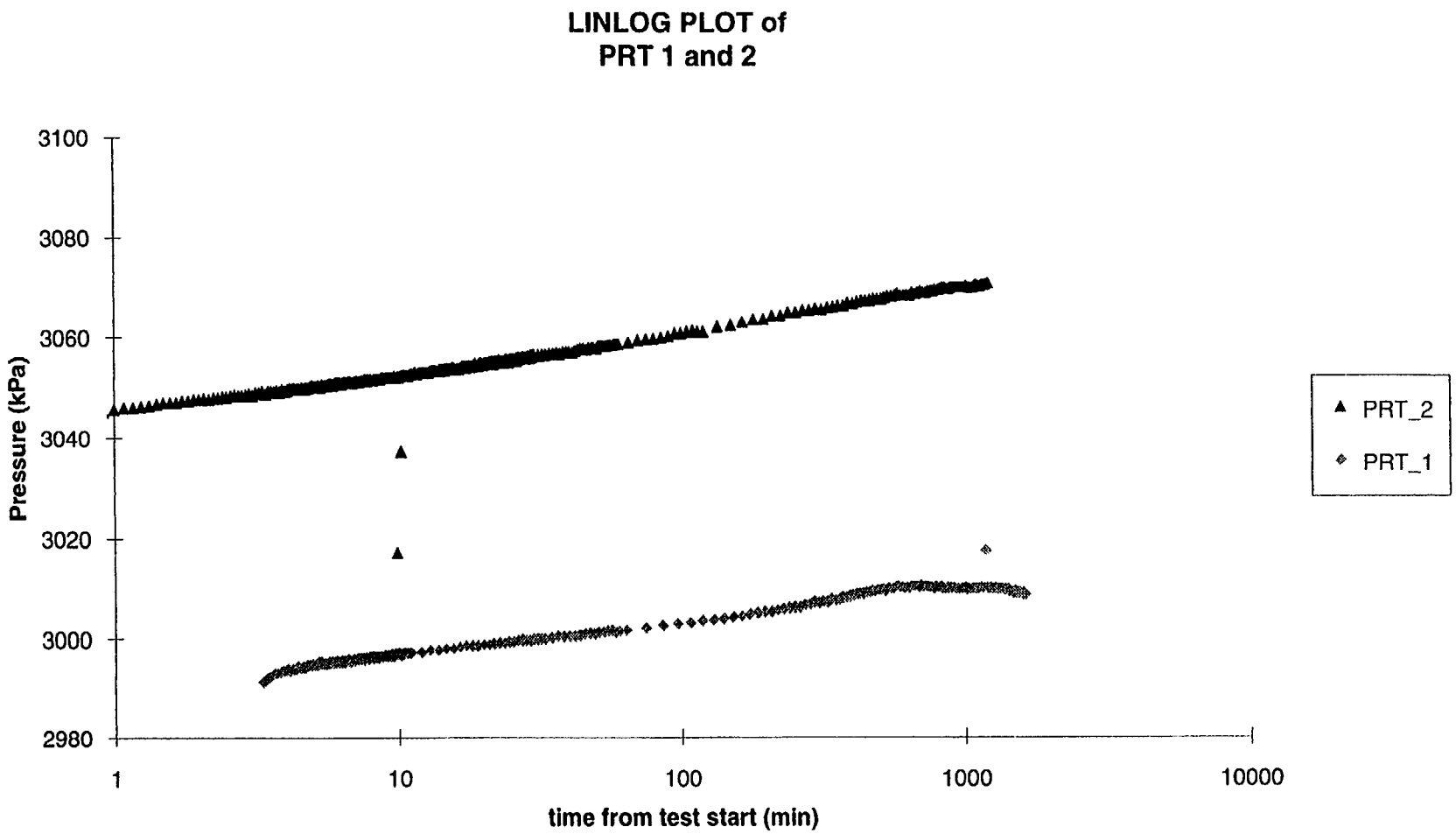
LINLOG PLOT of
PRT 1 and 2
3100
3080
3060
3040
3020
3000
2980
Pressure (kPa)
1
10
100
1000
10000
time from test start (min)
PRT_2
PRT_1

Fig. 3-36

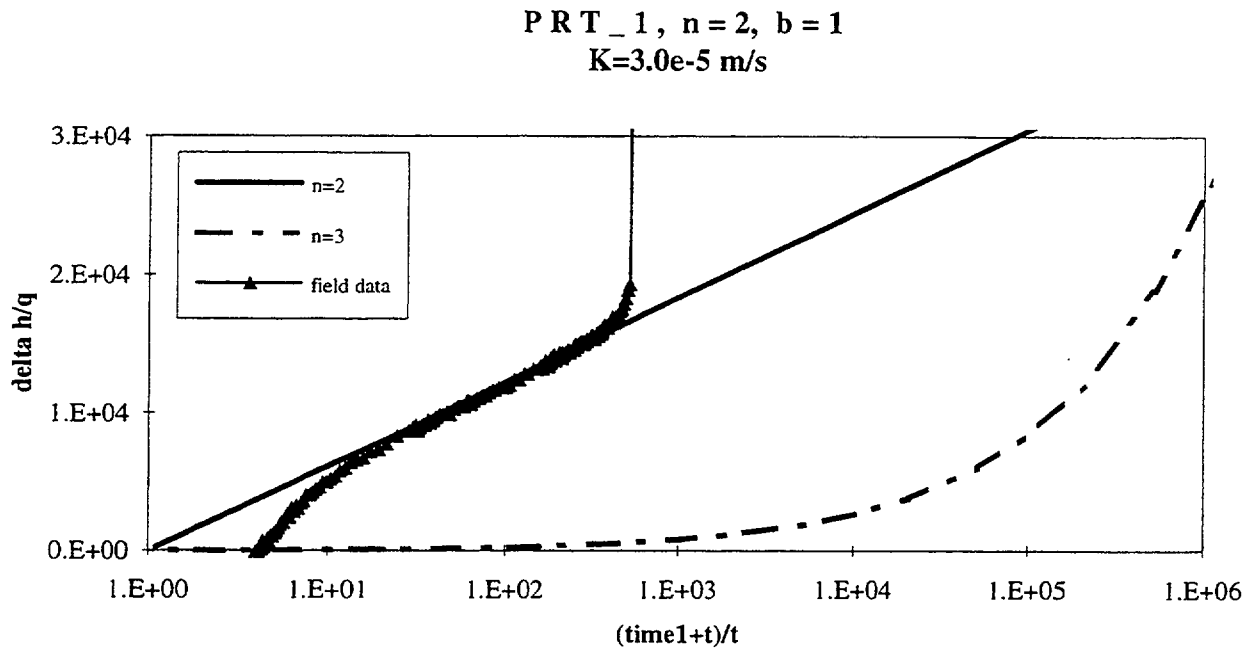

Fig. 3-37

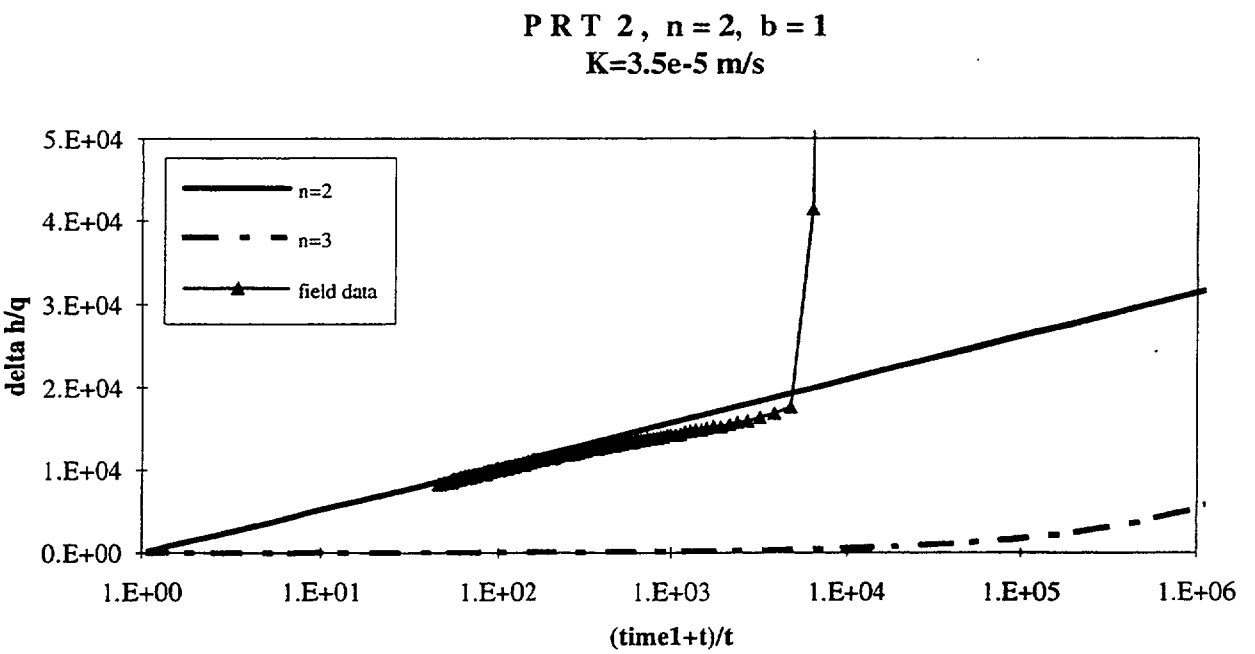

Fig. 3-38

P R T _ 1 , n = 3
K=1.2e-6 m/s, Ss=1e-3 1/m

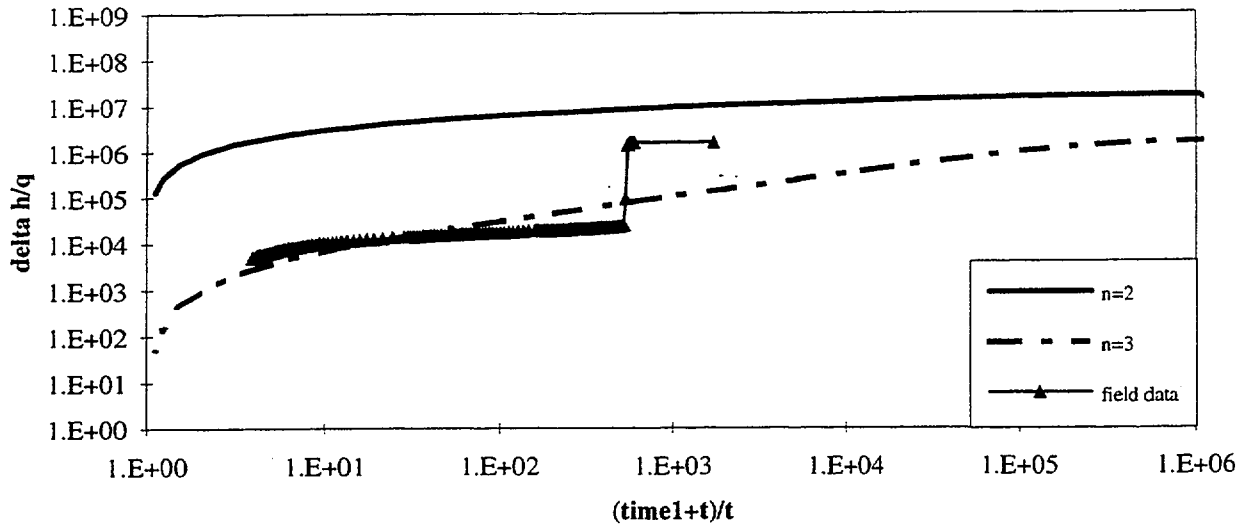

Fig. 3-39

P R T 2 , n = 3
K=1.1e-6 m/s, Ss=6.0e-5 1/m (as best fit for CPT_8)

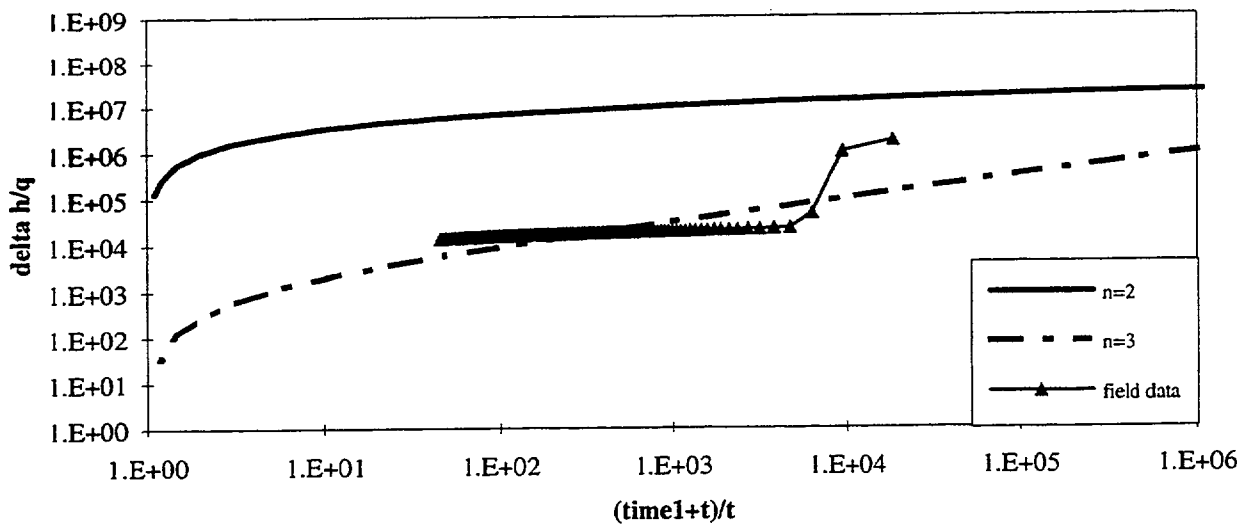

Fig. 3-40

4. CONCLUSIONS AND RECOMMENDATIONS

The pilot hole experiment tested the application of borehole inflow tests to measure the effects of groundwater degassing on hydraulic parameters when pressure is reduced. The test sequence was designed to detect degassing effects by comparing flow behavior above the bubble pressure where single-liquid-phase conditions definitely exist with borehole inflow below the bubble pressure where two-phase flow conditions may evolve.

The hydraulic conductivity measured in borehole KA2512A was constant for borehole pressures ranging from 1500 kPa (abs) to 120 kPa (abs) during tests conducted in December, 1994. The low gas contents measured in KA2512A during these tests (0.5% v/v STP) indicate that water pressures below the bubble pressure may not have been achieved with the equipment configuration used. The estimated bubble pressure at this gas content is about 130 kPa (abs), which is close to the estimated minimum pressure attained at the end of the borehole where the flowing fracture occurred. Previous values of total gas contents measured in other boreholes at Äspö were around 4%, which are within the range of values measured at Stripa where groundwater degassing effects were thought to have occurred. These gas contents would result in a bubble pressure on the order of 300 kPa(abs).

A constant pressure test conducted in January, 1995, indicated a 20% decrease in the hydraulic conductivity with a reduction in borehole pressure from 1500 kPa (abs) to 120 kPa (abs). The gas contents measured at this time were about twice as high (1% v/v) as in December, suggesting that degassing may have caused the flow reduction. Although not enough testing was done above the bubble pressure to exclude the possibility that the observed flow reduction was caused by a change in boundary conditions, the decrease in hydraulic conductivity is approximately two times the standard deviation of measurements made in December. These tests ran about ten times longer than the tests conducted in December 1994, however there was no net decrease in flowrate associated with time.

The findings of this experiment have important implications for further testing. Testing a borehole with low gas contents provided a fortuitous opportunity to assess other factors that might cause borehole inflow rates to decrease at lower borehole pressures. Calcite precipitation, turbulence and the increase of effective stress could all cause a decrease in flowrates at lower borehole pressures. It would be difficult to distinguish which low-pressure effect is significant because they all cause a reduction in transmissivity. As no decrease in flowrate was observed at low borehole pressures, we can conclude that these three effects did not occur to any

measurable degree. This should aid in the interpretation of future borehole inflow tests.

Single-well and cross-well analyses of transient test data were used to estimate hydraulic conductivity/ transmissivity and specific storage/ storativity of the formation. In addition, steady-state flowrates as a function of borehole pressures were used to estimate hydraulic conductivity. The single-well constant pressure tests and pressure recovery tests provided relatively good estimates of hydraulic conductivity, but the fast response of the system caused by the relatively high transmissivity led to non-unique fits between field data and the analytical solutions, which led to ambiguous estimates at the specific storage. The analytical solutions for pressure response at the monitoring well contain the hydraulic diffusivity, which is the ratio of the conductivity and the specific storage. These solutions, in combination with the hydraulic conductivity value obtained in the single-well analysis, provided unambiguous type-curve fits for the determination of the specific storage. This experience illustrates the importance of a pressure monitoring well in the vicinity of the test well for the estimation of hydraulic parameters. Furthermore, it was observed that different tests suggested different inflow geometries to the borehole, and depending on choice of flow geometry, the hydraulic conductivity values differed by one order of magnitude.

The above hydraulic diffusivity is an important parameter for detection of degassing effects in the field. Two-phase conditions should cause a decrease in hydraulic conductivity and an increase in specific storage, resulting in a large overall decrease in the hydraulic diffusivity. Consequently, the change in this parameter relative to single-phase conditions should be readily detectable even if an absolute value of storativity cannot be measured with confidence. The requirement to use changes in the storativity and hydraulic conductivity to detect two-phase conditions reinforces the need of a thorough characterization of single-phase flow conditions before reducing borehole pressure below the bubble pressure.

A gas sampling tube was developed for measuring the volume of evolved gas from groundwater samples acquired under pressure. This device is connected to a valve on the borehole casing with a valve on the other end to maintain pressure. Once the sample is obtained, the pressure is relieved and the volume of gas evolving is measured from the length of the gas bubble in the translucent portion of the tube. In the continued use of this sampler, evolved gas volumes should be measured at 15-minute intervals to determine the optimum time required for the dissolved gas to come out of solution. Our experience indicates that a 2-hour equilibration time is adequate, however further calibration of this device is recommended.

Future degassing tests should be conducted in a borehole with significantly higher gas contents than in KA2512A. Experimental results by Geller et al. (1995) indicate that fracture geometry has a first order effect on flow reduction due to degassing and that gas content is a second order effect. However, the relationship between degassing effects and such low gas contents measured in KA2512A has not been tested and it is possible that flowrate changes cannot be detected at such low values. In order to test the degassing hypothesis with greater confidence, gas contents should be closer to the values measured at Stripa, where degassing is hypothesized to have caused the observed flow reductions.

A series of consistent gas content measurements should be performed in order to increase the understanding of the significant spatial and temporal variability of gas contents indicated by measurements in the pilot hole and in other boreholes. The test series should include repeated volumetric gas content measurements and chemical analysis in several boreholes as a function of borehole inflow volume to detect changes with time and location. The measurements reported here suggest that elevated dissolved gases occur in the near-borehole and that the gas content of the formation water away from the borehole is lower. If this is the case, then gas contents in water sampled from a borehole that has been shut-in for a long time should be higher than in water sampled from a flowing borehole, as indicated by the data in this report. Laboratory analysis shows that over 70% of the dissolved gas is nitrogen and that the nitrogen is of atmospheric origin. Biogenic gases (CO_2 and CH_4) and radiogenic He, make up most of the remaining fraction. The bubble pressures of CO_2 and CH_4 are much lower than atmospheric pressure, consequently only nitrogen, and possibly helium, are expected to evolve at atmospheric pressure.

The experience of the pilot hole test has shown that for low gas contents and with a standard borehole configuration, the groundwater pressure in the fracture may not be reduced to below the bubble pressure. The order-of-magnitude flow reductions measured at Stripa were for water flowing into the drift where the fractures were directly subjected to atmospheric pressure, allowing pressures below the bubble pressure to exist in the formation. Due to the dip of KA2512A and frictional losses during flow, the pressure at the fracture intersection with the borehole was greater than atmospheric pressure. The test equipment should be configured to ensure that pressures below the bubble pressure of the groundwater are obtained in the formation. Lower borehole pressures can be achieved by maintaining a water-filled drain line and extending it to an elevation significantly lower than the test borehole.

Another consideration in borehole selection is the transmissivity of the fracture and its characteristic geometry. Degassing is most likely to cause measurable effects in rough, relatively tight fractures where gas can be

trapped, as compared to smooth, highly transmissive fractures that do not provide conditions for gas trapping and subsequent flow reduction.

In addition to the degassing problem, there are compelling reasons to continue the investigation of two-phase flow effects at Äspö. Groundwater degassing may be important at other sites. Other two-phase flow effects can interfere with the interpretation of hydrologic tests from excavations, such as ventilation and air invasion. Two-phase flow studies are also relevant to the prediction of repository performance following closure in terms of resaturation rates and the fate of waste-generated gas.

Injection-withdrawal tests using gas-saturated water should be considered to demonstrate the occurrence of flow reduction in the presence of higher gas contents. Changes in hydrologic properties of the test region are then measured for controlled boundary conditions due to the presence of the gas phase and as resaturation occurs. The tests could be conducted from a single hole, or as a dipole test, where two wells intersect the same fracture. Much greater flexibility in test design and control of boundary conditions would exist for the dipole test configuration. Subsequent testing should also include air injection for the determination of two-phase flow parameters.

REFERENCES

Almén, K.E., Andersson, J.E., Carlsson, L, Hansson K. and Larsson N.Ä., 1986. Hydraulic testing in crystalline rock. A comparative study of single-hole test methods. SKB Technical Report 86-27, Stockholm.

Andres, J.N., Hussain, N. and Youngman, M.J., 1989. Atmospheric and radiogenic gases in groundwaters from the Stripa granite. Geochemica et Cosmochimica Acta, Vol 53, pp 1831-1841.

Arvidsson, L., 1994. Elkraftteknik VU-EP, Vattenfall utveckling, report no. 219-224.94, Project no 34002, March 23, 1994.

Barker, J.A., 1988. A general radial flow model for hydraulic tests in fractured rock. Water Resour. Res, Vol 10, pp 1796-1804.

Carslaw, H.S. and Jaeger, J.C., 1959. Conduction of heat in solids. Oxford University Press, 2nd edition, pp 54 and 257.

Doughty, C., 1995. Personal communication. Earth Sciences Division, Lawrence Berkeley Laboratory, Berkeley, California.

Earlougher, R.C., Jr., 1977. Advances in well test analysis. Soc. Pet. Engr. Monograph Series, Vol 5, SPE, Dallas.

Gass, R. and Ramqvist, G., 1995. Degassing of ground-water and two phase flow, Technical Note, Drilling under formation pressure, March 1995.

Gass et al., 1995. (core logging report for KA2512A) (in preparation).

Geller, J.T., Doughty C., Glass R.J. and Long, J.C.S., 1995. Disturbed zone effects: Two-phase flow in fractures of regionally water-saturated crystalline rock, FY94 annual report to the International Program under the cooperative agreement between SKB and U.S. DOE Radioactive Waste Management (LBL-36848).

Gentzschein, B., 1993. Frontborre: mätning och handhavande. In: Nyberg, G., Manual för Hydro Monitoring System (HMS), del 1:1. SKB Tekniskt PM nr 25-94-014, Äspö HRL.

Horner, D.R., 1951. Pressure buildup in wells. Proc. Third World Pet. Cong., The Hague, Sect II, pp 503-523.

Jacob, C.E., and Loman, S.W., 1952. Nonsteady flow to a well of constant drawdown in an extensive aquifer. Trans., Am. Geophys. Union, Vol 33, pp 559-569.

Kennedy, B.M., 1995. Earth Sciences Division, Lawrence Berkeley Laboratory, personal communication.

Lif, M., 1993. Elkraftteknik VU-EP, Vattenfall utveckling, report no. 1113.93, project no. 33116, December 7, 1993.

Long, J.C.S., Olsson, O., Martel, S. and Black, J., 1992. Effects of excavation on water inflow to a drift. Proceedings of the U. S. Rock Mechanics Meeting, Lake Tahoe, CA..

Mishra, S., 1992. Methods for analyzing single- and multi-well hydraulic test data. In: Vomvoris, S. and Frieg, B. (eds), Interpretation of crosshole hydraulic tests and a pilot fluid logging test for selected boreholes within the BK.-site. NAGRA Technical Report 91-09.

Nyberg, G., Jönsson, S. and Ekman, L., 1994. Groundwater level program report for 1993, SKB Progress Report 25-94-23, Äspö HRL, pp 40.

Olsson, O., ed, 1992. Site characterization and validation - final report, Stripa Project Technical Report 92-22, Swedish Nuclear Fuel and Waste Management Co., Stockholm, Sweden, 364 pp.

Pedersen, K., 1995. Personal communication.

SKB-TR 90-05

Theis, C.V., 1935. The relation between the lowering of the piezometric surface and the rate and duration of discharge of a well using ground-water storage. Am. Geophys. Union Trans. 16, pp 519-524.

APPENDIX I

Estimation of gas contents and bubble pressure

Henry's Law describes the equilibrium of a species between the gas and liquid phases as follows:

$$P_g = Hx_g$$

where P_g is the partial pressure (absolute) of species g in the gas phase, H is Henry's Law constant, and x_g is the mole fraction of species g in the liquid phase.

At Stripa, gas bubbles were observed in the borehole after the pressure was decreased from 800 to 270 kPa(abs). Assuming nitrogen is the main component of the gas and H equals 6.77 x 10^6 kPa (mole fraction)$^{-1}$ at 10°C, Henry's Law predicts a gas contents of 3.4 to 5.9% v/v STP if the gas evolves at 270 to 400 kPa(abs) respectively. Measurements of dissolved gas concentrations reported by Andres et al. (1989) were approximately 4% consisting mainly of nitrogen of atmospheric origin. Dissolved nitrogen concentrations of atmospheric origin in groundwater can be higher than surface water equilibrated with the atmosphere because of the dissolution of residual air in the formation at higher pressures. Andres et al. (1989) did not report any values for CO_2, O_2 or CH_4.

At HRL, Pedersen (1993) reported a value of 3.8% total gas contents in borehole KA2598A; 74% of the gas was N_2, 12% was CO_2, 4% was H_2+He, 2% was O_2, 0.3% was CH_4 and the rest unidentified. Gas contents measured in surface boreholes at depths of 200 to 400m range from 3.9 to 5.4% (SKB-TR-90-5), where N_2 is the major component of the gas. The estimates of the bubble pressure of the dissolved gas in KA2512A are bracketed for total gas contents of 3.5 to 5% using Henry's Law constants for nitrogen in both pure water and water with 15% chlorinity. The values are summarized in Table I-1 :

Table I- 1. Estimate of bubble pressure in borehole KA2512A

Percent Chlorinity	*H* (kPa/mole fraction, 10°C)	Bubble Pressure (kPa, abs) 3.5% gas v/v STP	5.0% gas v/v STP
0	6.77×10^6	292	373
15	8.14×10^6	330	428

APPENDIX II

Table II-1. Record of blasting activities during pilot hole test

Date	Time	Tunnel Length (m)	Comments
11/30/94	11:14	3370	niche, 4 m
11/30/94	14:30	3370	ceiling
11/30/94	20:05	3370	niche, ~4 m
12/01/94	10:43	3370	niche, ~3 m
12/05/94	16:30	3450/3490	floor
12/05/94	19:45	3450/3490	reblast
12/06/94	11:17	3503/3505	broadening
12/06/94	19:55	3503/3505	broadening
12/07/94	14:05	3503/3505	broadening
12/08/94	16:15	3503/3505	broadening
12/12/94	12:38	?	?
12/13/94	19:53	3500	left niche
12/14/94	15:13	3500	left niche

Table II-2. Record of blasting from January 9 to February 6, 1995

Date	Time	Number	Comments
01/09/95	09:40	salva #215	
01/10/95	12:52	" #216	
01/10/95	21:25	" #B2	Bomsalva
01/11/95	13:11	" B2	Omskjutning
01/12/95	01:35	" Z1	Z = ZEDEX
01/12/95	12:54	" #218	
01/12/95	13:03	" Z1	Omskjutning
01/12/95	23:40	" Z2	
01/13/95	12:25	" #219	
01/13/95	12:19	" Z2	Omskjutning
01/14/95	01:55	" Z3	
01/15/95	22:00	" Z4	
01/16/95	11:55	" Z4	Omskjutning
01/16/95	13:15	" #220	
01/16/95	21:50	" Z5	
01/17/95	10:05	" #221	
01/17/95	19:48	" #222	
01/17/95	19:52	" Z6	
01/18/95	10:45	" #223	
01/18/95	12:15	" Z6	Omskjutning
01/18/95	20:18	" #224	
01/19/95	10:19	" #225	
01/20/95	08:30	" #226	
01/23/95	11:16	" #227	
01/24/95	10:48	" #228	
01/24/95	20:30	" 229	
01/25/95	11:09	" #230	
01/25/95	20:50	" 231	
01/26/95	09:45	" #226	
01/26/95	19:50	" #233	
01/26/95	21:03	" Z7	
01/27/95	10:50	" #234	
01/27/95	22:20	" Z8	

Table II-2. (cont'd.)

01/28/95	10:30	" Z8	Omskjutning
01/28/95	23:10	" Z9	
01/30/95	17:36	" #235	
02/01/95	12:15	" #236	
02/01/95	16:00	" #237	Trappschakt
02/01/95	22:00	" #238	"
02/02/95	07:30	" 239	"
02/02/95	10:10	" #240	"
02/02/95	13:20	" #241	"
02/02/95	17:00	" #247	
02/04/95	15:04	" 243	
02/05/95	15:10	" 244	
02/06/95	09:00	" #245	

Z* = Blasting in tunnel

List of International Cooperation Reports

ICR 93-01
Flowmeter measurement in borehole KAS 16
P Rouhiainen
June 1993
Supported by TVO, Finland

ICR 93-02
Development of ROCK-CAD model for Äspö Hard Rock Laboratory site
Pauli Saksa, Juha Lindh,
Eero Heikkinen
Fintact KY, Helsinki, Finland
December 1993
Supported by TVO, Finland

ICR 93-03
Scoping calculations for the Matrix Diffusion Experiment
Lars Birgersson[1], Hans Widén[1],
Thomas Ågren[1], Ivars Neretnieks[2],
Luis Moreno[2]
1 Kemakta Konsult AB, Stockholm, Sweden
2 Royal Institute of Technology, Stockholm, Sweden
November 1993
Supported by SKB, Sweden

ICR 93-04
Scoping calculations for the Multiple Well Tracer Experiment - efficient design for identifying transport processes
Rune Nordqvist, Erik Gustafsson,
Peter Andersson
Geosigma AB, Uppsala, Sweden
December 1993
Supported by SKB, Sweden

ICR 94-01
Scoping calculations for the Multiple Well Tracer Experiment using a variable aperture model
Luis Moreno, Ivars Neretnieks
Dept. of Chemical Engineering and Technology,
Royal Institute of Technology, Stockholm, Sweden
January 1994
Supported by SKB, Sweden

ICR 94-02
Äspö Hard Rock Laboratory. Test plan for ZEDEX - Zone of Excavation Disturbance EXperiment. Release 1.0
February 1994
Supported by ANDRA, NIREX, SKB

ICR 94-03
The Multiple Well Tracer Experiment - Scoping calculations
Urban Svensson
Computer-Aided Fluid Engineering
March 1994
Supported by SKB, Sweden

ICR 94-04
Design constraints and process discrimination for the Detailed Scale Tracer Experiments at Äspö - Multiple Well Tracer Experiment and Matrix Diffusion Experiment
Jan-Olof Selroos[1], Anders Winberg[2], Vladimir Cvetkovic[2]
1 Water Resources Eng., KTH
2 Conterra AB
April 1994
Supported by SKB, Sweden

ICR 94-05
Analysis of LPT2 using the Channel Network model
Björn Gylling[1], Luis Moreno[1], Ivars Neretnieks[1], Lars Birgersson[2]
1 Department of Chemical Engineering and Technology, Royal Institute of Technology, Stockholm, Sweden
2 Kemakta Konsult AB, Stockholm, Sweden
April 1994
Supported by SKB, Sweden

ICR 94-06
SKB/DOE Hard Rock Laboratory Studies Task 3. Geochemical investigations using stable and radiogenic isotopic methods
Bill Wallin[1], Zell Peterman[2]
1 Geokema AB, Lidingö, Sweden
2 U.S. Geological Survey, Denver, Colorado, USA
January 1994
Supported by SKB and U.S.DOE

ICR 94-07
Analyses of LPT2 in the Äspö HRL with continuous anisotropic heterogeneous model
Akira Kobayashi[1], Ryo Yamashita[2], Masakazu Chijimatsu[2], Hiroyuki Nishiyama[3], Yuzo Ohnishi[3]
1 Iwate University, Iwate, Japan
2 Hazama Corporation, Ibaraki, Japan
3 Kyoto University, Kyoto, Japan
September 1994
Supported by PNC, Japan

ICR 94-08
Application of three-dimensional smeared fracture model to the groundwater flow and the solute migration of LPT-2 experiment
T Igarashi, Y Tanaka, M Kawanishi
Abiko Research Laboratory, Central Research Institute of Electric Power Industry, Abiko, Japan
October 1994
Supported by CRIEPI, Japan

ICR 94-09
Discrete-fracture modelling of the Äspö LPT-2, large-scale pumping and tracer test
Masahiro Uchida[1], Thomas Doe[2], William Dershowitz[2], Andrew Thomas[2], Peter Wallmann[2], Atsushi Sawada[1]
1 Power Reactor and Nuclear Fuel Development Co., Tokai, Japan
2 Golder Associates Inc., Seattle, WA, USA
March 1994
Supported by PNC, Japan

ICR 94-10
Äspö Hard Rock Laboratory
International workshop on the use of tunnel boring machines for deep repositories
Äspö, June 13-14 1994
Göran Bäckblom (ed.)
Swedish Nuclear Fuel and Waste Management Co.
October 1994
Supported by SKB, Sweden

ICR 94-11
Data analysis and modelling of the LPT2 Pumping and Tracer Transport Test at Äspö.
Tracer experiment
Aimo Hautojärvi
VTT Energy
November 1994
Supported by TVO, Finland

ICR 94-12
Modelling the LPT2 Pumping and Tracer Test at Äspö. Pumping test
Veikko Taivassalo, Lasse Koskinen,
Mikko Laitinen, Jari Löfman, Ferenc Mészáros
VTT Energy
November 1994
Supported by TVO, Finland

ICR 94-13
Proceedings of The Äspö International Geochemistry Workshop, June 2-3, 1994, Äspö Hard Rock Laboratory
Peter Wikberg (chairman), Steven Banwart (proc. ed.)
December 1994
Supported by SKB, TVO, Nirex, ANDRA, CRIEPI

ICR 94-14
Hydrodynamic modelling of the Äspö HRL. Discrete fracture model
D Billaux[1], F Guérin[2], J Wendling[2]
1 ITASCA
2 ANTEA
November 1994
Supported by ANDRA, France

ICR 94-15
Hydrodynamic modelling of the Äspö Hard Rock Laboratory. ROCKFLOW code
M L Noyer, E Fillion
ANTEA
December 1994
Supported by ANDRA, France

ICR 94-16
Hydrodynamic modelling of the original steady state and LPT2 experiments. MARTHE and SESAME codes
Y Barthelemy, J Schwartz, K Sebti
ANTEA
December 1994
Supported by ANDRA, France

ICR 95-01
Simulations of pressure and salinity fields at Äspö
Jari Löfman, Veikko Taivassalo
VTT Energy, Espoo, Finland
June 1995
Supported by TVO, Finland

ICR 95-02

Definition and characterisation of the N-S fracture system - tunnel sections 1/600m to 2/400m.
Relationships to grouted sections - some remarks -

W Kickmaier

June 1993
Supported by NAGRA, Switzerland